NEAR-SURFACE GROUND ICE CONDITIONS IN UNIVERSITY VALLEY, MCMURDO DRY VALLEYS OF ANTARCTICA

Caitlin Lapalme

A thesis submitted to the
Faculty of Graduate and Postdoctoral Studies
in partial fulfillment of the requirements
for the degree of
Master of Science in Geography

Department of Geography
Faculty of Arts
University of Ottawa

Acknowledgements

I would first like to extend my gratitude toward my thesis committee: Dr. Bernard Lauriol and Dr. Antoni Lewkowicz. Thank you both for your comments and discussions during this process - your time and expertise were both greatly appreciated.

Financial assistance provided by NASA's ASTEP program and operated by the National Science Foundation (NSF) Office of Polar Programs and the Natural Science and Engineering Research Council of Canada (NSERC) Discovery Grant are acknowledged as they helped fund the programs, travel and laboratory analyses that made this work possible. I would also like to thank Dr. Alfonso Davila and Dr. Denis Lacelle for collecting the permafrost cores analysed in this thesis.

I thank the GéoCryolab at the Université de Montréal for technical support related to CT scanning and image processing. Additionally, I thank Jean Bjornson at the University of Ottawa for his assistance with the laboratory analyses of the permafrost core samples.

A very important extension of my gratitude is toward my supervisor, Dr. Denis Lacelle, without whom this thesis would not be possible. D, it was in your class that I was first introduced to the Polar Regions and I have developed a love for them ever since (even while in the field, knee-deep in mud, trying to free a corer frozen in permafrost). I appreciate all your comments, support, expertise, knowledge, patience and ability to put up with us all the time (I am sure it was not always easy). Thank you for helping make my dive into the field of science a truly positive experience (and for keeping me up to date with the latest LEGO sets and Ottawa Senators news).

To the Basement Bitties: thank you for being the best office-mates I could have asked for throughout this adventure. Thank you Phil for watching out for me, both by keeping me organized and reminding me that I spill too much coffee to wear white (as much as I know it drove you crazy). Brit, thank you for all the chats and storytelling sessions – a great example of our ability to procrastinate at its finest. MF, thank you for being beside me (quite literally) every step of the way – through R happy dances when we succeeded in running our code, to picking up each other's catch-phrases that no one else understood or liked; I am incredibly grateful and lucky to have done my degree alongside you.

To my friends, thank you all for continuing to be my friends even through my year-long hiatus – you all make life just a little more special. A special thank you must be given to Linda for always checking in on my thesis (and me) while convincingly pretending to be interested in my work. I also wish to thank Simone for keeping me “in shape” and feeding me over these past years. To my adopted family (my roommates), thank you for being my favourite people to come home to; I am very fortunate to have you in my life. Kaitie, thank you for giving me the “tips of the trade” and reminding me that it will get easier. Ame, thank you for being my voice of reason and an overall kind and understanding person to be around; Netflix marathons were that much better with you by my side. Sav, thank you for being my number 1 fan and offering endless support and encouragement through tireless fights over who The Nin loves more (me). Sundy, thank you for keeping my life fun, exciting, entertaining and full of country and Vevo (I still argue that “Bailando” is best danced to when listening to the English version). Lastly, I want to extend my gratitude to Rob for all the stats talks, the discovery of the slow cooker, the subsequent meals that it/you provided and for being a key participant in our Mario Kart tournaments (that, of course, I always “win”). I am fortunate to have someone in my life that actually shares my excitement in discussing all things cold. I am very lucky and grateful to have had your continued patience, help, support and kindness throughout the completion of this degree – you made long weekend nights thesis-ing seem much more manageable (dare I say - fun?).

Last, but certainly not least, I would like to extend my gratitude to my family. Thank you all for offering endless support and encouragement throughout my thesis; it never went unappreciated or unnoticed. Particularly, I would like to extend my thanks to both my sisters. Brièle, thank you for still being happy to see me the few times I do come to visit (even if it means that you need to share the computer a little more than you may like). Élise, thanks for being my big-little sister; you have helped me through paper readings, present buying and overall acceptance of my busy life over the past years (even if you end up having to roll your eyes at me a few times). I would also like acknowledge “The Mom”. Momma, thank you for single-handedly allowing me to achieve this thesis. Your support, understanding and encouragement have been amazing and I could not have done it without you (even if I sometimes forgot to call you back). Finalement, j’aimerais remercier mon père. Papa, you also played a role in shaping my interests. Although I would have never believed it, my interests led to the completion of this thesis as part of a M.Sc. (!?) degree (while still finding time for a few card games); incredibly, I think this is where you would want me to be.

Abstract

This study aims to quantify ground ice content and describe the cryostructures and sediment in 15 ice-bearing permafrost cores collected from nine sand-wedge polygons in University Valley. The objectives were reached through laboratory measurements and computed tomodensitometric (CT) scanned image analysis of the permafrost cores. The soils in the valley were predominantly medium-sand. Four types of cryostructures were present in the cores: structureless, suspended, crustal and porphyritic. Excess ice content ranged from 0 to 93%, gravimetric water content ranged from 13 to 1881% and volumetric ice content varied from 28 to 93%. Median excess ice, volumetric ice and gravimetric water contents significantly increased in the top 20 cm of the cores taken from the polygon shoulders with increasing distance from University Glacier. Ground ice was preferentially stored in the centre of the investigated polygons where the ground surface remains cryotic throughout the year. Conversely, higher ground ice contents were measured in the shoulders of the investigated polygon where the ground surface is seasonally non-cryotic. CT-scanned images were shown to reasonably assess the distribution and presence of excess ice in permafrost cores taken from a cold and hyper-arid environment. The results of this thesis provide the first cryostratigraphic study in the McMurdo Dry Valleys of Antarctica.

Table of Contents

List of figures

List of tables

List of abbreviations

a.s.l.	Above sea level
ASTER	Advanced Spaceborne Thermal Emission and Reflection Radiometer
BV	Beacon Valley
BW	Lake Brownworth
CRREL	Cold Regions Research and Engineering Laboratory
CT	Computed tomodensitometric
CTVIC	Computed tomodensitometric volumetric ice content
CTZ	Coastal thaw zone
EC	Explorer's Cove
EI	Excess ice
ecdf	Empirical cumulative distribution function
FDD	Freezing degree days
FR	Ferrar Glacier
GSRH	Ground surface relative humidity
GWC	Gravimetric water content
HU	Hounsfield units
IMZ	Inland mixed zone
K-S test	Kolmogrov-Smirnov test
LB	Lake Bonney
LiDAR	Light detection and ranging
LH	Lake Hoare
LTER	Long-term ecological research
LV	Lake Vanda
MAAT	Mean annual air temperature
MAGSRH	Mean annual ground surface relative humidity
MAGST	Mean annual ground surface temperature
MDV	McMurdo Dry Valleys
MSGST	Mean summer ground surface temperature
NCZ	Non-cryotic ground zone
PCZ	Perennially cryotic ground zone
PISR	Potential incoming solar radiation
RH	Relative humidity
SUZ	Stable upland zone
SWE	Snow water equivalent
SWIr	Short wave incoming radiation
TDD	Thawing degree days
UV	University Valley
VIC	Volumetric ice content

1. Introduction

Ground ice is one of the most important and dynamic geologic components of permafrost. Unlike other minerals in frozen soils, ground ice can rapidly adjust to changing environmental conditions, and as such, measurements of the amount, distribution and the shape of ground ice in frozen soils can provide insight into the thermal history of permafrost (French, 1998; French and Shur, 2010). According to Pollard and French (1980) and Mackay and Dallimore (1992) who investigated ground ice content in the uppermost 10 m of permafrost in the western Canadian Arctic, higher ground ice contents tend to be found in the uppermost 2 m of permafrost. Similar ground ice distribution was observed in Alaska (e.g. Kanevskiy *et al.*, 2013; 2014) and Siberia (e.g. Iwahana *et al.*, 2014). Based on observations and measurements from Arctic permafrost, Mackay (1972) proposed a classification of ground ice based on the source of the water immediately prior to its freezing (i.e. water vapour, surface water or groundwater) and the principal transfer processes responsible for moving the water to the freezing plane (i.e. vapour diffusion, gravity migration, pressure potential and in situ freezing). The classification includes 10 types of ground ice: open-cavity ice, vein ice, ice wedge, tension-crack ice, closed-cavity ice, epigenetic ice, aggradational ice, sill ice, pingo ice and pore ice. The freezing of liquid water is responsible for the formation of eight of these ice types, whereas vapour diffusion is responsible for the remaining two types of ice (open and closed cavity ice).

There are numerous studies on ground ice content and distribution in Arctic permafrost, but few examine these components in Antarctic permafrost. To date, most studies from the McMurdo Dry Valleys (MDV) of Antarctica have focused on soil properties and salt concentrations in the dry soil layer (e.g. Campbell and Claridge, 1969; 1975; 1978; 1981; Bockheim, 1997; 2002; Bockheim and McLeod, 2015), active layer depths (e.g. Bockheim and Hall, 2002; Campbell and Claridge, 2006; Adlam *et al.*, 2010) and on the stability of the *ice table*, the boundary surface between the dry and ice-bearing permafrost (e.g. Hindmarsch *et al.*, 1998; McKay *et al.*, 1998; Ng *et al.*, 2005; Kowalewski *et al*., 2006; 2012; Hagedorn *et al.*, 2007; McKay, 2009; Lacelle *et al.*, 2011; Mellon *et al.*, 2014; Liu *et al.*, 2015; Fisher *et al.*, in review). Investigations of ground ice abundance in MDV permafrost have only been addressed in a limited number of studies (e.g. Marchant *et al.*, 2002; Dickinson and Rosen, 2003; Bockheim *et al.*, 2007; Levy *et al.*, 2008; Hagedorn *et al.*, 2010; Pollard *et al.*, 2012; Lacelle *et al.*, 2013), mostly at very coarse resolutions and none have described cryostructures in the permafrost. The permafrost classification map of the McMurdo Dry Valleys of Antarctica depicts ground ice in permafrost as occurring in: i) dry permafrost, characterized by low ice contents, usually < 3%wt; ii) ice-cemented or ice-bonded permafrost, where ice occupies the pore space of sediments; and iii) ground ice, in the form of ice wedges or buried ice (Bockheim *et al.*, 2007). This broad classification mixes the abundance (i.e. dry or ice-cemented) and origin (i.e. buried ice, ice wedges or ground ice) of ground ice, highlighting a lack of understanding of its distribution, quantity and origin in MDV permafrost. The presence of ice-cemented permafrost in the cold and hyper-arid environments of the MDV, where liquid water is rare, seemingly defies the conventional understanding of ground ice forming processes (e.g. Mackay, 1972). As such, the amount, distribution and origin of ground ice in MDV permafrost remains poorly understood, yet these are essential components of the dynamic relations between the climate and landscape evolution in this region.

Cryostratigraphy emphasizes the description of cryostructures (distribution and shape of ground ice), the quantification of ground ice content and associated cryofacies, and the identification of discontinuities in permafrost revealed by a change in cryostructure and/or cryofacies. As a result, cryostratigraphy is used to reconstruct the history of permafrost and the origin of ground ice (e.g. French, 1998; French and Shur, 2010). This thesis investigates the cryostratigraphy of near-surface permafrost in University Valley, a small hanging glacial valley in the Quartermain Mountains of the MDV of Antarctica. Overall, the results presented in this study contribute towards our understanding of the processes and environmental factors that form the ice-cemented permafrost in the Quartermain Range.

1.1. Objective of thesis

This thesis is the first cryostratigraphic study in the MDV. The objectives of this study are to describe the cryostructures and quantify the ground ice content in shallow permafrost cores from University Valley by combining laboratory measurements with computed tomodensitometric (CT) scans that produce high-resolution images (sub-mm scale). Relations between sediment properties, cryostructures and ice content are explored. These objectives are accomplished using the following methods: i) field sampling of 15 shallow permafrost cores taken from nine sand-wedge polygons (< 1.5 m deep at varying ice table depths); ii) CT scanning of select permafrost cores with the resulting images analyzed for ice distribution, shape and content; iii) quantifying the ground ice content of the cores and characterizing the associated cryofacies; and iv) determining the particle size distribution and dry colour of the mineral soils. The spatial sampling method employed for the collection of the permafrost cores, taken across the valley and within individual polygons, allows for a preliminary assessment of the spatial (horizontal and vertical) variation of ground ice content within the valley.

This study is of importance due to the limited understanding of the impact of climate change on Antarctic permafrost. Paleoclimatic studies on the effects of historical climate change in Antarctica have largely focused on the response of ice-sheets and sea-ice to insolation-driven changes in temperatures (e.g. Jouzel *et al.*, 2007; Kawamura *et al.*, 2007) and the response of permafrost to past and future climate change remains largely unexplored (e.g. Fountain *et al.,* 2014). Investigating changes in ground ice content and cryostructures in MDV permafrost may have important paleoclimatic implications. For example, previous permafrost studies (i.e. French and Shur, 2010 and references therein) have shown that former surface conditions (e.g. temperature and humidity) can be recorded through the analysis of ice content, cryostructures and/or geochemical discontinuities. This contribution helps further our current understanding of ground ice conditions in cold and hyper-arid environments and evaluates the applicability of Arctic-centric cryostratigraphic classification schemes to permafrost found in University Valley.

2. Study area

2.1. McMurdo Dry Valleys of Antarctica

The McMurdo Dry Valleys in southern Victoria Land form the largest ice-free area in Antarctica where only 0.35% of the Antarctic continent is considered to be ice-free (Bockheim *et al.*, 2008; Levy, 2013). Situated between 76°-79°S and 158°-170°E, the MDV are located within the Trans-Antarctic Mountains, constrained between the East Antarctic Ice Sheet and the western coast of the seasonally open water of the Ross Sea (Denton *et al.*, 1993) (Figure 1). The Trans-Antarctic Mountains act as a barrier to the ice flow of the East Antarctic Ice Sheet into the MDV; however, Taylor and Ferrar glaciers override the mountains to occupy the MDV (Fountain *et al.,* 2009). The total area of the MDV is 22,700 km^2, while the ice-free areas comprise 4500 km^2. The central MDV have a total area of 12,200 km^2 with the ice-free areas occupying 3000 km^2. However, recent inter-comparisons of mapping thresholds suggest that the actual ice-free areas of the MDV could be within ca. 10% of the previously reported values (Levy, 2013). Elevations in the MDV range from sea level at the Ross Sea to 2000 m above sea level (a.s.l.) near the Polar Plateau. The landscape of the valleys includes perennial ice-covered lakes, ephemeral streams fed by snow and glacier meltwater, arid-rocky and ice-cemented soils and the surrounding glaciers (Doran *et al.*, 2002). The soil texture in the region is characterized as rocky-sandy (Fountain *et al.*, 2009) and the soil surface is characterized by desert pavement (Bockheim, 2015) and a lack of vascular vegetation (Fountain *et al.*, 2009; Bockheim, 2015). The region experiences continuous daylight in the midsummer and constant darkness in the midwinter (Fountain *et al.*, 2009).

The climate in the MDV is classified as cold and dry, with mean annual air temperatures in the range of ca. -14 to -30°C and mean annual water-equivalent precipitation of ca. < 100 mm (Doran *et al.*, 2002; Fountain *et al.*, 2009). However, a steep gradient in summer air temperature and relative humidity (RH) exists between the coastal lowlands of the Ross Island area and the high elevation valleys, with summer air temperatures largely set by the dry adiabatic lapse rate (Doran *et al.*, 2002; McKay, 2015). The extremely arid conditions lead to the region experiencing low precipitation relative to potential evaporation, low surface albedo and katabatic winds descending from the Polar Plateau and removing available moisture from the air (Doran *et al.*, 2002).

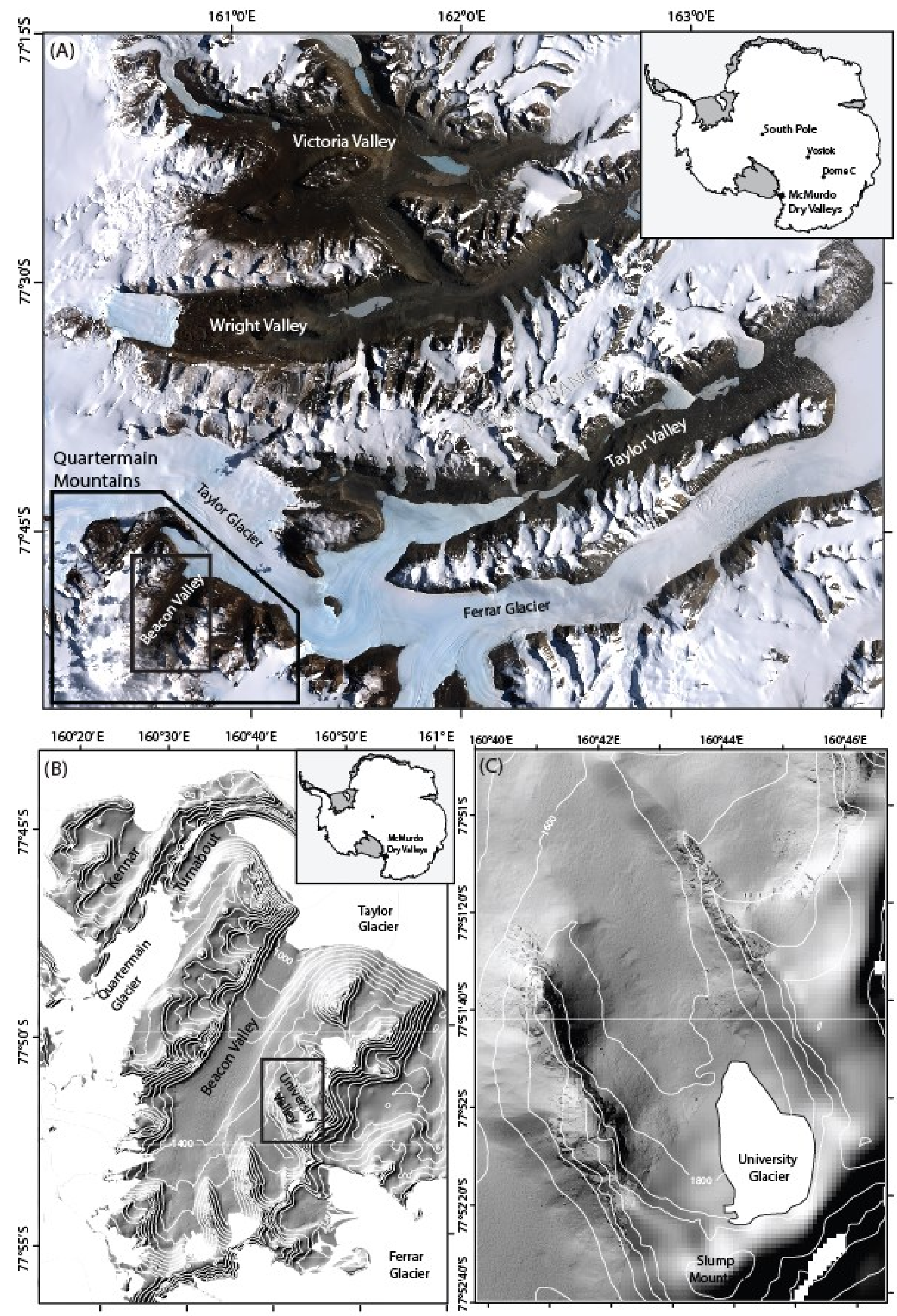

Figure 1: (A) Landsat image showing the location of the McMurdo Dry Valleys relative to Antarctica. (B) Map showing the location of the Upper McMurdo Dry Valleys. (C) Map of University Valley; the hillshade image was derived from a light detection and ranging (LiDAR) digital elevation model (http://usarc.usgs.gov/lida_dload.shtml) embedded into a 15 m Advanced Spaceborne Thermal Emission and Reflection Radiometer (ASTER) digital elevation model of the upper McMurdo Dry Valley's region (http://asterweb.jpl.nasa.gov/data/asp).

Katabatic winds are one of the main influences on local climate in the MDV (Clow *et al.*, 1998; Doran *et al.*, 2002; Nylen *et al.*, 2004). A katabatic force is described as the wind pattern of a surface which is steered by the long-wave radiative cooling of the continental snow surface. This process cools the atmospheric surface layer that overlies the snow surface; if a slope is present, this prompts a downslope pressure-gradient force (i.e. wind is katabatic if the flow is caused by a downslope buoyancy forcing) (Renfrew and Anderson, 2002). Katabatic winds in the MDV flow off the East Antarctic Ice Sheet at speeds typically reaching 20 m s^{-1} (Nylen *et al.*, 2004) and occur more frequently in the summer than the winter (Doran *et al.*, 2002; Nylen *et al.*, 2004). The winds are considered an important factor in explaining the variation in mean annual air temperature between valleys. These inter-valley temperature differences are related, in part, to temperature contrasts during the winter months and the slowing and/or forcing of the winds from the ground by phenomenon similar to hydraulic jumps (Doran *et al.*, 2002). Inter-valley variability in the frequency of katabatic winds is attributed to the location of the valley relative to the East Antarctic Ice Sheet and the persistency and force of temperature inversions throughout the non-summer months. Katabatic vs. non katabatic conditions can result in monthly average temperature and RH differences of 10 to 30°C and 20 to 30%, respectively (Nylen *et al.*, 2004). For example, a local air temperature increase of up to 30°C can be felt within a few hours of a katabatic wind event as a result of the wind's adiabatic warming (Fountain *et al.*, 2009).

Annual snowfall values in the region range from 3 to less than 100 mm water equivalent where the highest snowfall values occur in coastal areas and decrease further inland. Snowfall patterns can influence the spatial distribution of ground ice conditions (Hagedorn *et al.*, 2007; McKay, 2009) in addition to the stability of subsurface ice deposits (McKay, 2009; Liu *et al.*, 2015) and the maintenance of glaciers (Fountain *et al.*, 2006). Snow can also influence the hydrological system of the MDV; for example, glacial melt can cease as a result of as little as a few centimeters of snow accumulation, which will lead to a lower amount of glacier runoff (Fountain *et al.*, 2009). Summer snowfall also produces an increased albedo of the snow-covered surface. As a result, the energy balance changes and less energy is available to allocate toward melting and thawing (Fountain *et al.*, 1999). Snowfall may not occur during katabatic wind events as they are typically triggered by conditions that do not favour precipitation. However, half of the accumulated snow in the MDV can be attributed to wind dispersion. For example, local snow from valley walls can be transported through katabatic winds to the surrounding valley floors (Fountain *et al.*, 2009). Additionally, the winds are able to transport snow from the large interior Polar Plateau resulting in the deposition of snow on the leeside of topography within the MDV (Marchant and Head, 2007).

Solar radiation is a driving factor in the hydrological and biological systems in the valleys as it warms the air and the soil surface, impacts the sublimation process and glacier melt and gives energy for photosynthesis by microbial communities within soils, streams and perennially ice-covered lakes. Inter-valley variations in solar radiation are related to the mountainous topography and the resulting steep-sided valleys in the region and differing cloud covers (Dana *et al.*, 2002).

2.1.1. Climate zones in the McMurdo Dry Valleys of Antarctica

Marchant and Head (2007), following the work of Marchant and Denton (1996), distinguished three climatic zones in the MDV that incorporate summer air temperatures and RH: 1) the coastal thaw zone (CTZ), 2) the inland mixed zone (IMZ), and 3) the stable upland zone (SUZ). The low elevation valleys (< 400 m) are situated in the CTZ where the summer air temperature and RH average -5°C and 64%, respectively. The sum of thawing degree-days ranges between 20 and 100 yr^{-1} (Doran *et al.*, 2002) and snow accumulation, as snow water equivalent (SWE) ranges between 25 to 100 mm yr^{-1} (Fountain *et al.*, 2009). The high elevation valleys (> 1000 m) are located in the SUZ where the summer air temperature and RH values are lower than the CTZ averaging -10°C and 41%, respectively. The sum of thawing degree-days is < 5 yr^{-1} and snow accumulation is rare (SWE < 10 mm yr^{-1}) (Doran *et al.*, 2002, Fountain *et al.*, 2009). The spatial pattern of summer climate conditions in the climatic zones of the MDV appears to be related to distinct periglacial processes (Bockheim *et al.*, 2007, Marchant and Head, 2007; Adlam *et al.*, 2010; Levy *et al.*, 2011; Fountain *et al.*, 2014). For example, the CTZ is characterized by a thick and moist active layer (< 60 cm and > 30%wt) and geomorphic features such as intermittent meltwater streams, ice wedge polygons, thermokarst and gullies. Comparatively, the SUZ is distinguished by a shallow and dry active layer (< 15 cm and < 3%wt) with sand wedge and sublimation-type polygons.

Figure 2 depicts temperature-related indices for multiple long-term ecological research (LTER) meteorological stations within the MDV: Lake Bonney (LB), Lake Hoare (LH), Ferrar Glacier (FR), Explorer's Cove (EC), Lake Vanda (LV), Beacon Valley (BV), University Valley

(UV) and Lake Brownworth (BW). University Valley had the lowest temperatures of the recorded stations with a mean annual air temperature (MAAT) of ca. -24°C (Figure 2A), a mean annual ground surface temperature (MAGST) of ca. -25.5 °C (Figure 2B); zero days where air and soil surface temperature were above freezing (Figure 2C and 2D, respectively); and zero thawing degree-days measured from the air (Figure 2E) and soil surface (Figure 2F).

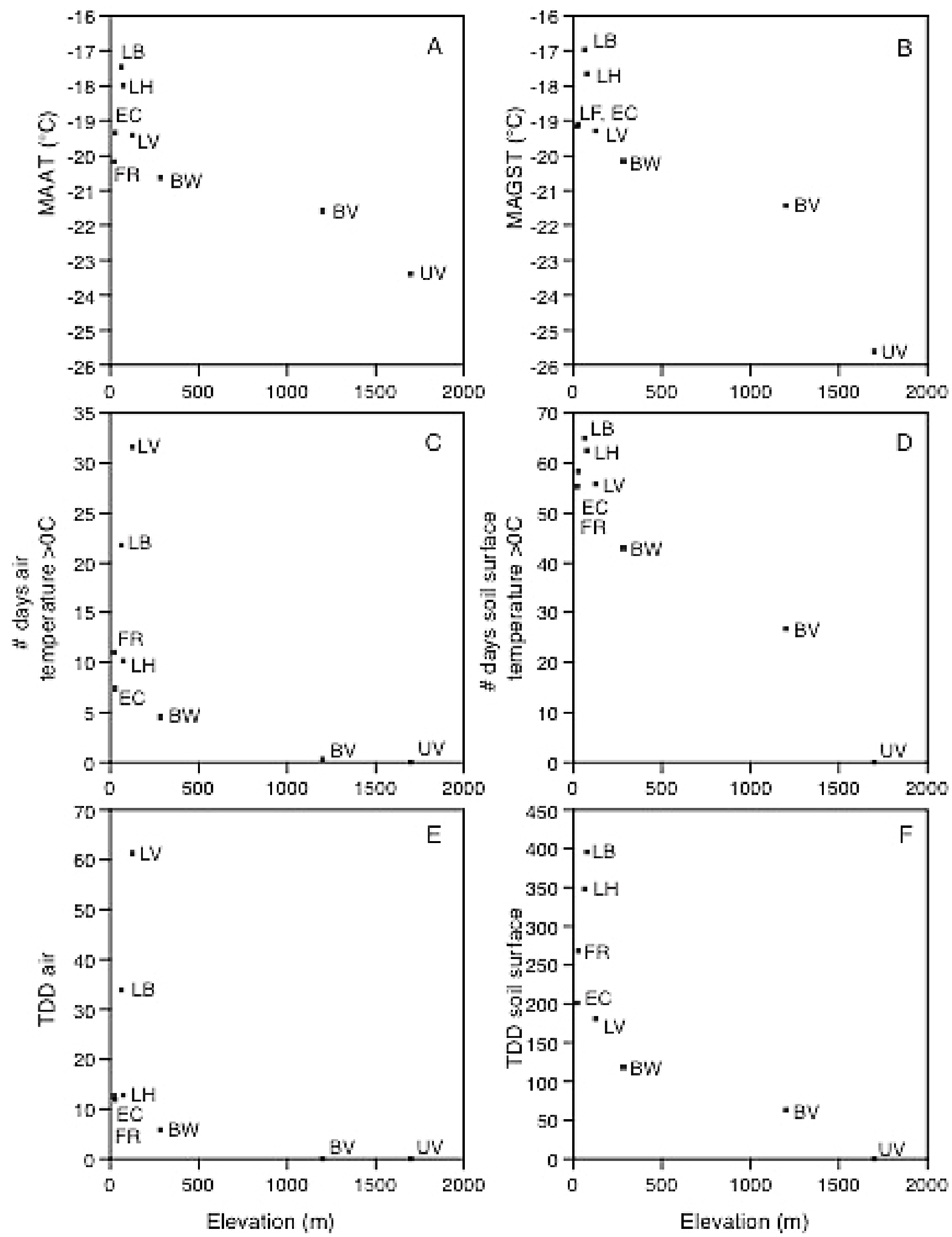

Figure 2: Graphs illustrating: A) mean annual air temperature (MAAT), B) mean annual ground surface temperature (MAGST), C) the number of days where air temperature was above 0°C, D) the number of days where soil surface temperature was above 0°C, E) the number of thawing degree days (TDD) calculated from air temperatures and F) the number of thawing degree days (TDD) calculated from soil surface temperatures for stations in the McMurdo Dry Valleys. Stations are located at Lake Bonney (LB), Lake Hoare (LH), Ferrar Glacier (FR), Explorer's Cove (EC), Lake Vanda (LV), Beacon Valley (BV), University Valley (UV) and Lake Brownworth (BW). Data taken from LTER database (https://portal.lternet.edu/nis/browseServlet?searchValue=MCM).

2.1.2. Permafrost and active layer thickness across the McMurdo Dry Valleys of Antarctica

The cold climate conditions in the MDV cause permafrost to be continuous throughout the region (Bockheim and Hall, 2002). The permafrost classification map of the MDV depicts the Quartermain Mountains to contain an estimated 59% of dry permafrost, 37% of ice-cemented permafrost and the remaining 4% of permafrost contains ground ice (Figure 3). The type of permafrost present has been suggested to relate to the age of the surface. For example, ground ice is present in Holocene age surfaces while ice-cemented permafrost occurs on late Quaternary surfaces. However, distribution patterns of ice-cemented permafrost and ground ice can also be influenced by local environmental factors. The development of dry permafrost is suggested to occur on surfaces > 115 ka as a result of sublimation (Bockheim *et al.*, 2007).

Active layer thicknesses in the MDV vary with respect to the three climatic zones and decrease with elevation ($r^2 = 0.67$, p-value = < 0.05; Figure 4). In the CTZ, an active layer forms over permafrost containing variable amounts of ground ice ranging from ice-bonded permafrost to massive ground ice (buried ice). Here, the active layers are thickest, ranging from 30 to 70 cm, and decrease in thickness to < 40 cm within the IMZ (Bockheim and Hall, 2002; Campbell and Claridge, 2006; Bockheim *et al.*, 2007). Portions of the low elevation valleys occupied by the Ross Sea Drift and glacio-lacustrine sediments have salty and moist permafrost. In the IMZ and SUZ, the extreme cold and aridity ensure that a dry cryotic soil layer is found between the active layer and underlying ice-bearing permafrost (e.g. Marchant and Head, 2007) (Figure 5). The boundary between the bottom of the dry cryotic soils and the top of the ice-bearing permafrost is referred to as the ice table (Figure 6). Active layers are thinner within the SUZ and the plateau fringe varying between 0 to 25 cm and 15 to 20 cm, respectively (Bockheim and Hall, 2002). Lastly, active layer depths are < 2 cm along the Polar Plateau (Bockheim *et al.*, 2007). Overall, the variability in the thickness of the active layer in the MDV is influenced by the proximity to the coast (Bockheim and Hall, 2002; Campbell and Claridge, 2006; Adlam *et al.*, 2010), elevation (Bockheim and Hall, 2002), mean summer air temperature, wind speed, and mean winter air temperatures (Adlam *et al*., 2010). The trend also correlates well with the dry adiabatic lapse rate (Campbell and Claridge, 2006).

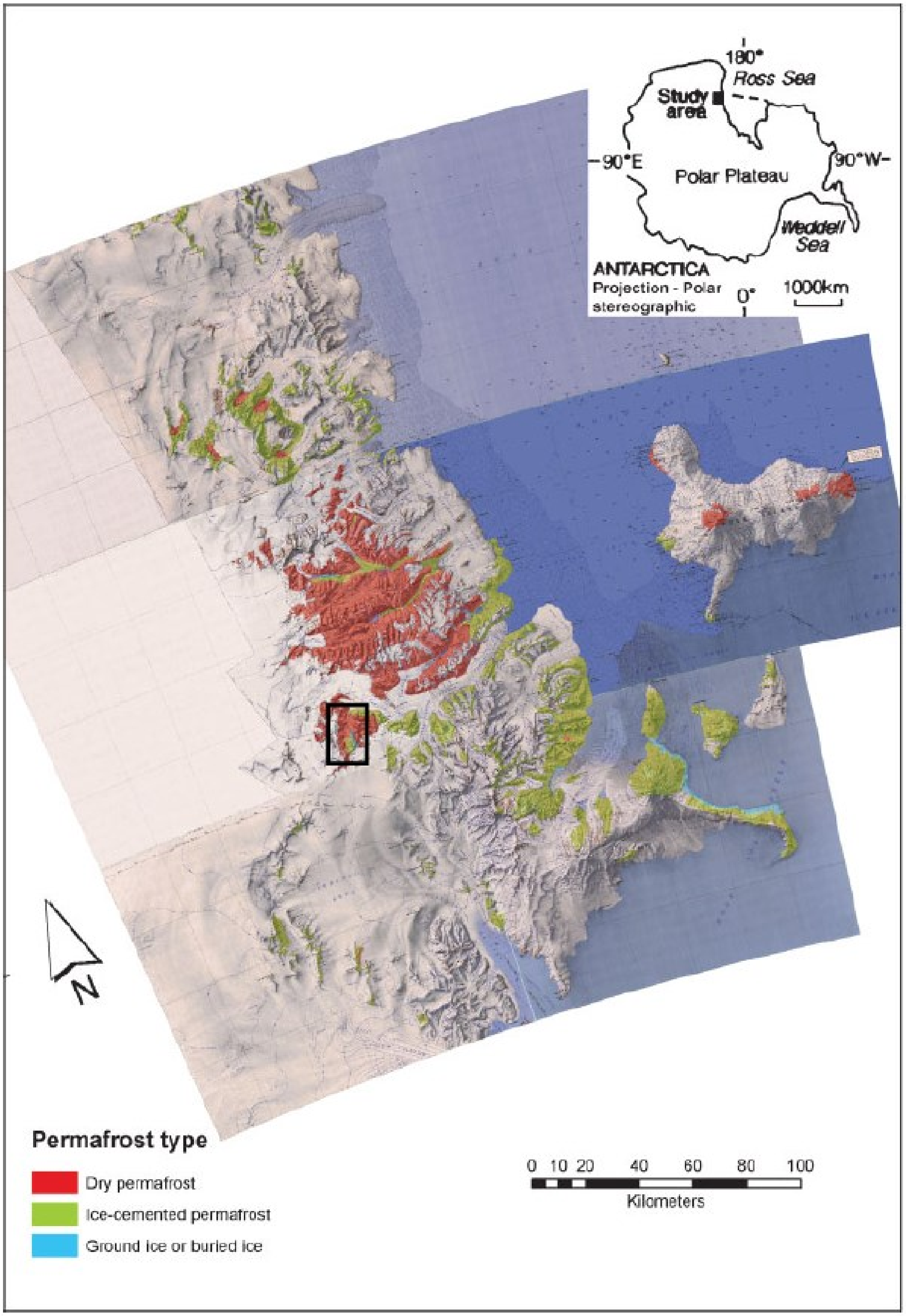

Figure 3: Distribution of permafrost, by form, in the McMurdo Dry Valleys of Antarctica. The Quartermain Range is located in the black rectangle. Source: Bockheim *et al.* (2007).

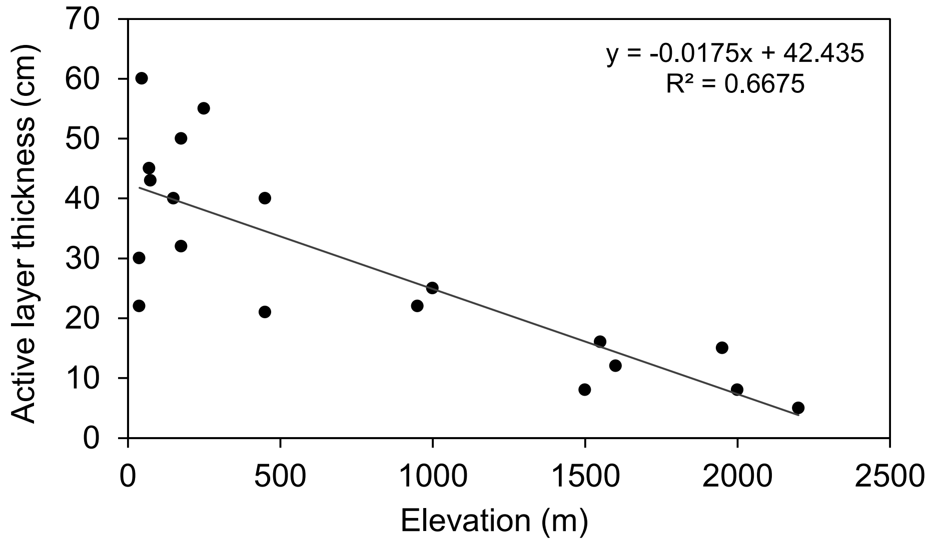

Figure 4: Active layer thicknesses (cm) across the McMurdo Dry Valleys compared with associated elevations (m). Data from the database for active-layer depths in the McMurdo Dry Valleys from Bockheim *et al.* (2007).

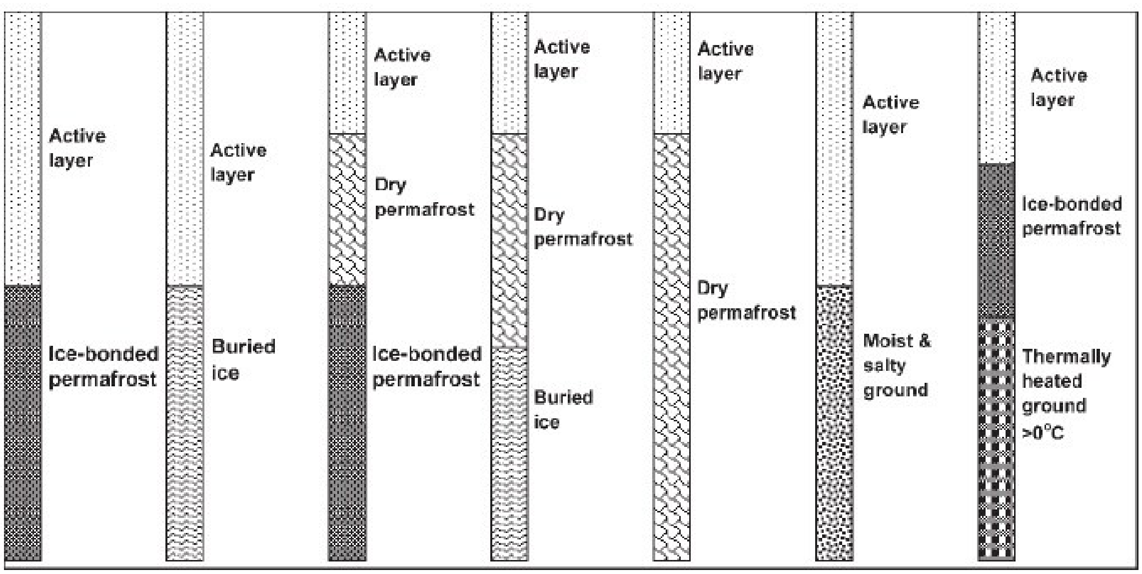

Figure 5: The different types of permafrost found in the Transantarctic Mountains, Antarctica. Source: Campbell and Claridge (2006).

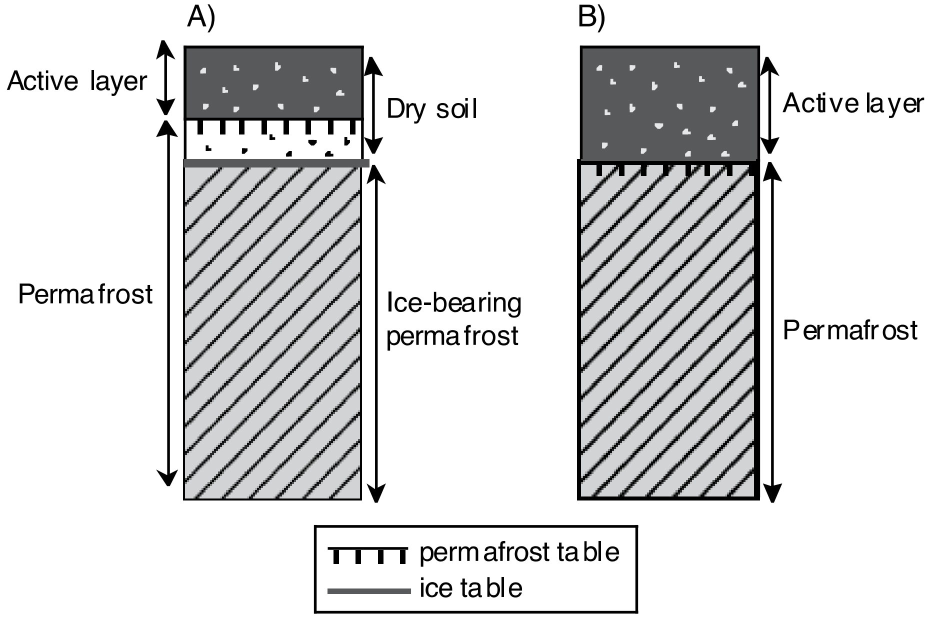

Figure 6: Schematic illustrating: A) permafrost containing a dry soil layer between the top of the permafrost table and the top of the ice-table (ice-bearing permafrost) typical of Antarctic soils in the stable upland zone and B) permafrost where the top of the permafrost table intersects with the top of the ice-bearing permafrost (typical of cryotic soils with higher moisture contents).

2.2. University Valley, McMurdo Dry Valleys of Antarctica

University Valley (77°52’S; 163°45’E; 1600-1800 m a.s.l.) is located in the Quartermain Mountains of the MDV (Figure 7). The valley is a 1.5 km long and 500 m wide northwest facing upper hanging glacial valley situated ca. 450 m above the floor of the adjacent Beacon Valley (Figure 1B, p.5). A small glacier, informally named University Glacier, is located at the head of the valley and has a maximum thickness of ca. 150 m. Permanent snow patches are found in depressions scattered along the western portion of the valley floor.

The local geology for the region consists of sills of Ferrar Dolerite (Jurassic age intrusives) and sedimentary rock of the Beacon Supergroup (Devonian to Triassic age sandstones and conglomerates) (Barrett, 1981; Marchant *et al.*, 1993; Cox *et al.*, 2012). Surficial sediments are fairly heterogeneous throughout the valley including areas comprised of large rocks and boulders and others composed of sand-sized particles. The surface sediments consist of colluvium and talus cones at the base of the valley walls and undifferentiated till and alpine drift on the valley floor (Figure 7). The alpine drifts are found only in the central and upper areas of the valley in addition to dispersed outcrops of sandstone bedrock (Cox *et al.*, 2012). Sand wedge polygonal terrain developed on the valley floor and on some of the talus cones.

University Valley is located within the SUZ of the MDV, which is characterized by summer air temperatures < 0°C and RH values < 50%; the latter can be attributed, in part, to the dry katabatic winds that pass through the region (Marchant and Head, 2007). Climate data collected over a three year period (2010-12) from a weather station in University Valley (77°51.729'S; 160°42.606'E; elevation = 1677 m; ice table depth = 42 cm) by Lacelle *et al.* (2015) reported a MAAT of -23.4 ± 0.8°C and a mean annual relative humidity of 45.5 ± 14%. Mean summer air temperature was -13.9 ± 0.4°C and air temperatures were always < 0°C. The maximum individual daily and hourly air temperature values were -5.7 and -2.8°C, respectively.

These cold and hyper-arid climate conditions lead to ice-bearing permafrost in the valley overlain by dry permafrost of varying thicknesses (McKay, 2009; Lacelle *et al.*, 2011; 2013; Marinova *et al.*, 2013). The depth to ground ice increases as a function of distance from University Glacier, from less than 1 cm in proximity to the glacier, to more than 70 cm at the mouth of the valley (McKay, 2009; Marinova *et al.*, 2013). McKay (2009) suggested that differences in ice table depths could be controlled by snow recurrence with a more continued snow cover near the head of the valley. Fisher *et al.* (in review) suggested that the ice table depth is set by ground surface temperature, humidity and advective air flow in the dry soil layer responding to changing surface conditions occurring over decades to centuries. Mellon *et al.* (2014) investigated the morphological characteristics and size of the polygonal ground in the valley with respect to the depth to ice table and found a positive correlation between ice table depth and polygon size. As a result, it was suggested that the ice table has been at its present-day position for longer than 10,000 years, the time-scale for polygon development.

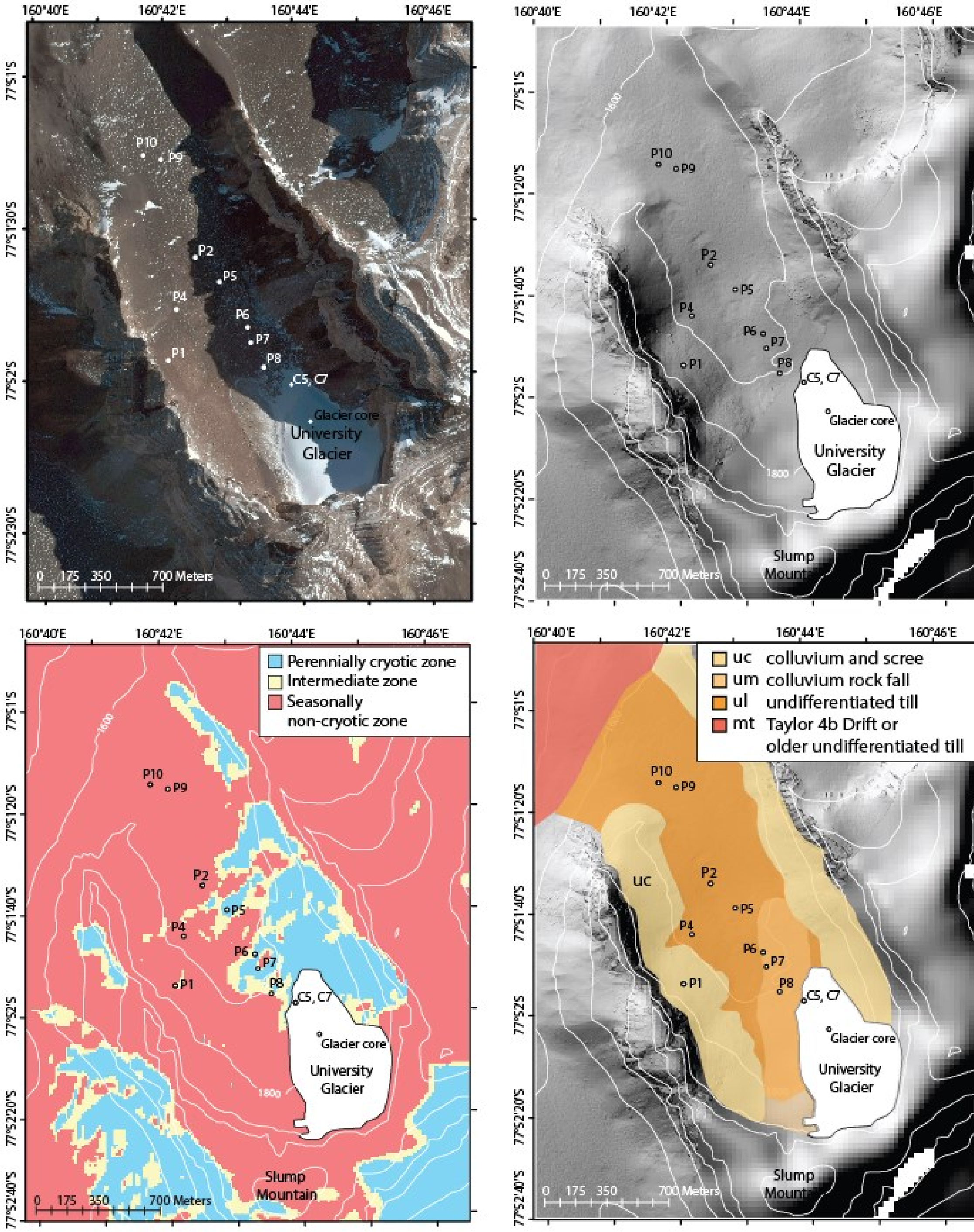

Figure 7: Top left) Nextview Imagery of University Valley (Source: DigitalGlobe, Inc.). Top right) Hillshade image of University Valley showing the location of the polygon cores generated from a LiDAR digital elevation model and a 15 m resolution ASTER digital elevation model (http://asterweb.jpl.nasa.gov/data.asp). Bottom left) Map delineating three distinct ground surface temperature zones within University valley derived from ground surface temperatures and potential incoming solar radiation (Lacelle *et al*., 2015). Bottom right) Image delineating four surficial sediment covers that characterize University Valley (Cox *et al*., 2012). Contour lines on the maps are given at 100 m intervals and delineated by white lines. The polygon core locations are marked on all four images.

2.2.1. Micro-climates in University Valley

Ground surface and air temperatures (2010-12 with some missing values) and incoming short-wave radiation data in University Valley were obtained by Lacelle *et al.* (2015). Mean monthly and maximum daily air temperatures in University Valley are summarized in Table 1.

Table 1: Mean monthly and maximum daily air temperature (°C) in University Valley, McMurdo Dry Valleys of Antarctica.

	Mean monthly			Max daily		
Month	2010	2011	2012	2010	2011	2012
1	-12.1	-12.6	-12.6	-8.0	-8.1	-6.4
2	-18.1	-17.4	-17.0	-12.9	-13.1	-6.3
3	-23.0	-24.6	-23.7	-13.2	-18.2	-15.5
4	-27.0	-26.7	-28.7	-18.1	-15.0	-21.6
5	-29.9	-28.5	-26.1	-18.8	-19.0	-14.7
6	-31.4	-27.8	-30.4	-20.5	-19.9	-20.3
7	-33.9	-26.8	-32.1	-25.6	-18.8	-25.4
8	-31.4	-26.7	-30.0	-23.3	-18.4	-22.1
9	-30.3	-26.7	-29.1	-23.8	-19.3	-21.7
10	-24.0	-24.2	-24.6	-19.7	-17.4	-19.7
11	-18.2	-15.2	-17.3	-8.7	-11.5	-11.7
12	-11.0	-12.0	-10.9	-6.3	-6.8	-5.7
MAAT	-24.2	-22.5	-23.5			

Temperatures at the soil surface and the top of the ice table were measured at increasing distances from University Glacier at varying ice table depths (250, 550, 750 and 950 m distance from University Glacier with corresponding ice table depths of 8, 22, 42 and 36 cm, respectively) (Figure 8). Results show mean summer ground surface temperatures (MSGST) near -26°C along the valley but the summer ground surface temperatures exhibit a warming trend from the upper to lower areas of the valley. Mean daily ground surface temperatures were always < 0°C. However, hourly ground surface temperatures rose above 0°C in some locations along the valley floor. For example, ground surface temperatures were above 0°C for one hour near the head of the valley (thaw degree-hours = 0.3) and 110 hours at 950 m down valley (thaw degree hours = 442). The findings for the mean monthly soil temperatures and maximum daily soil temperatures (surface and ice table) for the shallowest (8 cm depth; 250 m from glacier) and deepest (36 cm depth; 950 m from glacier) ice table sites are summarized in Tables 2 and 3, respectively. Maximum daily soil surface temperatures are ca. 1°C warmer at the deepest ice table depth site

(42 cm depth; -2.7°C; 2010) than at the shallowest ice table depth site (8 cm depth; -3.8°C; 2010-2011). In contrast, maximum daily ice table temperatures were ca. 2°C warmer at the shallowest ice table site (-7.7°C; 2010-2011) than at the deepest ice table depth site (-9.6°C) (Lacelle *et al.*, 2015).

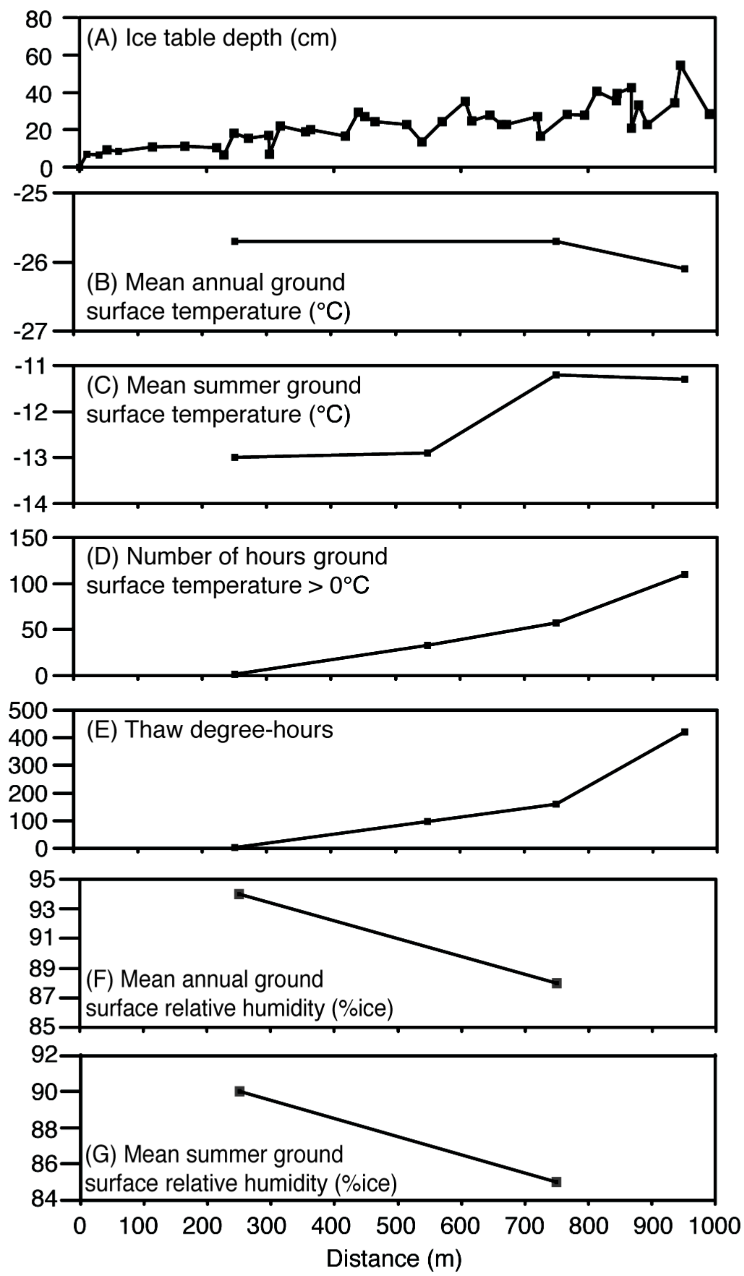

Figure 8: (A) Ice table depth in University Valley measured with distance from University Glacier (data from Marinova *et al.* (2013)). (B–G) Ground surface temperatures and humidity as a function of distance from University Glacier. Data were collected in 2010 at four different sites.

Table 2: Mean monthly soil temperatures (°C) (surface and ice table) at 42 cm ice table depth (750 m from glacier) and 8 cm ice table depth (250 m distance from glacier) in University Valley, McMurdo Dry Valleys of Antarctica.

	2010		2011		2012	
Month	Soil surface	Ice table	Soil surface	Ice table	Soil surface	Ice table
			42cm ice table depth			
1	-8.3	-12.5		-11.1		-10.8
2	-15.6	-15.2		-14.9	-13.0	-14.7
3	-23.3	-20.2		-21.4		-21.4
4	-30.7	-26.2		-26.8	-30.7	-27.0
5	-34.5	-29.9		-28.9	-29.4	-27.0
6	-36.7	-32.3		-28.8	-35.3	-30.8
7	-38.8	-34.0		-30.4	-36.9	-32.8
8	-36.0	-34.1		-29.8	-33.8	-32.2
9	-34.6	-33.0		-28.8	-33.5	-31.2
10	-25.1	-27.8		-26.6	-24.8	-27.6
11	-14.3	-20.5		-19.1	-13.8	-20.4
12	-9.9	-13.6	-2.6	-13.2	-5.6	-13.2
MAGT	-25.7	-25.0		-23.4	-27.9	-24.1
			8 cm ice table depth			
1	-10.8	-11.5	-10.9	-11.6	-8.9	-9.9
2	-16.9	-16.8	-16.7	-16.6	-15.7	-15.6
3	-23.4	-22.9	-25.3	-24.7	-24.9	-23.3
4	-28.5	-28.0	-29.2	-28.8		
5	-32.1	-31.5	-30.6	-30.2		
6	-33.7	-33.3	-30.2	-29.9		
7	-36.0	-35.4	-30.2	-30.2		
8	-34.7	-34.6	-29.8	-29.7		
9	-33.8	-33.7	-29.6	-29.2		
10	-28.0	-28.4	-26.2	-26.4		
11	-20.5	-21.2	-14.9	-16.2		
12	-9.8	-12.6	-9.3	-11.3		
MAGT	-25.7	-25.9	-23.6	-23.8		

Table 3: Maximum daily soil temperatures (°C) (surface and ice table) at 42 cm and 8 cm ice table depths in University Valley, McMurdo Dry Valleys of Antarctica.

	2010		2011		2012	
Month	Soil surface	Ice table	Soil surface	Ice table	Soil surface	Ice table
42 cm ice table depth						
1	-3.0	-11.1		-9.9		-9.6
2	-10.1	-12.6		-12.5	-9.0	-13.1
3	-15.2	-17.4		-16.6		-17.9
4	-23.9	-24.5		-23.9	-24.4	-22.4
5	-24.6	-25.9		-25.7	-20.1	-24.4
6	-25.3	-29.7		-25.6	-23.9	-28.1
7	-28.5	-31.2		-27.0	-28.9	-30.8
8	-26.9	-31.8		-26.6	-26.3	-29.9
9	-26.4	-30.9		-26.6	-25.6	-29.5
10	-20.1	-24.8		-24.4	-19.5	-24.7
11	-7.9	-17.7		-15.7	-7.6	-16.8
12	-2.7	-9.9	-2.6	-10.0	-0.1	-10.0
8 cm ice table depth						
1	-7.4	-8.9	-6.2	-8.7	-3.3	-6.3
2	-11.8	-13.7	-13.1	-13.5	-11.1	-12.6
3	-18.6	-18.8	-20.1	-19.7	-22.7	-21.3
4	-24.9	-25.3	-21.6	-22.5		
5	-26.1	-26.3	-24.3	-25.1		
6	-27.9	-29.3	-24.8	-25.2		
7	-30.1	-30.6	-24.3	-25.2		
8	-29.4	-30.6	-23.3	-24.7		
9	-28.8	-30.1	-24.3	-25.0		
10	-25.1	-25.8	-21.1	-22.4		
11	-17.1	-18.1	-9.7	-12.8		
12	-3.8	-8.3	-4.7	-7.7		

Short wave incoming radiation (SWIr) was measured for University Valley for the summer of 2010 by Lacelle *et al.* (2015) collected from an automated Campbell Scientific CR1000 weather station located near the centre of the valley (77°51.729'S; 160°42.606'E; elevation = 1677 m; 42 cm ice table depth). The reported values for mean daily SWIr for the summer season ranged from 61 to 347 W m^{-2} with an average of 208 ± 7 W m^{-2} (226 ± 12 W m^{-2} on clear days only). The results of a correlation analysis by Lacelle *et al.* (2015) between mean daily and monthly SWIr and measured ground surface temperature show a significant positive relation suggesting that solar heating influences summer ground temperatures in the valley. Based on this correlation, potential incoming solar radiation (PISR) was modeled for the summer of 2010 in University Valley. The results indicated that the southeast portion of University Valley received the lowest average summer PISR (values = < 225 W m^{-2}) as most of the valley was shaded throughout the day. PISR increased with distance from the glacier to values reaching 300 W m^{-2} where the mouth of the valley meets Beacon Valley. Based on the PISR map and the ground surface temperature measurements, Lacelle *et al.* (2015) differentiated two zones in University Valley with distinct ground surface temperatures and one transition zone (Figure 7, p.15): i) the perennially cryotic ground zone (PCZ); ii) the seasonally non-cryotic ground zone (NCZ); and iii) the transition zone. The PCZ is distinguished by hourly ground surface temperatures that remain below 0°C throughout the year; in contrast, the NCZ is characterized by ground surface temperatures that rise above 0°C for a minimum of a few hours on clear summer days. The transition area between the two aforementioned zones can include ground surface temperatures characteristic of either zone.

3. Methodologies

3.1. Field sampling

In January 2013, 15 shallow ice-bearing permafrost cores were collected from sand-wedge polygons in University Valley (Figure 9). The cores were collected from nine different polygons along the valley floor at different locations inside each polygon (centres and shoulders; Table 4). Previous studies (e.g. Pollard *et al.*, 2012; Lacelle *et al.*, 2013; 2014) observed high variability in ground ice content within distances as a little as 5 m. As such, the spatial sampling method used was intended to explore potentially changing ground ice conditions within a single polygon and throughout the valley floor. Polygons 5, 7 and 8 are mainly situated in the perennially cryotic zone, whereas polygons 1, 2, 3, 4, 9 and 10 are located in the seasonally non-cryotic zone and Polygon 6 is located in the transition zone between the two categories (Figure 7, p.15). All but two of the polygons are in the undifferentiated drift. Polygons 7 and 8 are in the colluvium derived from a rock fall.

The permafrost cores were collected using an 11.5 cm diameter Cold Regions Research and Engineering Laboratory (CRREL) core barrel equipped with a gas powerhead. Prior to coring, the dry soil layer above the ice-bearing permafrost was removed to prevent the surrounding dry loose mineral soil from infilling the borehole. Each core was retrieved in 10 to 50 cm long segments, wrapped in plastic core sleeves and shipped frozen in thermally insulated boxes to the CryoLab for Arctic, Antarctic and Planetary Studies at the University of Ottawa.

Figure 9: Photo illustrating field sampling of permafrost cores using the CRREL drill in University Valley, McMurdo Dry Valleys of Antarctica (Photo Source: Dr. Denis Lacelle).

Table 4: Details of the permafrost cores collected in University Valley.

Site	Latitude (South)	Longitude (East)	Core ID	Length of core (cm)	Ice table depth (cm)	Distance from glacier (m)	Position in polygon
Polygon 8 (P8)	77.86563	160.72627	13-P8-C3	68	2	304	Centre
			13-P8-C5	73	2	304	Right shoulder
			13-P8-C6	39	2	304	Left shoulder
Polygon 7 (P7)	77.86422	160.72297	13-P7-C1	27	22	466	Centre
Polygon 6 (P6)	77.86341	160.72222	13-P6-C3	100	25	545	Centre
			13-P6-C5	70	20	545	Left shoulder
Polygon 1 (P1)	77.86508	160.70158	13-P1-C1	107	30	860	Centre
			13-P1-C2	102	19	860	Right shoulder
			13-P1-C3	60	28	860	Left shoulder
Polygon 5 (P5)	77.86091	160.71527	13-P5-C1	23	19	866	Centre
Polygon 4 (P4)	77.86233	160.70402	13-P4-C1	15	2	943	Centre
Polygon 2 (P2)	77.8595	160.70936	13-P2-C2	22	20	1076	Deflation surface
Polygon 9 (P9)	77.85408	160.70086	13-P9-C1	20	30	1692	Right shoulder
			13-P9-C2	10	30	1692	Left shoulder
Polygon 10 (P10)	77.85383	160.69633	13-P10-C1	167	16	1771	Right shoulder

3.2. Ground ice content measurements

Ice content in the 15 cores was determined in the Physical Geography Laboratory at the University of Ottawa following CT scanning. The frozen permafrost cores were cut into ca. 2 cm thick slices using a RIGID circular saw with a 0.8 mm thick diamond blade and allowed to thaw in sealed plastic bags. Once thawed, the cores were transferred into graduated 50 ml polypropylene tubes where the sediments settled. The volume of supernatant water (if present) and sediments were then recorded and the polypropylene tubes were weighed. The supernatant water was extracted and filtered (0.45 μm pore diameter filter) into 20 ml vials for geochemical and isotopic analysis (not included in this thesis). The 50 ml tubes with the remaining sediment were placed into an oven at 105°C for 24 hours to dry and the weight of the dried sediment was subsequently recorded.

Excess ice (defined as the volume of ice in the ground exceeding the total pore volume that the ground would have under natural unfrozen conditions; van Everdingen, 1988) was calculated using eq. [1] from Kokelj and Burn (2003):

$$[1]\ Excess\ ice\ (\%) = \frac{volume\ supernatant\ water\ x\ 1.09}{volume\ supernatant\ water\ x\ 1.09 + volume\ sediments}\ x\ 100$$

The number 1.09 is employed to convert the measured volume of supernatant water to the equivalent volume of ice (9% volumetric expansion of water to ice). The measurements are within 1 ml precision, which results in ± 1% error in the reported values.

The gravimetric water content was subsequently determined from the weight of the wet and dry sample using eq. [2] from van Everdingen (1988):

$$[2]\ Gravimetric\ water\ content\ (\%) = \frac{weight\ water}{weight\ dry\ sample}\ x\ 100$$

Additional material properties, such as porosity and volumetric ice content, were calculated based on eq. [1] and [2]. The porosity (*θ*) for the sediments was calculated from the measured mass of water and divided by the volume of sediments.

The total volume of water was subsequently estimated using the calculated sediment porosity for each sample and eq. [3]

$$[3]\ Volume\ water\ (ml) = volume\ supernatant\ water + volume\ of\ sediment\ x\ porosity$$

The volumetric ice content in the sample was determined by modifying the equation for volumetric water content from Pollard and French (1980) to incorporate the 9% volumetric expansion of water to ice using eq. [4]:

$$[4]\ Volumetric\ ice\ content\ (\%) = \frac{(volume\ water)\ x\ 1.09}{volume\ of\ sediments + (volume\ water\ x\ 1.09)} * 100$$

Based on the calculated volumetric ice content, five cryofacies were described following the classification of Murton and French (1994) (Table 5). The mean porosity of 0.42, typical of sediment in University Valley (e.g. Lacelle *et al.*, 2013), may result in high volumetric ice contents (> 25%) without the presence of excess ice in the sample.

Table 5: Cryofacies identified from fieldwork in the Tuktoyaktuk coastlands (NWT). Source: Murton and French (1994).

Cryofacies type	Volumetric ice content (%)	Cryofacies	Code
Pure ice	100	Pure ice	I
Sediment-poor ice	> 75	Sand-poor ice	SPI
		Aggregate-poor ice	API
Sediment-rich ice	> 50 to ≤75	Sand-rich ice	SRI
		Aggregate-rich ice	ARI
Ice-rich sediment	> 25 to ≤50	Ice-rich sand	IRS
		Ice-rich mud	IRM
		Ice-rich diamicton	IRD
Ice-poor sediment	≤ 25	Ice-poor mud	IPM
		Ice-poor sand	IPS
		Ice-poor gravel	IPG
		Ice-poor diamicton	IPD
		Ice-poor peat	IPP

3.3. Cryostructures and ground ice content using computed tomodensitometric (CT) scanning

CT scanning was performed on select ice-bearing permafrost cores (P1-C1, P2-C2, P6-C5, P7-C1, P8-C3 and P8-C6) to investigate cryostructures and derive their respective volumetric ice content (CTVIC). CT scanning is a non-destructive method that has been employed in Arctic permafrost studies over the past decade (e.g. Calmels and Allard, 2004; 2008; Calmels *et al.*, 2008). The principles of CT scanning draw similarities to those of radiography as the two produce 3D images of density contrasts for a given sample. However, the density contrast in CT scanned images is greatly superior to that of X-Ray radiography. Additionally, the sedimentary structures of the core can be visualized in 3D from each spatial direction instead of using predefined visualization plans (Calmels and Allard, 2004). The non-destructive technique is particularly useful for the analysis of permafrost cores as the samples can subsequently be used for further sedimentological, geotechnical and geochemical analyses (Calmels *et al.*, 2010). The density measurements for CT scanning are made relative to water and expressed in Hounsfield Units (HU): water thus has a value of 0 HU. Density threshold values for ice, air and sediment can be estimated through the analysis of the histograms associated with CT scanned image stacks. For example, ice has values between ca. -250 and 750 HU, air has values near -1000 HU and sediments have values > 750 HU (e.g. Calmels *et al.*, 2010). The large difference in densities between ice, sediments and gases allows the identification of the distribution and shape of these components, and thus, the classification of cryostructures. Further processing of the CT scans using image analysis software (e.g. Osirix, ImageJ and Fiji) permits the estimation of volumetric ice content (e.g. Calmels *et al.*, 2010).

The CT scanning for the full P2-C2, P6-C5, P7-C1 and P8-C6 cores and sections of the P1-C1 and P8-C3 cores was performed using a medical scanner (Siemens Somaton Volume Access) at the Institut National de la Recherche Scientifique (Québec, Canada). The permafrost cores were placed on a bench in the centre of a ring containing the X-Ray source. The X-Ray source rotated around the core as the core moved down the ring resulting in an image produced through a helical movement. Once completed, the core was rotated 90° and the process was repeated. When combined, the images represented a two-section view with a 3D perception (e.g. Calmels and Allard, 2004; 2008) of the cores. The scanned image stacks, with a pixel resolution of 0.4 mm, were saved in DICOM format and analyzed using Fiji image analysis software (http://fiji.sc/Fiji). The resulting greyscale images used darker tones to indicate lower density materials (i.e. gas and ice) and lighter tones to indicate higher density material. The image stacks were subsequently processed to classify the ice component in the cores following the instructions of the GeoCryolab at the Université de Montréal. Image processing and analyses aimed at determining the ice shape and estimating its content are dependent on the threshold used to define ice in an image stack. Consequently, four ice thresholds were tested after analyzing the peaks in the image stacks' histograms: -200 to 700 HU, - 200 to 750 HU, -250 to 700 HU and -250 to 750 HU. The four tested thresholds yielded similar ice content results with ca. 4% difference for various parameters (Table 6). Therefore, the threshold that produced the highest ice content and closest values to the measured volumetric ice content (-250 to 750 HU) was used to convert the CT-scanned greyscale image stack into binary images representative of only the ice content (black represents ice while white represents all other components). CTVIC was derived from each slice (0.4 mm) of the stack of binary images using the *Z-axis Plot* function. The full description of the image analysis in Fiji is provided in Appendix 1.

The orthogonal views of the processed binary images were subsequently used to describe the cryostructures in the permafrost cores applying the classification of Murton and French (1994): structureless, suspended, layered, lenticular, crustal and reticulate (Figure 10). Cryostructures have previously been described at the centimeter scale (e.g. Shur *et al.*, 2004; Cold Regions Research and Engineering Laboratory, 2012) and at the meter scale (e.g. Murton and French, 1994). Structureless cryostructures form from pore water freezing in situ around mineral grains and thus are not visible to the naked eye and lack a structure. Lenticular cryostructures are lens-shaped bodies with horizontal or vertical inclinations (Murton and French, 1994). The orientation of lenticular cryostructures is a reflection of the direction of the freezing fronts and/or the sediment's mechanical properties and soil density (Smith and Williams, 1990). Layered cryostructures are continuous parallel bands of sediment and/or ice (Kudriavtsec, 1978; Popov *et al.*, 1985). The vertical or sub-vertical layering is formed by the infilling of thermal contraction and dilation cracks with either ice, clastic sediment, and/or organic material (Mackay, 1985); comparatively, horizontal or gently dipping layers are formed through segregated and intrusive ice, as well as buried glacier ice bodies (Murton and French, 1994). A reticulate cryostructure has a three-dimensional, net-like structure of ice veins that surround fine-grained sediment blocks (Mackay, 1974) and is divided into a regular or irregular type. Mackay (1974) hypothesized that reticulate structures (regular or irregular) form in a semi-closed freezing system through cracks in-filling with water or ice from surrounding muddy blocks. Reticulate cryostructures may represent the shrinkage and loss of water within sediment as moisture migrates to the advancing freezing front. A rim of ice surrounding a rock clast, or an ice crust, is termed a crustal cryostructure and is commonly found immediately below the permafrost table (Murton and French, 1994). Its formation is likely due to localized ice segregation surrounding clasts that are frost-susceptible in nature (Mackay, 1984). Aggregates, rock clasts and grains of variable size suspended in ice are termed a suspended cryostructure and are typical of massive ice bodies and commonly seen immediately below the permafrost table (Mackay, 1972; Cheng, 1983).

Many other cryostructural classifications existed, primarily from Russian literature, prior to the development of Murton and French's (1994) classification (e.g. Pihlainen and Johnston, 1963; Linell and Kaplar, 1966; Katasonov, 1969; Kudriavtsev, 1978; Popov *et al.,* 1985). Previous classifications were considered unsatisfactory, as some were complex and unwieldy. Moreover, classifications were applied to permafrost generally containing little excess ice, resulting in a description of ice distribution within sediment and neglecting to classify sediment within ice. Murton and French's (1994) classification, however, incorporates all ranges of ice contents within permafrost, ensuring a simple application.

Table 6: Descriptive statistics for volumetric ice content (CTVIC) in six permafrost cores derived from CT-scanned images and Fiji image analysis software.

Threshold	Mean	Median	Range	Min	Max
P1-C1					
-200 to 700	9.36	11.27	21.82	0.16	21.97
-200 to 750	11.16	14.03	25.26	0.00	25.26
-250 to 700	9.33	11.29	21.81	0.00	21.82
-250 to 750	11.58	14.04	25.22	0.27	25.49
P2-C2					
-200 to 700	0.85	0.63	3.84	0.05	3.89
-200 to 750	1.16	0.75	5.49	0.06	5.55
-250 to 700	0.72	0.37	4.06	0.06	4.11
-250 to 750	1.04	0.56	5.18	0.04	5.22
P6-C5					
-200 to 700	24.77	25.11	51.35	0.77	52.12
-200 to 750	27.02	27.58	54.46	0.80	55.26
-250 to 700	24.89	25.20	51.84	0.77	52.62
-250 to 750	27.35	27.85	55.13	0.99	56.13
P7-C1					
-200 to 700	2.98	2.66	4.74	1.02	5.76
-200 to 750	3.54	3.48	4.50	1.93	6.43
-250 to 700	2.88	2.75	3.87	1.56	5.43
-250 to 750	3.58	3.51	4.51	1.95	6.46
P8-C3					
-200 to 700	27.72	20.49	68.82	3.16	71.97
-200 to 750	29.94	23.96	67.71	4.41	72.12
-250 to 700	28.85	21.26	69.06	2.85	71.91
-250 to 750	30.42	23.92	68.99	4.24	73.23
P8-C6					
-200 to 700	1.69	1.06	5.92	0.29	6.21
-200 to 750	2.14	1.44	6.53	0.65	7.18
-250 to 700	1.65	1.06	5.86	0.41	6.27
-250 to 750	2.09	1.27	6.85	0.49	7.34

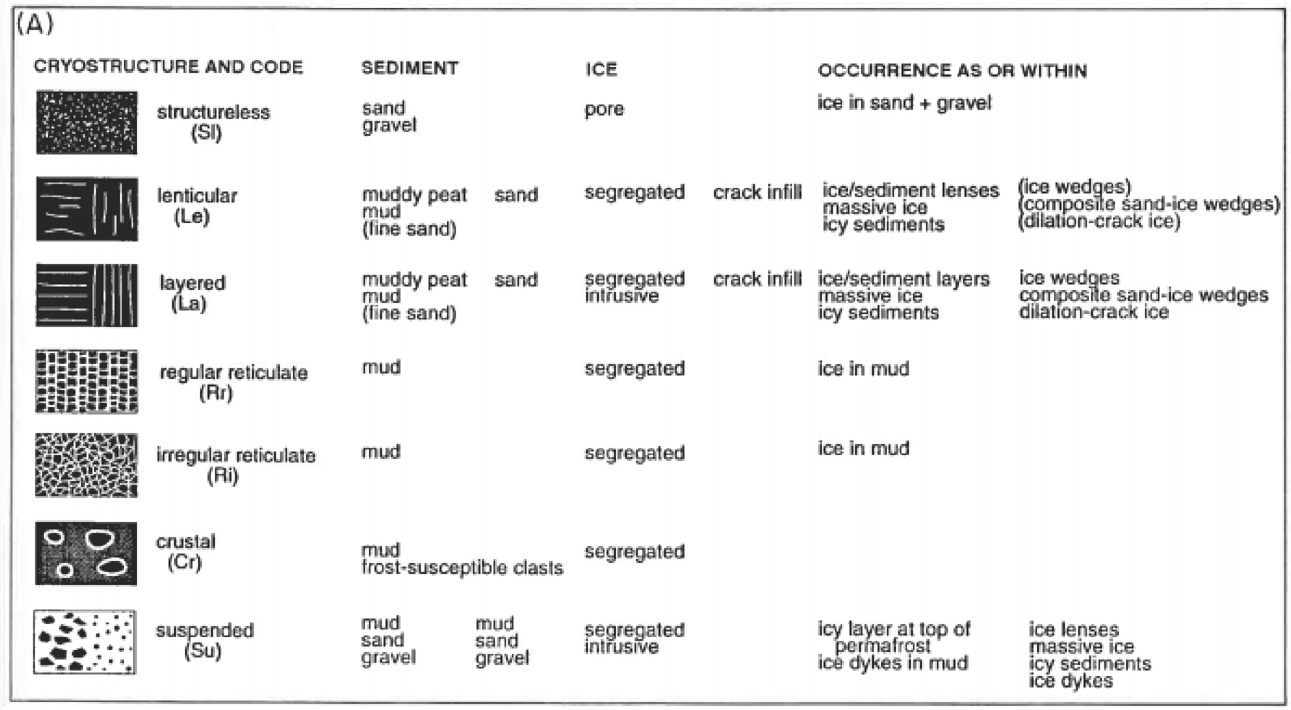

Figure 10: Murton and French's (1994) cryostructural classification where ice is represented in white and sediment in grey or black.

3.4. Grain size analysis

Soils have been used to increase the understanding of both the paleoclimate and glacial history in the MDV, specifically through the identification of the spatial extent of drift sheets (Bockheim and McLeod, 2006). Soil forming processes occurring in the soils of the Transantarctic Mountains include: i) rubification (the slow reddening of soil as a result of hematite formation); ii) salinization (the accumulation of soluble salts in the soil column); iii) the development of desert pavement (Bockheim, 1990); and iv) the sublimation of interstitial ice resulting in the conversion of ice-cemented permafrost into dry permafrost and rubification (Bockheim, 2015). Rubification is observed in cold desert soils through the increase in depth of profile staining and the colour development of the horizon underlying the desert pavement over time. Salinization is an indicator of soil age as the depth to which salts are found increases with time; additionally, salt form is altered as soil age increases. Desert pavement is more defined on older landscapes (Bockheim, 1982; Bockheim, 1990) as seen through more rounded clasts and larger quantities of desert varnish and ventifacts on older surfaces. The proportion of silt may also increase with depth with increasing soil age due to weathering (Bockheim, 1990).

Soils found in the MDV are largely in the Gelisol order (Bockheim, 2002; Bockheim and McLeod, 2006). Soils containing ice-cemented permafrost within the uppermost 70 cm of the surface are typically cryoturbated and classified in the Turbel suborder. While, soils in dry permafrost and with little cryoturbation are classified as Orthels. Anhydrous soil conditions typically receive < 30 mm year^{-1} water equivalent precipitation and are associated with dry permafrost (Bockheim and McLeod, 2015).

Soil texture partly influences the hydraulic conductivity of frozen soils through the dependence of unfrozen water content on particle size, pore size distribution, void ratio and surface area (Burt and Williams, 1976). Many studies have documented a positive association between near-surface ground ice content and silt content (e.g. Kokelj and Burn, 2005; Morse *et al.*, 2009; O'Neil and Burn, 2012). This relation is due to the higher hydraulic conductivity below 0°C and frost-susceptibility of silts compared to that of clays and sands (O'Neil and Burn, 2012). Consequently, potential relations between ground ice conditions, soil colour and particle size distribution of the sediments in the University Valley cores were investigated at ca. 10 cm depth intervals. The dry colour of the samples was determined using a Munsell chart and the grain size distribution of the sediments was determined using the stacked sieve method. The stacked sieve method was employed instead of laser particle size analysis because the sampled sediments are predominantly sand-sized. For each analysis, ca. 15 g to 250 g of sediment was passed through seven stainless steel stacked sieves (2 mm, 1 mm, 0.5 mm, 0.25 mm, 0.125 mm, 0.0625 mm and < 0.0625 mm). The dominant grain size class was determined using the Wentworth grain size classification where silt is < 0.0625 mm, very find sand is ≥ 0.0625 mm and < 0.125 mm, fine sand is ≥ 0.125 mm and < 0.25 mm, medium sand is ≥ 0.25 mm and < 0.5 mm, coarse sand is ≥ 0.5 mm and < 1 mm, very coarse sand is ≥ 1 mm and < 2 mm and gravel is ≥ 2 mm. Grain size distribution graphs were made by classifying the sediments into three soil sizes: gravel (≥ 2 mm), sand (< 2 mm to ≥ 0.0625 mm) and fine sediments (< 0.0625 mm). Errors in the calculation of the grain size distribution for the samples arose through the occasional retention of a small amount of the sample in the sieve mesh and through scale measurements errors. Overall, the error in the reported values for the total particle size distribution for a few samples is estimated to be ± 4%.

3.5. Statistical analysis

The Shapiro-Wilk test for normality was performed on the ground ice content data (gravimetric water and excess ice content) for all the cores. The test statistic *W* was calculated in R statistical analysis software (https://www.r-project.org/) using eq. [5] (e.g. Acevedo, 2013):

$$[5]\ W = \frac{(\sum_{i=1}^{n} a_i x_{(i)})^2}{\sum_{j=1}^{n}(x_i - \bar{x})^2}$$

where $x_{(i)}$ is the *i*th ordered statistic. The constants are a_i, calculated from variances, means and covariances of the *i*th order statistics.

The Spatial Autocorrelation (Global Moran's *I*) tool was used from the Spatial Statistics Tools in ArcGIS10 to determine if the mean VIC, GWC and excess ice content from the different cores were spatially autocorrelated or independent. The complete results for this test are provided in Appendix 2. Moran's *I* is calculated using eq. [6] (e.g. O'Sullivan and Unwin, 2003):

$$[6]\ I = \frac{n}{\sum_{i=1}^{n}(y_i - \bar{y})^2} \frac{\sum_{i=1}^{n}\sum_{j=1}^{n} w_{ij}(y_i - \bar{y})(y_i - \bar{y})}{\sum_{i=1}^{n}\sum_{j=1}^{n} w_{ij}}$$

where the subscripts *i* and *j* are different zones or areal units in the study and *y* is the data value in each; $\bar{y}$ is the overall mean, w_{ij} is an element from a weights matrix *W*. For example, $w_{ij} = 1$ if the zone *i* and *j* are adjacent and will otherwise equal 0. The core locations and mean VIC, excess ice content and GWC values were the input parameters used simultaneously to measure spatial autocorrelation. The inverse distance method was used to conceptualize the spatial relationships and the Euclidean distance method was used to calculate the distance from each feature to its neighbouring features as per the default for the tool.

The results of the Shapiro-Wilk test for normality on the mean excess ice content and GWC of the top 20 cm, 50 cm and 1 m of ice bearing permafrost indicated that 26 of 48 of the samples were normally distributed (Appendix 3A; 3B). Consequently, the Mann-Whitney *U* test was performed on the median ice content between the core samples (e.g. Kokelj *et al.*, 2013). If the result of the test was significant, it was concluded that there was a high likelihood that the samples were representative of populations taken from different median values. The assumption of homogeneity of variance between the populations of the underlying samples is commonly unacknowledged for this test. Further, it has been stated that the test is justified in place of the *t*-

test for two independent variables when the assumption of homogeneity of variance is violated in the data as the test may not be as affected by the lack of homogeneity of variance as the *t*-test (Sheskin, 2011). The test was computed using RStudio (v. 0.98.1103; https://www.r-project.org/) statistical analysis software. The complete results of the Mann-Whitney *U* test are provided in Appendix 4. The function ranked the subjects of both samples and the sums of the ranks for each of the groups (ΣR_1 , ΣR_2) were computed employing equations [7A] and [7B] (e.g. Sheskin, 2011):

$$[7A]\ U_1 = n_1 n_2 + \frac{n_1+(n_1+1)}{2} - \sum R_1$$

$$[7B]\ U_2 = n_1 n_2 + \frac{n_2+(n_2+1)}{2} - \sum R_2$$

The Kolomogrov-Smirnov (K-S) test for two independent samples was also performed on the permafrost core samples. The K-S test is a non-parametric alternative to the t-test involving the comparison of two cumulative frequency distributions. The K-S test is commonly employed when there is a lack of normality within the data, hence violating one of the assumptions of the t-test (Sheskin, 2011). The equation of the statistic for the K-S test was employed using eq. [8] (e.g. Acevedo, 2013):

$$[8]\ T = \max_{x} |F_1(x) - F_2(x)|$$

where F_1 (x) is the empirical cumulative distribution function (ecdf) of sample 1, F_2 (x) is the ecdf of sample 2, the bars represent absolute value and max is the maximum. The resulting test statistic is the largest departure between the two ecdf for the two samples. The complete results of the K-S test are provided in Appendix 5.

An analysis of variance was then performed on the GWC and excess ice content values for each core and their respective depths to assess the signal-to-noise ratio of the trends with depth. The results of the analysis of variance provide an estimated signal-to-noise variance ratio *F* by using eq. [9] (e.g. Reeh and Fisher, 1983; Fisher *et al.,* 1985):

$$[9]\ F = \frac{r_{xy}}{(1-r_{xy})}$$

where r_{xy} is the correlation coefficient between the GWC or excess ice content values and the depth values. The term noise is employed to the remaining uncorrelated parts between the ice content values and depth (i.e. Fisher *et al.*, 1985; Lacelle *et al*., 2014).

4. Results

4.1. Description of polygons in University Valley

4.1.1. Polygon morphology and age

Sand wedge polygonal terrain is pervasive along the floor of University Valley and occupies some of the talus cones. Observation of the Nextview satellite Imagery of University Valley (source: DigitalGlobe, Inc.) supported the previous findings of Mellon *et al.* (2014) and found that polygon size is variable in University Valley with the largest polygons located near the mouth of the valley and the smallest found in closer proximity to University Glacier (Table 7; Figure 11A, C and E). Although size variations exist among the polygons, their morphology is fairly homogenous with flat centres, raised shoulders and shallow troughs (on the order of 5 – 10 cm deep and 20 – 40 cm wide) (Figure 11B, D, F). The trough intersections are mainly triple junctions with a strong unimodal preference for equiangular junctions (Mellon *et al*., 2014).

The results of 14 optically stimulated luminescence ages for the sediments taken from two polygons discussed in this thesis (P1 and P8; Trinh-Le, unpublished data) and an additional polygon in University Valley (P12; Lacelle *et al.*, 2013) indicated deposition ages between 79.5 and 192.4 ka years for the sediments between 20 and 95 cm depth. The results for the sediments in the top 20 cm provided younger ages of < 102.2 ka years.

Table 7: Size of investigated polygons and the down-valley distance of the polygon from University Glacier. Distance is calculated from the "Glacier Core" point on University Glacier indicated in Figure 7.

Polygon ID	Core ID	Distance from glacier (m)	Polygon size (m)
Polygon 8	13-P8-C3	304	13 x 8
	13-P8-C5	304	13 x 8
	13-P8-C6	304	13 x 8
Polygon 7	13-P7-C1	466	18 x 17
Polygon 6	13-P6-C3	545	11 x 21
	13-P6-C5	545	11 x 21
Polygon 1	13-P1-C1	860	9 x 20
	13-P1-C2	860	9 x 20
	13-P1-C3	860	9 x 20
Polygon 5	13-P5-C1	866	23 x 20
Polygon 4	13-P4-C1	943	14 x 15
Polygon 2	13-P2-C2	1076	18 x 27
Polygon 9	13-P9-C1	1692	28 x 17
	13-P9-C2	1692	28 x 17
Polygon 10	13-P10-C1	1771	48 x 21

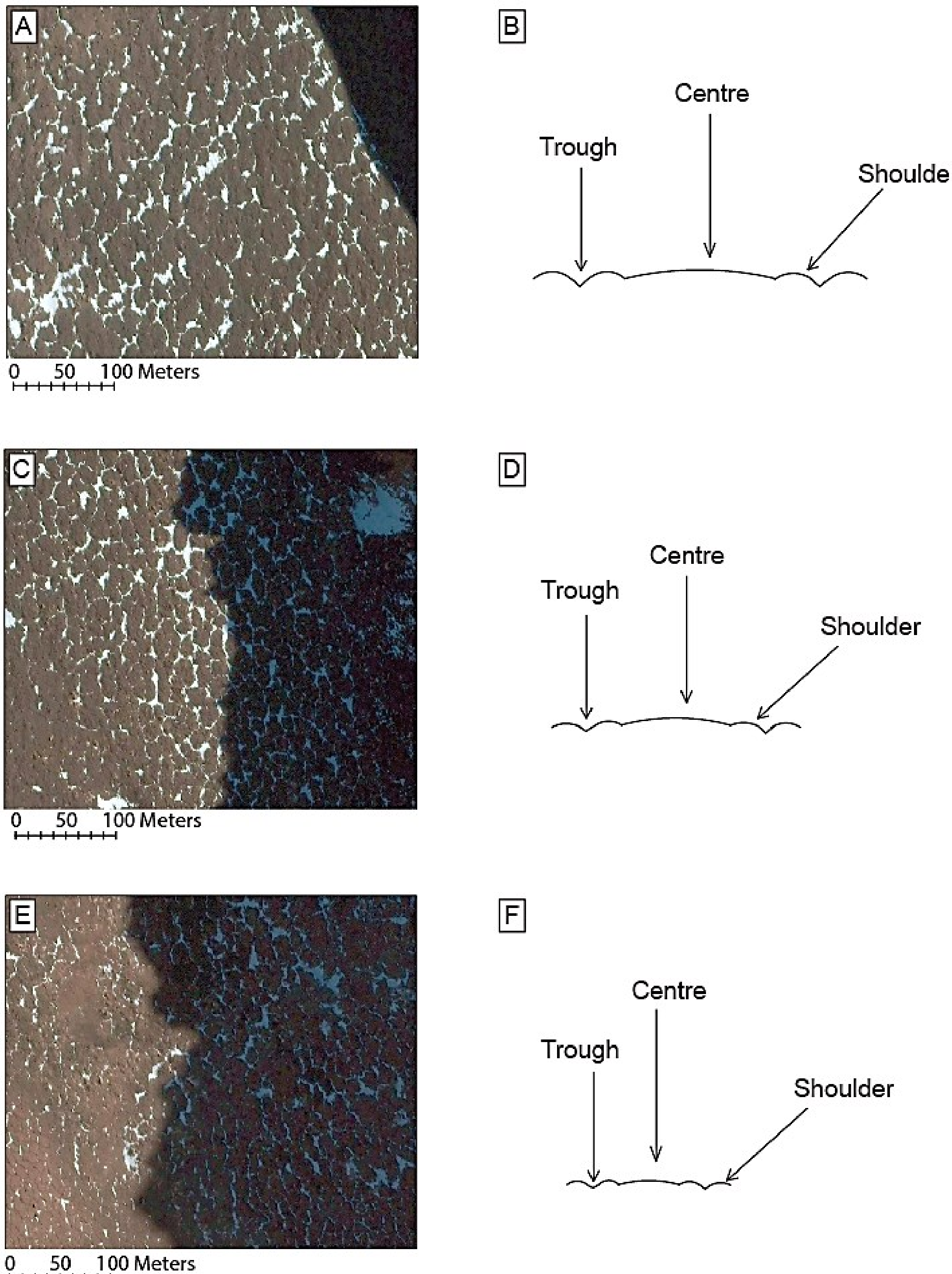

Figure 11: Polygon size in A) lower, C) middle and E) upper University Valley. Morphology of polygons located B) down valley, D) mid-valley and F) up-valley.

4.1.2. Soil texture and colour

The dry sediments in upper and middle University Valley were mainly pale to light brown (10YR 6/3, 7.5YR 6/4, 10YR 7/3); whereas, pale to light yellowish-brown sediments (2.5Y 7/3 and 2.5Y 6/4) were observed in lower University Valley. Table 8 includes the full description of the dry sediment colour of the analyzed cores organized in order of increasing distance from University Glacier.

Table 8: The dry colour of sediments in the cores taken from University Valley.

Core ID	Depth in core (cm)	Colour	Munsell hue, value and chroma
P8-C3	Full core	Pale brown	10YR 6/3
P8-C5	Full core	Pale brown	10YR 6/3
P8-C6	Full core	Pale brown	10YR 6/3
P7-C1	Full core	Pale brown	10YR 6/3
P6-C3	Full core	Pale brown	10YR 6/3
P6-C5	Full core	Light reddish brown	5YR 6/3
P1-C1	Full core	Pale brown	10YR 6/3
P1-C2	Full core	Pale brown	10YR 6/4
P1-C3	Full core	Pale brown	10YR 6/5
P5-C1	Full core	Pale brown	10YR 6/3
P4-C1	0 - 7 cm depth	Pale brown	10YR 6/2
	7 - 15 cm depth	Very pale brown	10YR 7/3
P2-C2	Full core	Light brown	7.5YR 6/4
P9-C1	Full core	Light yellowish brown	2.5Y 6/4
P9-C2	Full core	Light yellowish brown	2.5Y 6/4
P10-C1	70 – 140 cm depth	Pale yellow	2.5Y 7/3
	140 – 180 cm depth	Light yellowish brown	2.5Y 6/4

Soil texture analysis results from the different polygons are presented using the Wentworth grain size classification where: silt is < 0.0625 mm, very find sand is ≥ 0.0625 mm and < 0.125 mm, fine sand is ≥ 0.125 mm and < 0.25 mm, medium sand is ≥ 0.25 mm and < 0.5 mm, coarse sand is ≥ 0.5 mm and < 1 mm, very coarse sand is ≥ 1 mm and < 2 mm and gravel is ≥ 2 mm.

The soil texture class of the up-valley polygons (Polygon 7 (P7) and Polygon 8 (P8)) consisted of medium-sand. However, gravel-sized particles dominated the lower section (ca. 67 cm depth) of the left shoulder (P8-C6) of P8. In P8, sand-sized particle distribution ranged between 47 and 92% in the centre (P8-C3), between 91 and 96% in the right shoulder (P8-C5), and between 67 and 97% in the left shoulder (P8-C6). Gravel-sized particles ranged between 4 and 52%, between 0.5 and 5% and between 1 and 20% in the centre, right shoulder and left shoulder of P8, respectively. Fine-grained particles occupied < 4.5% of the three cores taken from P8 (Figures 12A, B and C). The sand-sized particles in the centre of P7 (P7-C1) ranged between 76 and 87% throughout the core while gravel-sized particles ranged between 10 and 21%. Fine-grained particles occupied < 2.6% of P7-C1 (Figure 12D).

The grain size class in two of the mid-valley polygons (Polygon 6 (P6) and Polygon 1 (P1)) consisted of medium sand. Although medium sand was mainly found throughout both cores in P6, coarse sand was the dominant grain size class at ca. 86 to 89 cm depth in the left shoulder (P6-C5). Sand-sized particle distribution was higher in the centre (P6-C3) than in the left shoulder of the polygon, ranging between 93 and 97% and between 74 and 94%, respectively. The left shoulder of the P6 contained more gravel-sized particles (ranging between 3 and 24%) than the centre (ranging between 0.75 to 5%). Fine-grained particles occupied < 4% of P6's cores (Figures 12E and F). The fraction of sand-sized particles ranged between 77 and 97% in the centre (P1-C1), between 81 and 92% in right shoulder (P1-C2) and between 86 and 99% in the left shoulder (P1-C3) of P1. Gravel-sized particles ranged between 0.3 and 19% in P1-C1, 1 and 6% in P1-C2 and 1.5 and 9% in P1-C3. Fine-grained sized particles occupied < 8%, < 3% and < 2.5% in cores P1-C1, P1-C2 and P1-C3, respectively (Figures 12G, H and I).

The dominant grain size class of the sediments in the remaining two mid-valley polygons (Polygon 5 (P5) and Polygon 4 (P4)) varied with depth. The dominant grain size class in the centre of P5 (P5-C1) varied from medium sand at ca. 19 to 27 cm depth to gravel from ca. 30 to 41 cm depth. As such, soil textures > 2 mm were the predominant grain size for the core. Sand-sized particles ranged between 16 to 95% and gravel-sized particles ranged between 1 and 82%. Fine-grained particles occupied < 4% of P5-C1 (Figure 12J). In the core taken from the centre of P4 (P4-C1), the gravel-sized grain class occupied the uppermost 7 cm of the core and transitioned to the very fine sand grain size class in the lower section (ca. 7 to 15 cm depth). Although the predominant grain size class varied with depth, the distribution of all sand-sized soil textures combined (ranging between 71 to 85% throughout the core) was much greater than the distribution of gravel-sized particles (ranging between 13 and 26%). Fine grained particles occupied < 2.5% of P4-C1 (Figure 12K).

The sediments in one of the down-valley polygons (Polygon 2 (P2)) consisted of the medium sand grain size class. The distribution of sand-sized particle ranged between 82 and 92% and gravel-sized particles comprised between 6 and 14% of the core taken from a deflation surface on the polygon (P2-C2). Fine-grained sediments occupied < 5% of the sediments in P2-C2 (Figure 12L).

The soil texture of the remaining two down-valley polygons (Polygon 9 (P9) and Polygon 10 (P10)) was somewhat variable with depth. Gravel was the dominant grain-size in the left shoulder of P9 (P9-C2). The dominant grain-size class in the right shoulder of P9 (P9-C1) was medium-sand in the uppermost 30 cm and gravel in the lower sections of the core. Sand-sized particles ranged between 42 and 76% and between 58 and 67% in P9-C1 and P9-C2, respectively. Gravel-sized particles ranged between 24 and 39% in the right shoulder and between 29 and 40% in the left shoulder of P9. Fine-grained particles occupied < 4% of both cores taken from P9 (Figures 12M and N). Grain size analyses for the right shoulder of P10 (P10-C1) were only performed for the core segment between ca. 70 and 178 cm depth as the uppermost section of the core did not contain enough remaining sediment to undergo analysis (sediment-rich ice cryofacies). Medium-sand was the dominant grain size class throughout the majority of P10-C1; however, some variation in the dominant grain-size class was observed at specific depths. For example, gravel-sized particles were the dominant grain size class between ca. 70 to 72 cm depth; the soil texture was predominantly of the fine-sand grain size class between ca. 98 to 100 cm and ca. 168 and 171 cm depth; and, the coarse-sand grain size class had the highest percent distribution between ca. 178 and 180 cm depth. Sand-sized particle distribution ranged between 68 and 113% while gravel-sized particles ranged between 3 and 28% throughout the right shoulder of P10. Fine-grained particles occupied < 7.5% of P10-C1 (Figure 12O).

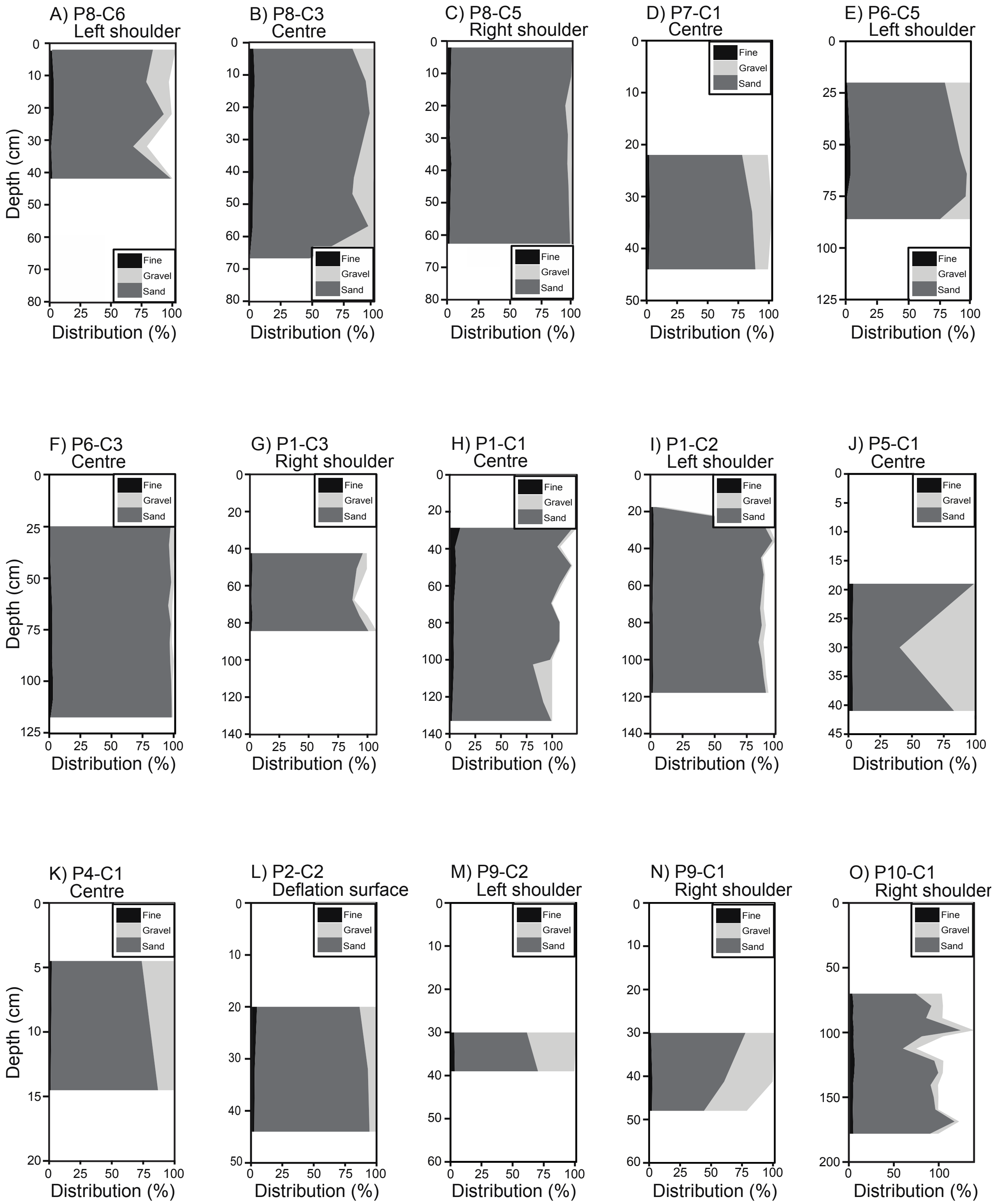

Figure 12: Particle size distribution (%) of the fine (< 0.0625 mm), sand (≥ 0.0625 mm to < 2 mm) and gravel (≥ 2 mm) sized particles in the cores taken from University Valley. Figures are arranged at increasing distance from University Glacier.

4.1.3. Summary

The mineral soils in in University Valley are classified predominantly as medium sand. In each polygon, little changes in grain size distribution were observed with depth. However, the gravel-size content increased down-valley for both the centres and shoulders of polygons (Figure 13). The increase in gravel content was significant for the shoulders of the polygons only (Table 9).

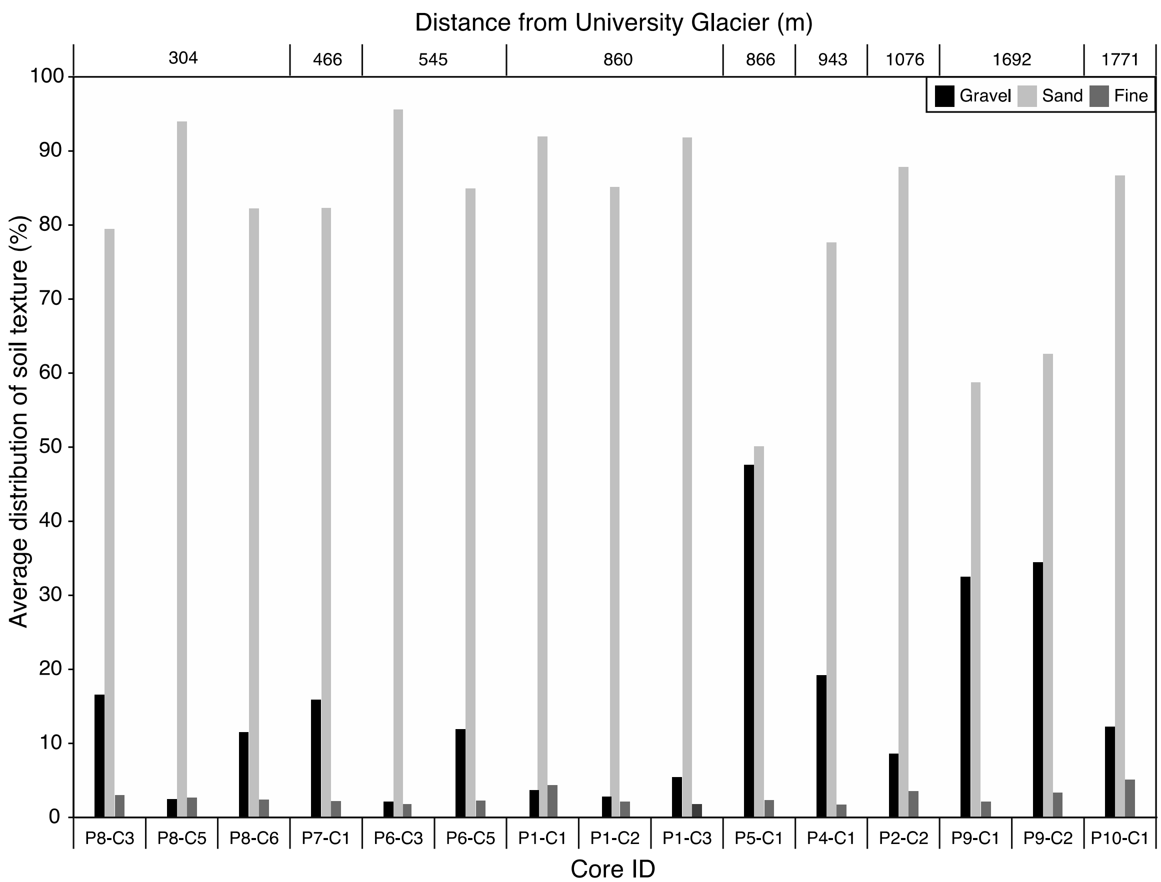

Figure 13: Average distribution of soil texture (%) for the 15 permafrost cores analyzed in University Valley arranged at increasing distance from University Glacier. Distances from University Glacier are calculated from the "Glacier core" point indicated on Figure 7.

Table 9: Regression coefficients between the down-valley distance from University Glacier and mean gravel content, sand content and fine content for all cores, the shoulders and centres of polygons in University Valley. Values significant at a 95 per cent level are bolded.

	Slope	Intercept	r^2	p-value
All				
Gravel content	0.0118	5.4529	0.1973	0.1114
Sand content	-0.0121	90.6455	0.2080	0.1011
Fine content	0.0008	1.9701	0.1725	0.1396
Shoulders				
Gravel content	0.0141	0.0215	0.4977	**0.0505**
Sand content	-0.0136	94.3944	0.4289	0.0779
Fine content	0.0009	1.8188	0.2938	0.1651
Centres				
Gravel content	0.0186	5.1673	0.0879	0.5682
Sand content	-0.0190	92.1103	0.0953	0.5515
Fine content	0.0001	2.4298	0.0023	0.9274

4.2. Ground ice content and cryofacies in University Valley

The results for ground ice content and cryofacies for the investigated polygons in University Valley are presented at increasing distance from University Glacier. The distance from University Glacier was calculated from the “Glacier core” point indicated in Figure 7. The descriptive statistics for these results are representative of the full sampled permafrost core unless otherwise stated.

4.2.1. Polygon 8

Polygon 8 is situated in the PCZ at 304 m from University Glacier within the colluvial rock fall deposit. In the left shoulder of P8 (core P8-C6; 39 cm core length), average excess ice content was 0.5 ± 1% and was only present below 30 cm depth where it ranged between 1 and 3%. Both the gravimetric water content (GWC) and the volumetric ice content (VIC) did not follow the same concentration pattern as excess ice until ca. 34 cm depth. The average GWC was 20 ± 4% resulting in a lower average than that of VIC (34 ± 3%). GWC ranged between 13 and 25% while VIC ranged from 28 to 38% (Figure 14A).

The average GWC (82 ± 52%) was much higher in the centre of P8 (P8-C3; 68 cm core length) than in the right and left shoulders ranging between 18% at 3 cm depth and 193% at 57 cm depth. Two distinct peaks in GWC were apparent with depth: the first was narrow and present in the upper part of the core (between 5 and 10 cm depth) with the maximum value of 57% observed at 5 cm depth; the second peak was broader and present between ca. 40 and 60 cm depth with the highest values > 65% and reaching a maximum of 193%. Average excess ice content was 36 ± 21%, ranging between 3 and 66% and followed a similar concentration pattern to that of GWC, albeit with lower values. The variations in VIC were similar to excess ice; however, values were higher and ranged from 35% to 69% with an average of 53 ± 11%. The VIC and excess ice content values at 57 cm depth are missing as a result of an error in volume calculation during laboratory analysis (Figure 14B).

The average GWC in the right shoulder of P8 (P8-C5; 73 cm core length) was 34 ± 10% ranging between 17% at ca. 4 cm depth and 53% at ca. 45 cm depth. GWC increased from ca. 17 to 32% in the upper section of the core between ca. 16 and 31 cm depth. A broad increase in GWC was observed between 31 and 49 cm depth with a maximum value of 53%. The distribution of excess ice within P8-C5 closely followed that of GWC; however, average excess ice content was 13 ± 6% resulting in lower excess ice content values than GWC throughout the core. VIC showed similar variations with depth to both GWC and excess ice content; however, the average VIC (42 ± 4% ranging between 34 and 48%) for the core was higher than both GWC and excess ice content (Figure 14C).

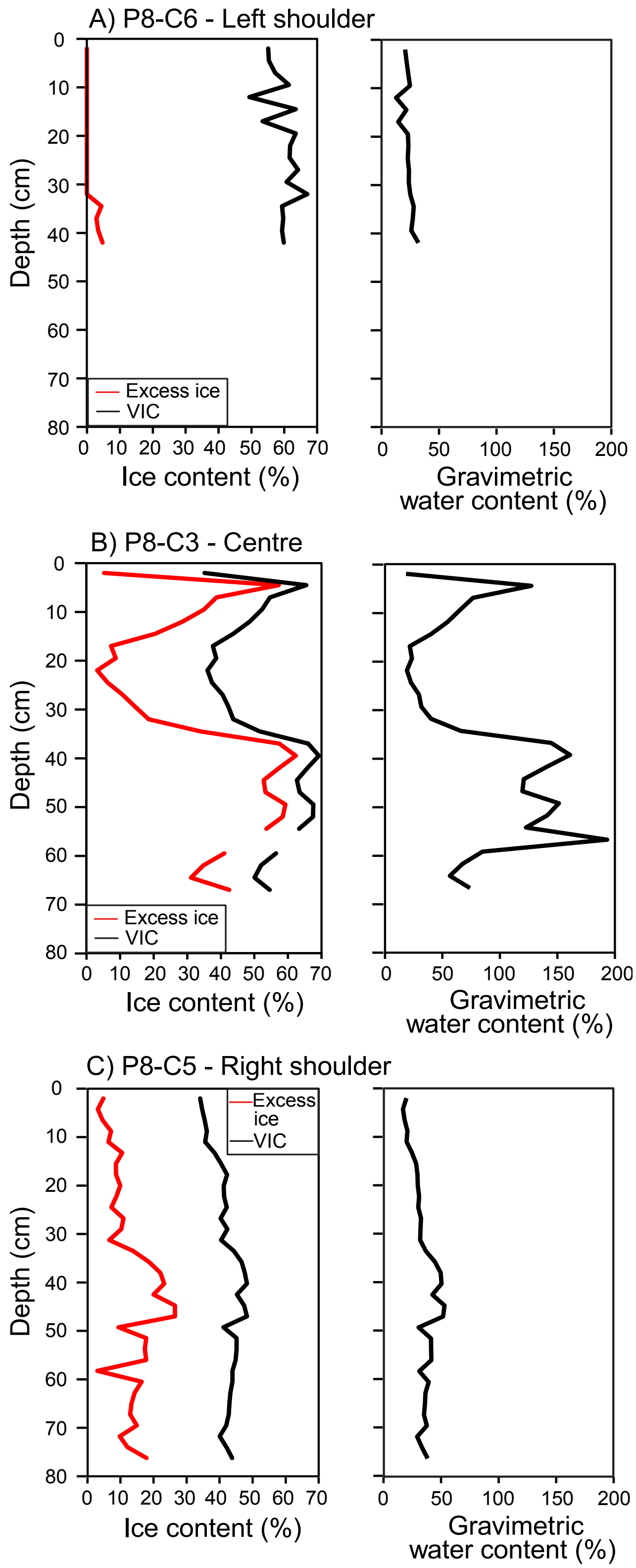

Figure 14: Excess ice and volumetric ice content (VIC) (%) (left) and gravimetric water content (%) (right) for the A) left shoulder (P8-C6), B) centre (P8-C3), and C) right shoulder (P8-C5) of P8. The ice table was at 2 cm depth for P8-C6, P8-C3 and P8-C5.

4.2.2. Polygon 7

Polygon 7 is predominantly situated in the PCZ at 466 m from University Glacier within the colluvial rock fall deposit. The average excess ice content in the centre of P7 (P7-C1; 27 cm core length) was 4 ± 1.7%, ranging from 2% at 22 cm depth to 7% at 44 cm depth. Excess ice content illustrated marked variations with depth although the largest peak was apparent between 38 and 49 cm depth with a maximum value of 7%. GWC followed a similar distribution pattern to that of excess ice; however, GWC values were greater than excess ice content with an average of 17 ± 3%. The minimum and maximum values for GWC were 13% and 22%, respectively, and were observed at the same depths as the minimum and maximum values of excess ice (22 and 43.6 cm, respectively). The average VIC in P7-C1 was 35 ± 1% and ranged between 34% and 37% at 30 and 46 cm depth, respectively. Two small peaks in VIC were apparent within the core. The first peak was the most pronounced and was observed between ca. 33 and 38 cm depth and reached a maximum of 37%. The second peak, observed between ca. 44 and 49 cm depth, was less pronounced and reached 37% (Figure 15).

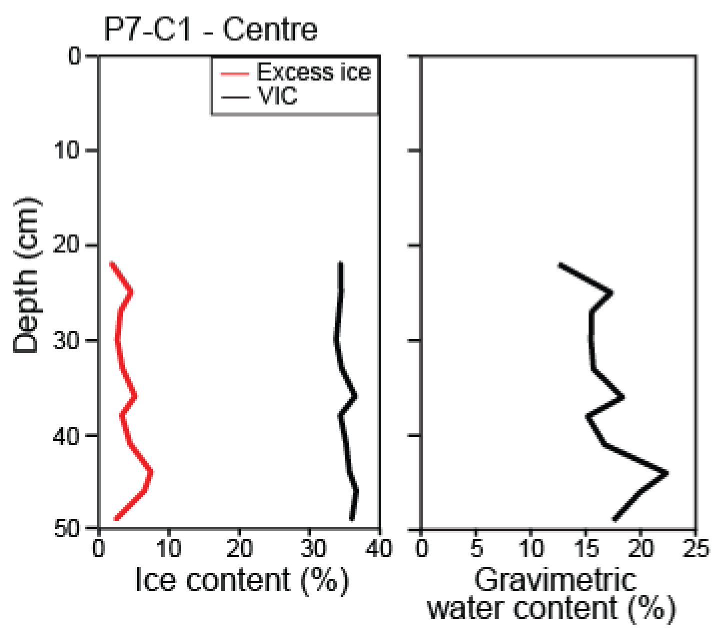

Figure 15: Excess ice and volumetric ice content (VIC) (%) (left) and gravimetric water content (%) (right) for the centre of P7 (P7-C1). The ice table for P7-C1 was at 22 cm depth.

4.2.3. Polygon 6

Polygon 6 is mainly situated in the PCZ at 545 m from University Glacier within a colluvium deposit linked to rock fall. The average GWC, VIC and excess ice contents were lower in the left shoulder (P6-C5; 70 cm core length) than in the centre (P6-C3; 100 cm core length) of P6. The average GWC in the left shoulder of the polygon was 37 ± 14%, ranging between 16% at 37 cm depth and 64% at 61 cm depth. Mean excess ice content was 14 ± 9% and ranged between 0 and 39% at ca. 20 and 78 cm depth, respectively. Three peaks were evident in the distribution of excess ice throughout the core. The first peak was observed between 20 and 37 cm depth with a maximum value of 11%. The second peak had higher excess ice contents than the first and was observed between ca. 15 and 70 cm depth with minimum and maximum values of 13 and 31%, respectively. The last peak was observed between ca. 75 and 83 cm depth with a maximum value of 39%. GWC and excess ice contents illustrated similar variations throughout the core; however, GWC values were always higher than those of excess ice. The average VIC in P6-C5 was 44 ± 8%, ranging between 33% and 64% at 20 and 78 cm depth, respectively. Five peaks in VIC were evident with depth; however, the three at the lower depths were more pronounced than the two in the upper sections of the core. The first peak was observed between ca. 20 and 37 cm depth, with the maximum value reaching 40%. The second peak, identified between ca. 59 cm and 67 cm depth, had higher values with a maximum VIC of 51%. The following three peaks were less broad and were observed between ca. 70 and 72 cm, 75 and 83 cm and between 83 and 89 cm depth with maximum VIC values of 60, 63 and 63%, respectively (Figure 16A).

The average GWC (150 ± 45%) in the centre of P6 (P6-C3) ranged between 75 and 303% at 25 and 81 cm depth, respectively. Three peaks in GWC were observed in P6-C3: the first peak was noted at ca. 50 cm depth and reached a maximum 205%, the second peak was observed between ca. 79 and 84 cm depth with the maximum value reaching 303%, the last peak was identified between ca. 90 and 97 cm depth with a maximum value of 286%. Average excess ice content in P6-C3 was 27 ± 11%, ranging between 3 and 44% at ca. 27 cm and 48 cm depth, respectively. GWC and excess ice followed similar concentration patterns until 79 cm depth, although GWC values were higher. Mean VIC in P6-C3 was 74 ± 4% ranging between 63 and 80% at ca. 25 and 50 cm, respectively. The distribution of VIC in the centre of the polygon illustrated more similarities to that of excess ice content than GWC; albeit, VIC was greater than excess ice content throughout the core (Figure 16B).

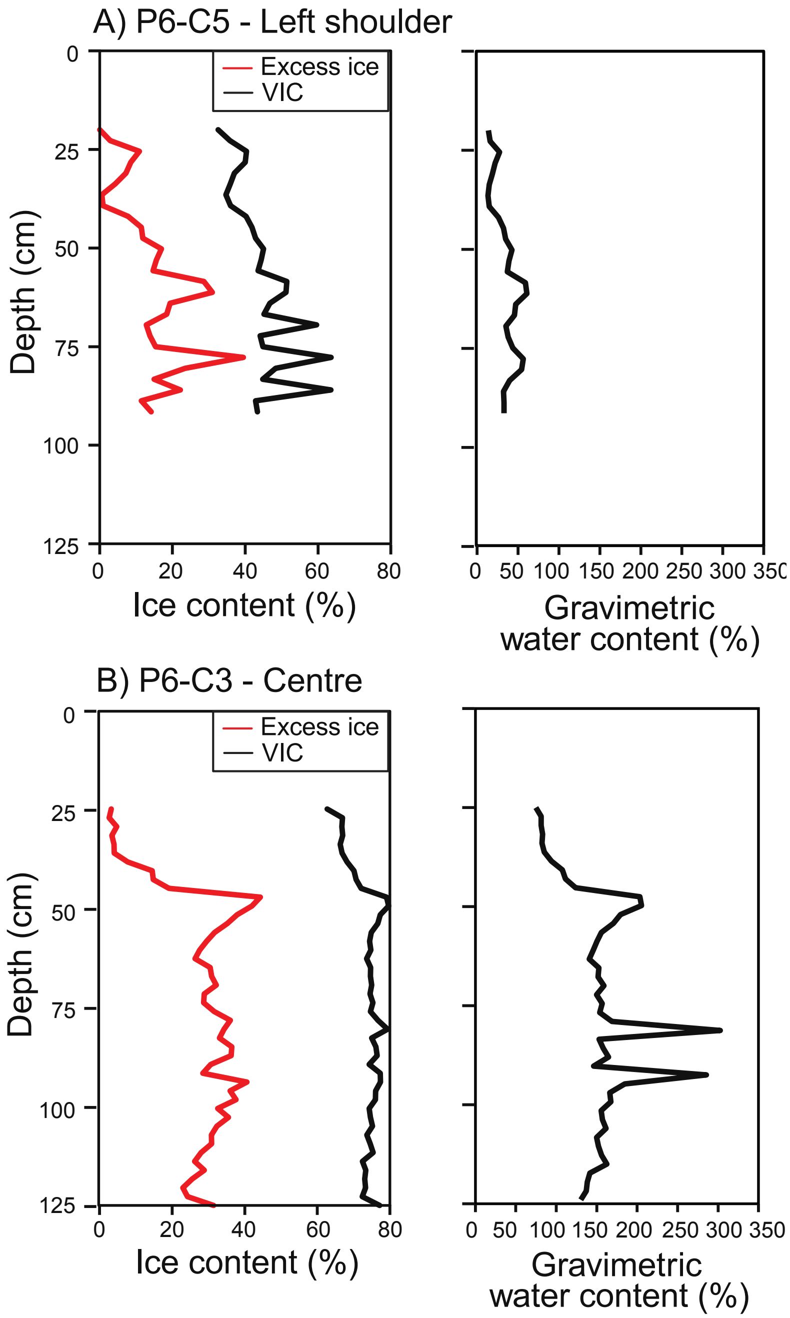

Figure 16: Excess ice and volumetric ice content (VIC) (%) (left) and gravimetric water content (%) (right) for the A) left shoulder (P6-C5) and B) centre (P6-C3) of P6. The ice table was at 25 cm depth for P6-C3 and at 20 cm depth for P6-C5.

4.2.4. Polygon 1

Polygon 1 is situated in the NCZ at 860 m from University Glacier within the undifferentiated drift deposit. The average GWC, VIC and excess ice content in the centre of P1 (P1-C1; 107 cm core length) were lower than both the right shoulder (P1-C2; 102 cm core length) and left shoulder (P1-C3; 60 cm core length) of the polygon. The average GWC in the left shoulder of P1 (128.5 ± 54%) was the highest of the three cores taken from this polygon. GWC values ranged between 24 and 272% at 42 and 82 cm depth, respectively. Although values decreased between 54 and 62 cm depth, GWC generally increased with depth. One distinct peak in GWC was evident between 76 and 84 cm depth with the maximum value reaching 272%. The mean excess ice content in P1-C3 was 48 ± 15% and values ranged between 7 and 66% at 42 and 82 cm depth, respectively. The concentration pattern in excess ice content with depth followed that of GWC. The average VIC in P1-C3 was 62 ± 9%, ranging from 38 to 71% at 42 and 82 cm depth, respectively. The distribution of VIC followed that of excess ice content throughout the core, although values for VIC were consistently higher at comparable depths (Figure 17A).

The average GWC in the core taken from the centre of the polygon was 42 ± 19%, ranging from 14.5% at 30 cm depth to 118% at 120 cm depth. The GWC gradually increased from 15% in the upper section of the core to 59% at 97.5 cm depth before beginning to fluctuate in values until 117.5 cm depth. One distinct narrow peak in GWC was present in the lower section of the core at ca. 120 cm depth with a maximum value of 118%. The mean excess ice content in P1-C1 was 19 ± 9%, ranging from 1.5% at 30 cm depth to 45% at 120 cm depth. Variations in excess ice content in the core followed those of GWC. The average VIC in P1-C1 was 44 ± 6%, ranging from 32% at 100 cm depth to 61% at 50 cm. VIC followed a similar pattern to that of excess ice, although the VIC values were always higher (Figure 17B).

The average GWC in the right shoulder of P1 was 73 ± 42%, ranging between 28% at ca. 89 cm depth and 152% at 42 cm depth. A broad increase in GWC was observed between ca. 42 and 57 cm depth reaching a maximum value of 152%. Values generally decreased with depth (between ca. 60 and 118 cm depth) to values ranging between 28 and 51%, following a similar pattern to that of excess ice. Mean excess ice content in P1-C2 was 20 ± 6%, ranging between 6 and 35% at 28 and 19 cm depth, respectively. Excess ice content variations with depth followed those of GWC. Mean VIC in P1-C2 was 55 ± 13%, ranging from 38% to 75% at ca. 89 and 42 cm depth, respectively. VIC values were greatest between ca. 19 and 57 cm depth ranging from

66 to 75%. A decrease in VIC occurred between ca. 57 and 61 cm depth. After this depth, VIC and excess ice content followed similar vertical variations; however, VIC values were always higher (Figure 17C).

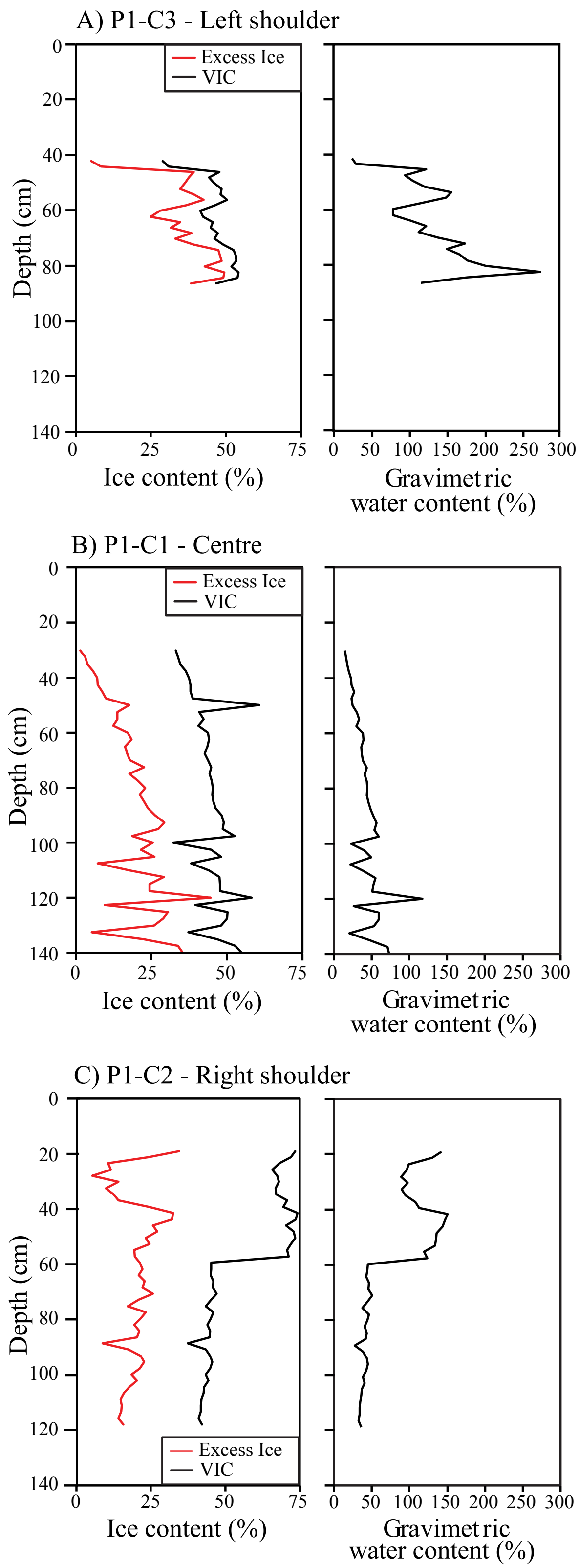

Figure 17: Excess ice and volumetric ice content (VIC) (%) (left) and gravimetric water content (%) (right) for the A) left shoulder (P1-C3), B) centre (P1-C1) and C) right shoulder (P1-C2) of P1. The ice table depth was at 28 cm for P1-C3, 30 cm for P1-C1 and at 19 cm for P1-C2.

4.2.5. Polygon 5

Polygon 5 is situated in the PCZ at 866 m from University Glacier within the undifferentiated till deposit. The average GWC in the centre of P5 (P5-C1; 23 cm core length) was 64 ± 47%, ranging from 14% at 19 cm depth to 132% at 38 cm depth. GWC increased with depth as was evident through a broad peak observed between ca. 27 and 41 cm depth, with the maximum value reaching 132%. Excess ice was not present between ca. 19 and 22 cm depth. Below 22 cm depth, the distribution of excess ice within the core closely followed that of GWC. However, values for excess ice were lower than GWC with an average of 35 ± 34% ranging between 0 and 71%. The average VIC for the core was 55 ± 21% and followed a similar pattern to that of excess ice, although values were always higher ranging between 34 and 76% (Figure 18).

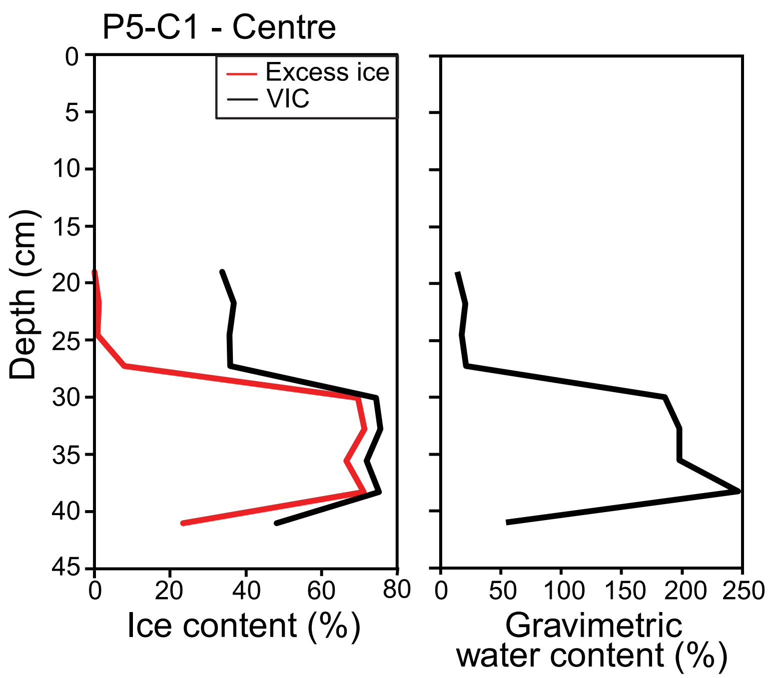

Figure 18: Excess ice and volumetric ice content (VIC) (%) (left) and gravimetric water content (%) (right) for the centre of P5 (P5-C1). The ice table was at 19 cm depth for P5-C1.

4.2.6. Polygon 4

Polygon 4 is situated in the NCZ at 943 m from University Glacier within the undifferentiated till deposit. The average GWC in the centre of P4 (P4-C1; 15 cm core length) was 47 ± 43%, ranging from 13 to 139% at 9.5 cm and 14.5 cm depth, respectively. GWC decreased in the top section of the core (from 2 to 4.5 cm depth). A large peak in GWC was observed between 12 and 17 cm depth, with the highest value reaching 129%. Mean excess ice content in P4-C1 was 14.5 ± 19%. Excess ice was not present at 2 and 4.5 cm depth, although it reached a maximum of 52% at ca. 15 cm depth. Excess ice content generally followed that of GWC, but the depths corresponding to the lowest excess ice contents (2 to 4.5 cm depth) were shallower than the depths with the lowest GWC (9.5 cm and 13%, respectively). The average VIC was 43 ± 10% and reached greater values than both GWC and excess ice between 4.5 and 12 cm depth. VIC showed less pronounced variations than excess ice and GWC with depth, although VIC also illustrated an observable increase at the same depths (12 to 17 cm) as both excess ice and GWC with a maximum value of 63%. The lowest VIC value was found at the same depth as GWC (9.5 cm) with a value of 33.5% (Figure 19).

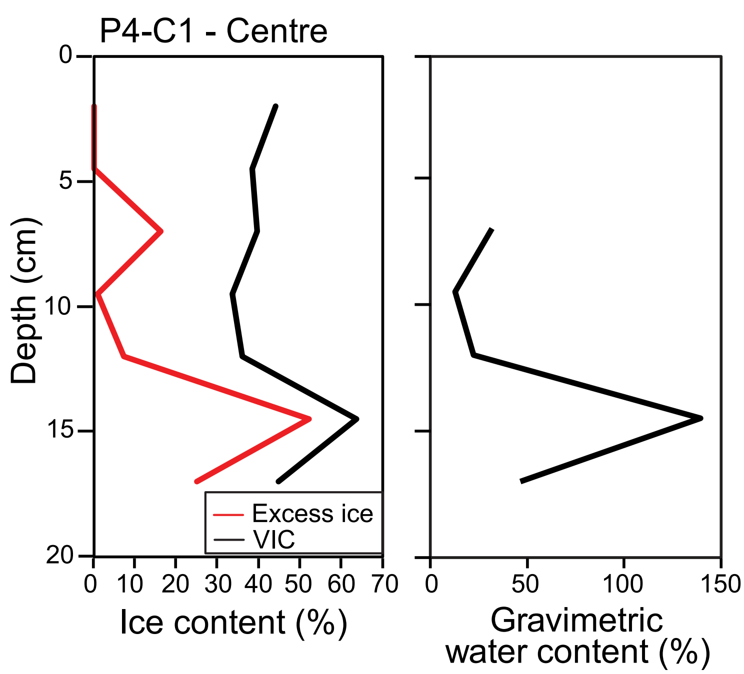

Figure 19: Excess ice and volumetric ice content (VIC) (%) (left) and gravimetric water content (%) (right) for the centre of P4 (P4-C1). The ice table for P4-C1 was at 2 cm depth.

4.2.7. Polygon 2

Polygon 2 is situated in the NCZ at 1076 m from University Glacier within the undifferentiated till deposit. The average GWC in P2-C2 (a deflation surface on P2 located near the shoulder of the polygon; 22 cm core length) was 22 ± 9% and ranged from 12% at 20 cm depth to 44% at 29 cm depth. GWC decreased sharply in the uppermost section of the core (from ca. 44 to 16% between 20 and 23 cm depth, respectively). After the initial decrease in GWC, values illustrated marked variations until 35 cm depth. GWC values gradually increased from 15% at 35 cm depth to 20% at the bottom of the core. Average excess ice content in core P2-C2 was ca. 0.2 ± 0.5% as excess ice was only present at 50 cm depth with a value of ca. 1.7%. Values for VIC were higher than both GWC and excess ice. Mean VIC in P2-C2 was 35 ± 4% and ranged between 29 and 46% at 20 and 29 cm depth, respectively (Figure 20).

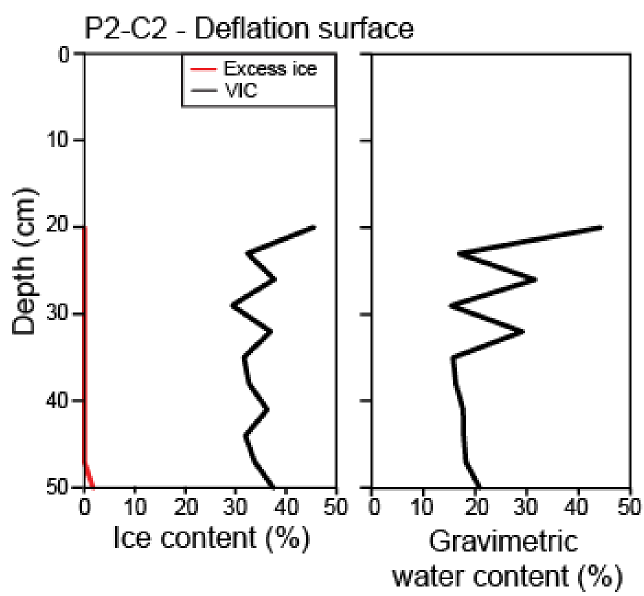

Figure 20: Excess ice and volumetric ice content (VIC) (%) (left) and gravimetric water content (%) (right) for a deflation surface on P2 (P2-C2). The ice table was at 20 cm depth for P2-C2.

4.2.8. Polygon 9

Polygon 9 is situated in the NCZ at 1692 m from University Glacier within an undifferentiated till deposit. The average GWC (333 ± 170%) was higher than both the average excess ice content and VIC within the left shoulder of P9 (P9-C2; 10 cm core length). GWC decreased with depth from the maximum value of 487% at 33 cm depth to the minimum value of 119% at 39 cm. The average excess ice content in the left shoulder was higher than the right shoulder at 75 ± 17% ranging between 51 and 88%. Excess ice content, GWC and VIC followed similar concentration patterns with depth; albeit, the average VIC (79 ± 13% ranging between 61 and 89%) was slightly higher than excess ice content (Figure 21A).

The average GWC in the right shoulder of P9 (P9-C1; 20 cm core length) was the highest of all the analyzed cores at 525 ± 690% ranging between 55% at 48 cm depth to 1881% at 30 cm depth. However, the GWC value at 39 cm depth is missing as a result of an error during laboratory analysis. The patterns of GWC and excess ice content were similar in the lower portion of the core (between ca. 41 and 50 cm depth); however, GWC values were higher than those of excess ice particularly at 30 cm (1881%) and 37 cm depth (1538%). The average excess ice content in the core was 64 ± 25% ranging between 28% at 48 cm depth and 93% at 30 cm depth. VIC and excess ice followed comparable concentration patterns throughout the core. However, the average VIC (73 ± 17%) and the minimum value for VIC (50%) were higher than excess ice, although the maximum value for VIC and excess ice were both 93% (Figure 21B).

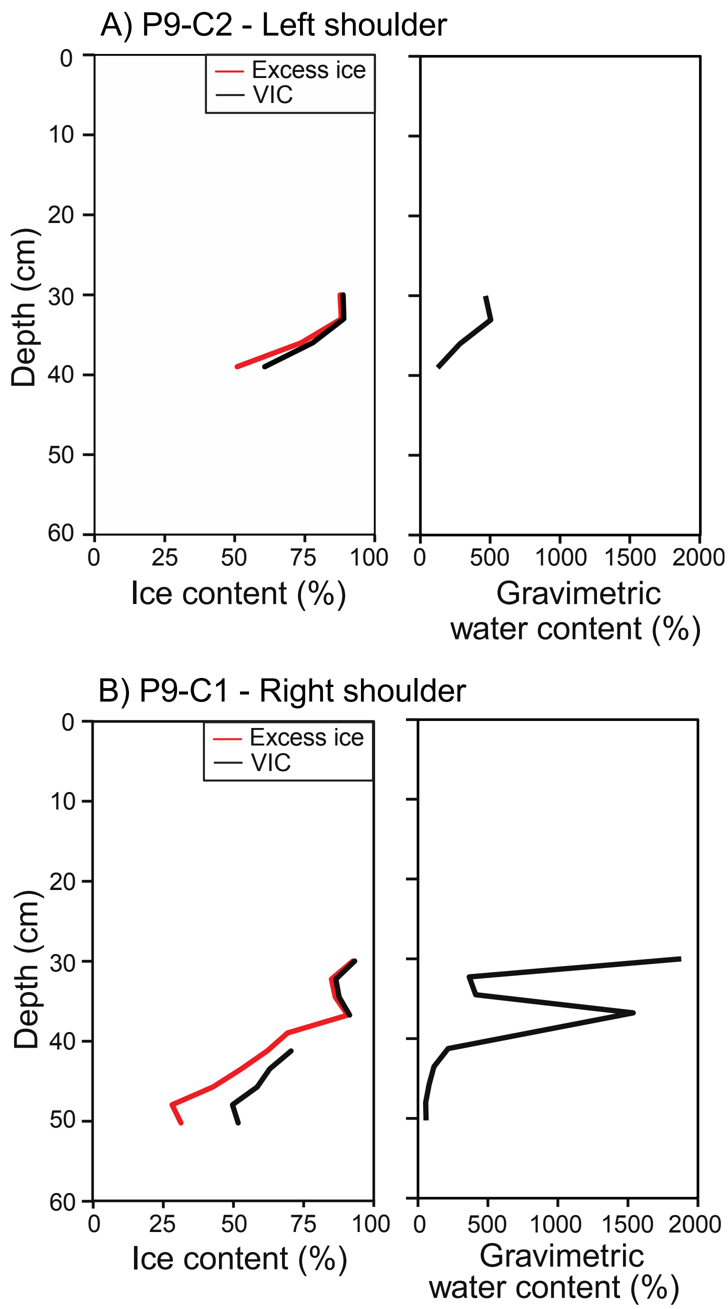

Figure 21: Excess ice and volumetric ice content (VIC) (%) (left) and gravimetric water content (%) (right) for the A) left shoulder (P9-C2) and B) right shoulder (P9-C1) of P9. The ice table was at 25 cm depth for P9-C2 and at 20 cm depth for P9-C1.

4.2.9. Polygon 10

Polygon 10 is situated in the NCZ at 1771 m from University Glacier within an undifferentiated till deposit. The average GWC for the right shoulder of P10 (P10-C1; 167 cm core length) was 207 ± 241% and ranged between 22% at 138 cm depth and 1174% at ca. 28 cm depth. The top of the core, between 16 and 86 cm depth, showed more pronounced peaks in GWC than both excess ice and VIC for the same core section. GWC decreased in the upper section of the core, from 1013% at 16 cm depth to 454% at ca. 21 cm depth. The first peak was observed between ca. 25 and 30 cm depth reaching a maximum GWC value of 1174%. The second peak was observed between 63 and 70 cm depth with GWC values > 327% and a maximum value of 726%. The concentration pattern for GWC at the bottom of the core, between ca. 86 and 182 cm depth, was similar to both excess ice content and VIC for the same depths; albeit, GWC values were higher than those of excess ice and slightly lower than those of VIC. The average excess ice content for the core was 47 ± 29% ranging between 9% at 138 cm depth and 90% at 16 cm depth. The concentration pattern for VIC with depth was very similar to that of excess ice, although values were higher as the average VIC was 61 ± 19 % ranging between 38 and 91%. Excess ice and VIC values are missing between ca. 25 and 28 cm depth due to an error in volume calculation during laboratory analysis (Figure 22).

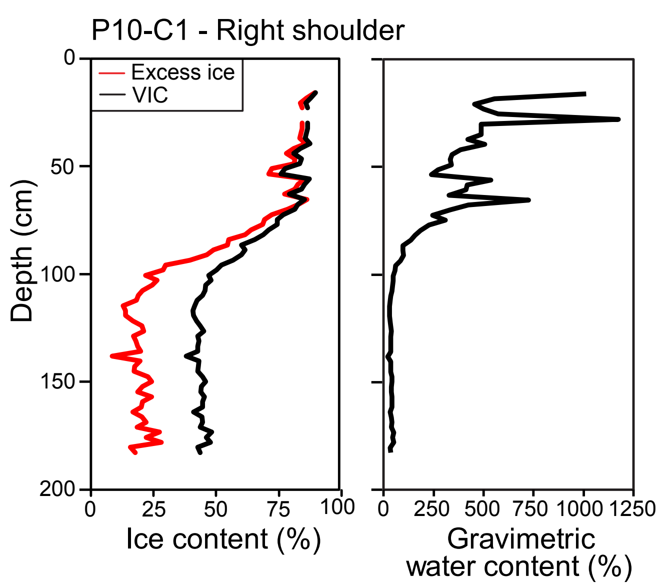

Figure 22: Excess ice and volumetric ice content (VIC) (%) (left) and gravimetric water content (%) (right) for the right shoulder of P10 (P10-C1). The ice table for P10-C1 was at 16 cm depth.

4.2.10. Cryofacies in University Valley

Based on the VIC throughout the cores taken from University Valley, the ice-rich sediment (> 25% to ≤ 50% VIC), sediment-rich ice (> 50% to ≤ 75% VIC) and sediment-poor ice (> 75% to > 100%) cryofacies were present throughout the investigated polygons.

The cryofacies present in the up-valley polygons were ice-rich sediment (> 25 to ≤ 50% VIC) in P8 and P7 and sediment-rich ice (> 50 to ≤ 75% VIC) in P8 (Figures 23A, B, C and D). In the mid-valley polygons, the ice-rich sediment (> 25% to ≤ 50% VIC) and sediment-rich ice (> 50% to ≤ 75% VIC) cryofacies were present in P6, P1, P5 and P4. The sediment-poor ice (> 75% to > 100%) cryofacies was present in P5 (Figures 23E, F, G, H, I, J and K). The ice-rich sediment (> 25 to ≤ 50% VIC) cryofacies was present in all three of the down-valley polygons (P2, P9 and P10). P9 and P10 also included the sediment-rich ice (> 50 to ≤ 75% VIC) and sediment-poor ice (> 75% to < 100%) cryofacies (Figures 23L, M, N and O).

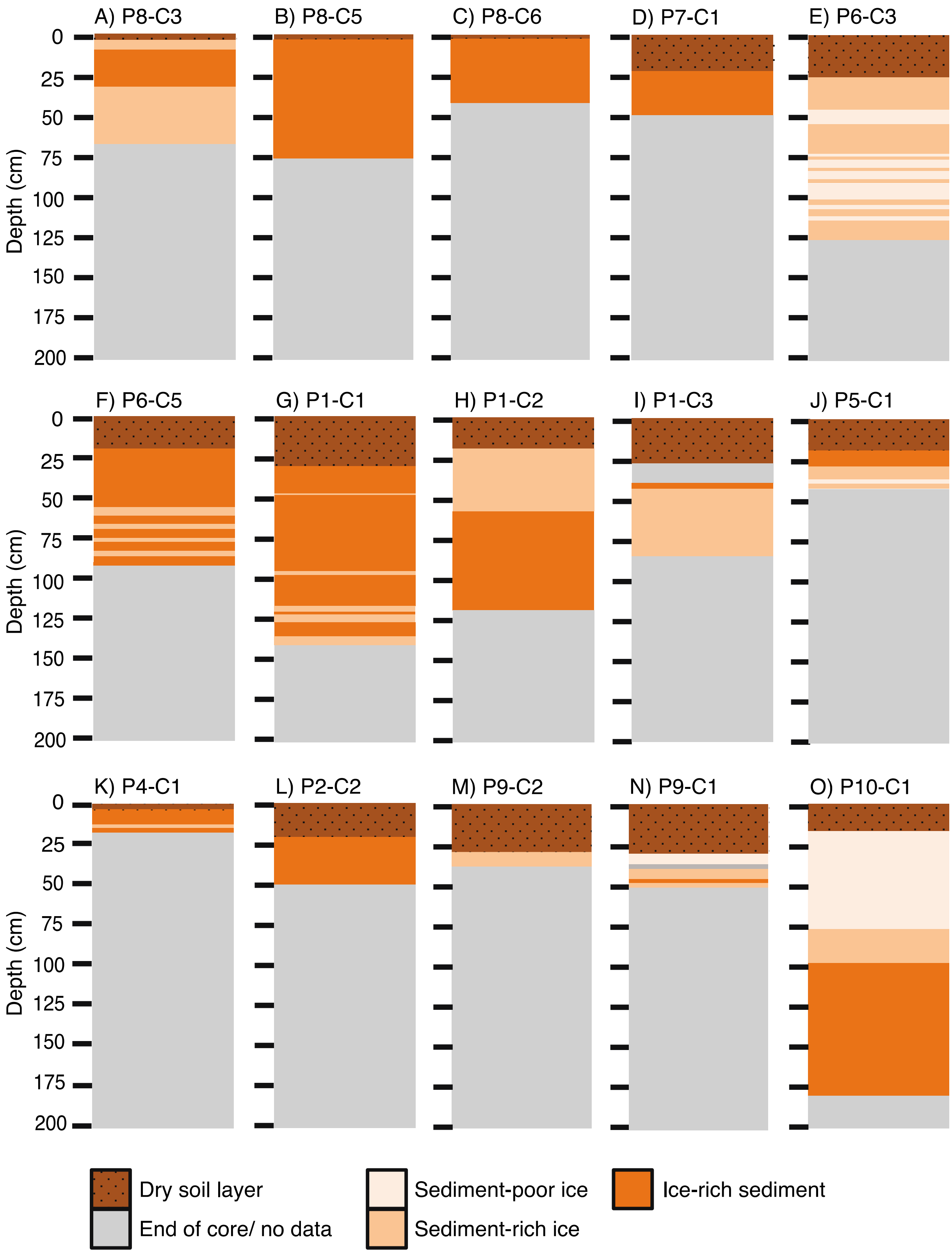

Figure 23: Cryofacies present in the 15 cores taken from University Valley. Figures are arranged at increasing distance from University Glacier.

4.2.11. Summary and statistical analyses

Ground ice content was measured in nine polygons along the floor of University Valley allowing the assessment of ice content variations. The ice content in individual polygons was highly variable, at increasing distances from University Glacier and with depth. In the 15 cores, excess ice content ranged from 0 to 93%, GWC ranged from 13 to 1881% and VIC varied from 28 to 93%. Summary statistics for excess ice content, GWC and VIC in the top 20 cm, 50 cm and 1 m of ice bearing permafrost cores taken from University Valley are presented in Tables 10, 11 and 12, respectively.

The Shapiro-Wilk test indicated that 26 out of the 48 groups of samples were normally distributed; the others showed a non-normal distribution (Appendix 3). As such, the Mann-Whitney *U* test was used to assess the significance of the differences between the medians (e.g. Kokelj *et al*., 2013) (Appendix 4). The Kolmogorov-Smirnov (K-S) test was also performed and yielded similar results to the Mann-Whitney *U* test; however, less significant results were returned in the K-S test due to its lower sensitivity to that of the Mann-Whitney *U* test. The K-S test results are shown in Appendix 5.

Table 10: Summary statistics of excess ice content (%) in the top 20 cm, 50 cm and 1 m of ice bearing permafrost for 15 cores taken from University Valley. N/A values delineate core lengths that did not reach the specified depths.

			Top 20 cm					Top 50 cm					Top 1 m				
Polygon	Core ID	Location	Mean	Median	Max	Min	SD	Mean	Median	Max	Min	SD	Mean	Median	Max	Min	SD
	P1-C1	Centre	7.2	7.1	17.7	1.5	4.8	13.1	13.8	44.3	14.5	6.5	18.5	18.4	44.5	1.5	9
1	P1-C2	Right shoulder	16.5	13.7	34.9	5.7	8.8	21.1	22.6	34.9	5.7	7.6	20.1	20.8	34.9	5.8	6.1
	P1-C3	Right shoulder	30	30.6	52.2	6.8	24.4	45.8	48.9	64.4	6.8	15.4	N/A	N/A	N/A	N/A	N/A
2	P2-C2	Deflation surface	0	0.0	0	0	0	N/A	N/A	N/A	N/A	N/A	N/A	N/A	N/A	N/A	N/A
4	P4-C1	Centre	N/A	N/A	N/A	N/A	N/A	N/A	N/A	N/A	N/A	N/A	N/A	N/A	N/A	N/A	N/A
5	P5-C1	Centre	36.1	37.2	71.3	0	36	N/A	N/A	N/A	N/A	N/A	N/A	N/A	N/A	N/A	N/A
6	P6-C3	Centre	8	4.6	19.3	2.9	6	22.1	27.7	44.4	2.9	13.8	26.9	30.6	44.4	2.9	11.4
	P6-C5	Left shoulder	4.4	3.6	10.9	0	4.1	11.8	11.4	30.9	0	8.7	N/A	N/A	N/A	N/A	N/A
7	P7-C1	Centre	4	3.4	7.4	1.9	1.6	N/A	N/A	N/A	N/A	N/A	N/A	N/A	N/A	N/A	N/A
	P8-C3	Centre	22.8	20.4	57.3	3.3	18.6	32.9	34.0	62.3	3.3	21.9	N/A	N/A	N/A	N/A	N/A
8	P8-C5	Right shoulder	7.2	7.8	10.4	3.1	2.5	12.3	9.8	26.3	3.1	7.1	N/A	N/A	N/A	N/A	N/A
	P8-C6	Left shoulder	0	0.0	0	0	0	N/A	N/A	N/A	N/A	N/A	N/A	N/A	N/A	N/A	N/A
9	P9-C1	Right shoulder	64.2	65.7	92.6	28.3	24.5	N/A	N/A	N/A	N/A	N/A	N/A	N/A	N/A	N/A	N/A
	P9-C2	Left shoulder	N/A	N/A	N/A	N/A	N/A	N/A	N/A	N/A	N/A	N/A	N/A	N/A	N/A	N/A	N/A
10	P10-C1	Right shoulder	85.5	85.1	90.2	84	1.8	83.1	84.4	90.2	71.5	4.5	63.5	75.5	90.2	12.9	25.8

Table 11: Summary statistics of gravimetric water content (%) in the top 20 cm, 50 cm and 1 m of ice bearing permafrost for 15 cores taken from University Valley. N/A values delineate core lengths that did not reach the specified depths.

			Top 20 cm					Top 50 cm					Top 1 m				
Polygon	Core ID	Location	Mean	Median	Max	Min	SD	Mean	Median	Max	Min	SD	Mean	Median	Max	Min	SD
	P1-C1	Centre	20.8	22.6	26.9	14.5	4.2	30.6	30.5	44.3	14.5	9.7	40.1	39.2	117.6	14.5	18.1
1	P1-C2	Right shoulder	107.2	99.6	144	89.9	18.1	104.3	109.4	152.1	43.1	37.2	72.8	45.0	152.1	28	42
	P1-C3	Right shoulder	66.9	61.2	121.4	23.9	48.2	115.4	119.4	175.5	23.9	43	N/A	N/A	N/A	N/A	N/A
2	P2-C2	Deflation surface	23.4	17.3	44.4	15.4	10.6	N/A	N/A	N/A	N/A	N/A	N/A	N/A	N/A	N/A	N/A
4	P4-C1	Centre	N/A	N/A	N/A	N/A	N/A	N/A	N/A	N/A	N/A	N/A	N/A	N/A	N/A	N/A	N/A
5	P5-C1	Centre	64.9	60.7	132.1	14.2	50.6	N/A	N/A	N/A	N/A	N/A	N/A	N/A	N/A	N/A	N/A
6	P6-C3	Centre	92.5	84.2	123.8	74.9	16.2	132.4	145.7	205.4	74.9	40.4	149.7	152.6	302.7	74.9	44.8
	P6-C5	Left shoulder	20.5	18.3	30.4	16.2	4.9	34.5	35.2	63.7	16.2	14.9	N/A	N/A	N/A	N/A	N/A
7	P7-C1	Centre	16.6	15.7	22.3	12.6	2.7	N/A	N/A	N/A	N/A	N/A	N/A	N/A	N/A	N/A	N/A
	P8-C3	Centre	49.5	40.1	127.3	18.3	36.2	76.9	65.2	161.1	18.3	52.5	N/A	N/A	N/A	N/A	N/A
8	P8-C5	Right shoulder	23.8	22.6	30.7	16.7	5.4	33.2	30.7	52.9	16.7	11.2	N/A	N/A	N/A	N/A	N/A
	P8-C6	Left shoulder	20.8	22.0	25	12.8	4.2	N/A	N/A	N/A	N/A	N/A	N/A	N/A	N/A	N/A	N/A
9	P9-C1	Right shoulder	524.9	215.7	1881.4	55.3	689.6	N/A	N/A	N/A	N/A	N/A	N/A	N/A	N/A	N/A	N/A
	P9-C2	Left shoulder	N/A	N/A	N/A	N/A	N/A	N/A	N/A	N/A	N/A	N/A	N/A	N/A	N/A	N/A	N/A
10	P10-C1	Right shoulder	615.8	494.6	1173.8	421	258.4	499.8	471.1	1173.8	238.1	222.9	314.1	317.8	1173.8	28.9	256.5

Table 12: Summary statistics of volumetric ice content (%) in the top 20 cm, 50 cm and 1 m of ice bearing permafrost for 15 cores taken from University Valley. N/A values delineate core lengths that did not reach the specified depths.

			Top 20 cm					Top 50 cm					Top 1 m				
Polygon	Core ID	Location	Mean	Median	Max	Min	SD	Mean	Median	Max	Min	SD	Mean	Median	Max	Min	SD
1	P1-C1	Centre	38.9	37.4	60.6	33	8.4	41.4	42.2	60.6	33	5.9	43.9	44.2	60.6	32.1	6.1
	P1-C2	Right shoulder	69.4	68.6	74	66.2	2.5	65.5	70.0	74.6	45.5	10.8	55	46.1	74.6	37.9	13.3
	P1-C3	Right shoulder	50.5	50.0	63.5	38.4	12.6	60.7	61.6	70.9	38.4	8.6	N/A	N/A	N/A	N/A	N/A
2	P2-C2	Deflation surface	35.3	34.5	45.6	29.4	5	N/A	N/A	N/A	N/A	N/A	N/A	N/A	N/A	N/A	N/A
4	P4-C1	Centre	N/A	N/A	N/A	N/A	N/A	N/A	N/A	N/A	N/A	N/A	N/A	N/A	N/A	N/A	N/A
5	P5-C1	Centre	54.8	54.3	75.5	33.8	20.7	N/A	N/A	N/A	N/A	N/A	N/A	N/A	N/A	N/A	N/A
6	P6-C3	Centre	67.8	67.0	72.1	62.8	2.6	72.3	74.4	79.6	62.8	4.6	73.6	74.6	79.6	62.8	3.7
	P6-C5	Left shoulder	36.5	35.9	40.3	32.5	2.6	42.3	41.8	59.5	32.5	6.8	N/A	N/A	N/A	N/A	N/A
7	P7-C1	Centre	34.8	34.5	36.5	33.8	0.8	N/A	N/A	N/A	N/A	N/A	N/A	N/A	N/A	N/A	N/A
8	P8-C3	Centre	45.8	43.7	65.4	35.2	10.3	51.9	51.6	69.2	35.2	12.5	N/A	N/A	N/A	N/A	N/A
	P8-C5	Right shoulder	37.8	37.2	42.1	34	3	41.6	41.2	48.1	34	4.5	N/A	N/A	N/A	N/A	N/A
	P8-C6	Left shoulder	33.1	32.7	36.3	28.2	2.9	N/A	N/A	N/A	N/A	N/A	N/A	N/A	N/A	N/A	N/A
9	P9-C1	Right shoulder	72.5	70.6	93.2	49.8	17.5	N/A	N/A	N/A	N/A	N/A	N/A	N/A	N/A	N/A	N/A
	P9-C2	Left shoulder	N/A	N/A	N/A	N/A	N/A	N/A	N/A	N/A	N/A	N/A	N/A	N/A	N/A	N/A	N/A
10	P10-C1	Right shoulder	86.1	87.0	90.5	78.4	3.4	84.7	86.1	90.5	76.6	3.7	72	78.4	90.5	41.1	16.4

4.2.11.1. Intra-polygon ice content variations

Ice-bearing permafrost cores were collected from both the centre and shoulders of three polygons: P8 (304 m distance from glacier), P6 (545 m distance from glacier) and P1 (860 m distance from glacier), which allowed an assessment of the minimum degree of ice content variations within a single polygon (Figure 24).

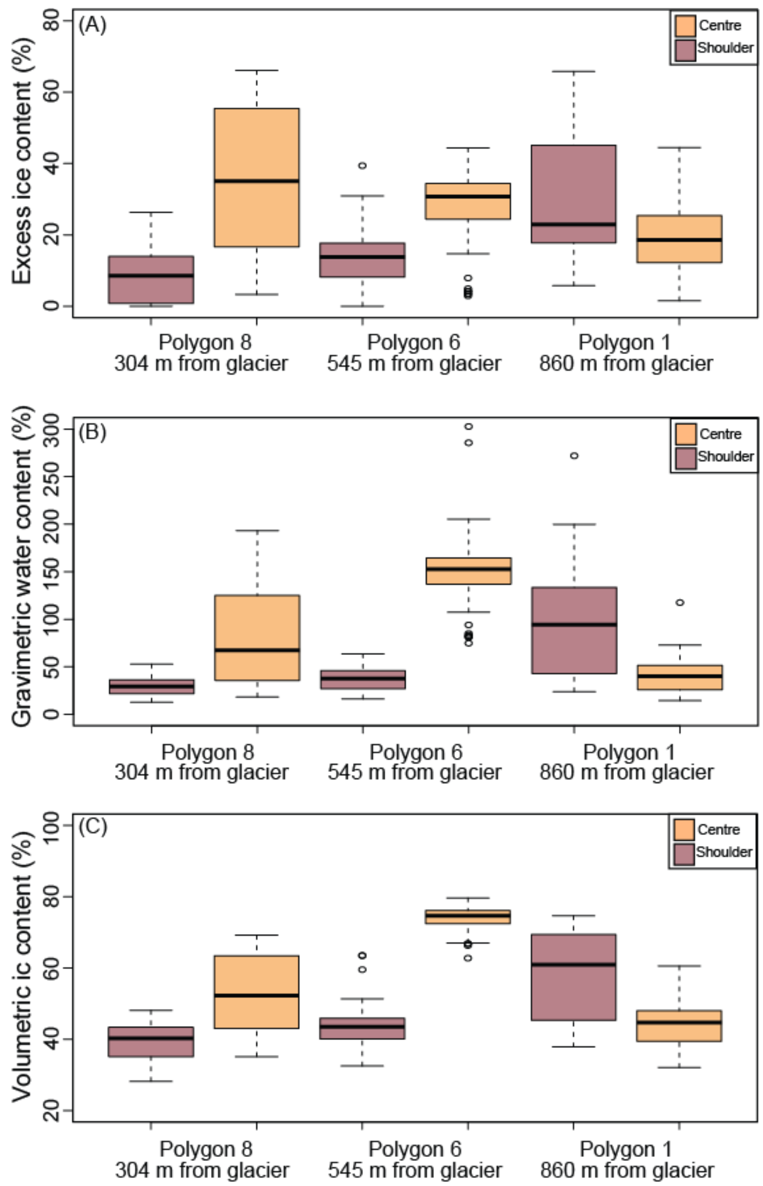

Figure 24: Intra-polygon comparison of the A) excess ice content (%), B) gravimetric water content (%) and C) volumetric ice content (%) in the entire cores taken from the centres and shoulders of Polygons 8, 6 and 1 at increasing distances from University Glacier.

In P8, the median excess ice content in the top 20 cm of ice bearing permafrost was significantly higher in the centre (20.4 %) than in the right and left shoulders (7.8% and 0%, respectively). However, no significant difference was found between the median GWC of the centre (40.1 %) and right and left shoulders (22.6% and 22%, respectively) for the same depth interval. In the uppermost 50 cm of ice-bearing permafrost, the median excess ice content and GWC were significantly higher in the centre (34% and 65%, respectively) than in the right shoulder (9.8% and 30%, respectively) of the polygon (Tables 13 and 14).

In P6, the median excess ice content in the top 20 cm of ice-bearing permafrost was statistically similar between the centre (4.6%) and left shoulder (3.6%); however the GWC was significantly higher in the centre (92.5%) than in the shoulder (20.5%). A similar observation was made in the uppermost 50 cm, where the median excess ice content was not statistically different between the centre (27.7%) and shoulder (11.4%), whereas the GWC was significantly higher in the centre (145.7%) compared to the shoulder (35.2%) (Tables 13 and 14).

In P1, the median excess ice content in the top 20 cm was significantly lower in the centre (7.1%) compared to the right shoulder (30.6%); no statistical difference was found between the left shoulder (13.7%) and the centre. Conversely, the median GWC was significantly lower in the centre (20.8%) compared to the right and left shoulders (61.2% and 99.6%, respectively). In the uppermost 50 cm, the median excess ice content was significantly lower in the centre (13.8%) compared to the right and left shoulders (48.9% and 22.6%, respectively). The same observation is made for the median GWC, where the median GWC in the centre was 30.5% and 119.4% and 109.4% in the right and left shoulders, respectively. The Mann-Whitney *U* test between median ice contents in the uppermost 1 m of ice-bearing permafrost could only be performed on P1 as the P6 and P8 cores did not reach the specified depth. The difference in median excess ice content between the centre (18.4%, P1-C1) and shoulder (20.8%, P1-C2) was not significant over this depth; however, a significant difference was shown between both median GWC (Tables 13, 14 and 15).

Overall, the median ice content was higher in the centre than in the shoulders in Polygons 6 and 8. The results for P1, however, show that median ice content was higher in the shoulders of the polygon than in the centre. When the ground ice content data for the three polygons are averaged together, the median excess ice content, GWC and VIC are significantly higher in the centres relative to the shoulders of the polygons (Figures 25A, B and C; Appendix 4G).

Table 13: Mann-Whitney *U* test comparison of the median excess ice content and gravimetric water content in the top 20 cm of ice bearing permafrost in 13 cores taken from University Valley. Only results indicative of a statistically significant (p-value = < 0.05) *W* statistic value are presented. A statistically significant result allows the rejection of the null hypothesis that the medians of variable x and variable y are equal. Cores P4-C1 and P9-C2 were not included as they measured less than 20 cm in length.

Excess ice content													
	P1-C1	P1-C2	P1-C3	P2-C2	P5-C1	P6-C3	P6-C5	P7-C1	P8-C3	P8-C5	P8-C6	P9-C1	P10-C1
P1-C1	--	**11**	--	**72**	--	--	--	--	--	--	**81**	**0**	**0**
P1-C2	**11**	--	--	**80**	--	**78**	**76**	**89**	--	**92**	**90**	**2**	**0**
P1-C3	--	--	--	**32**	--	--	**29**	**35**	--	--	**36**	--	**0**
P2-C2	**72**	**80**	**32**	--	**4**	**0**	**4**	**0**	**0**	**0**	N/A	**0**	**0**
P5-C1	--	--	--	**4**	--	--	--	--	--	--	**68**	--	**0**
P6-C3	--	**78**	--	**0**	--	--	--	--	**20**	--	**90**	**90**	**0**
P6-C5	--	**76**	**29**	**4**	--	--	--	--	**10**	--	**68**	**0**	**0**
P7-C1	--	**89**	**35**	**0**	--	--	--	--	**7**	**14**	**81**	**0**	**0**
P8-C3	--	--	--	**0**	--	**20**	**10**	**7**	--	--	**81**	**9**	**0**
P8-C5	--	**92**	--	**0**	--	--	--	**14**	--	--	**90**	**0**	**0**
P8-C6	**81**	**90**	**36**	N/A	**68**	**90**	**68**	**81**	**81**	**90**	--	**0**	**0**
P9-C1	**0**	**2**	--	**0**	--	**90**	**0**	**0**	**9**	**0**	**0**	--	--
P10-C1	**0**	**0**	**0**	**0**	**0**	**0**	**0**	**0**	**0**	**0**	**0**	--	--
Gravimetric water content													
	P1-C1	P1-C2	P1-C3	P2-C2	P5-C1	P6-C3	P6-C5	P7-C1	P8-C3	P8-C5	P8-C6	P9-C1	P10-C1
P1-C1	--	**0**	**2**	--	--	**0**	--	**65.5**	--	--	--	**0**	**0**
P1-C2	**0**	--	--	**80**	--	**77**	**80**	**90**	**82**	**100**	**90**	--	**0**
P1-C3	**2**	--	--	--	--	--	**29**	**36**	--	--	**35**	--	**0**
P2-C2	--	**80**	--	--	--	**0**	--	--	**13**	--	--	**0**	**0**
P5-C1	--	--	--	--	--	--	--	**60**	--	--	--	**13**	**0**
P6-C3	**0**	**77**	--	**0**	--	--	**80**	**90**	**79**	**100**	**90**	--	**0**
P6-C5	--	**80**	**29**	--	--	**80**	--	**13**	**11.5**	--	--	**0**	**0**
P7-C1	**65.5**	**90**	**36**	--	**60**	**90**	**13**	--	**3.5**	**8.5**	--	**0**	**0**
P8-C3	--	**82**	--	**13**	--	**79**	**11.5**	**3.5**	--	--	--	**8**	**0**
P8-C5	--	**100**	--	--	--	**100**	--	**8.5**	--	--	--	**0**	**0**
P8-C6	--	**90**	**35**	--	--	**90**	--	--	--	--	--	**0**	**0**
P9-C1	**0**	--	--	**0**	**13**	--	**0**	**0**	**8**	**0**	**0**	--	**20**
P10-C1	**0**	**0**	**0**	**0**	**0**	**0**	**0**	**0**	**0**	**0**	**0**	**20**	--

Table 14: Mann-Whitney *U* test comparison of the median excess ice content and gravimetric water content in the top 50 cm of ice bearing permafrost in eight cores taken from University Valley. Only results indicative of a statistically significant (p-value = < 0.05) *W* statistic value are presented. A statistically significant result allows the rejection of the null hypothesis that the medians of variable x and variable y are equal. A N/A value appears where cores were less than 50 cm in length.

Excess ice content

	P1-C1	P1-C2	P1-C3	P2-C2	P5-C1	P6-C3	P6-C5	P7-C1	P8-C3	P8-C5	P8-C6	P9-C1	P10-C1
P1-C1	--	**100**	**30**	N/A	N/A	**150**	--	N/A	**112**	--	N/A	N/A	**0**
P1-C2	**100**	--	**43**	N/A	N/A	--	**347**	N/A	--	**426**	N/A	N/A	**0**
P1-C3	**30**	**43**	--	N/A	N/A	**394**	**337**	N/A	--	**363**	N/A	N/A	**0**
P2-C2	N/A	N/A	N/A	--	N/A	N/A	N/A	N/A	N/A	N/A	N/A	N/A	N/A
P5-C1	N/A	N/A	N/A	N/A	--	N/A	N/A	N/A	N/A	N/A	N/A	N/A	N/A
P6-C3	**150**	--	**394**	N/A	N/A	--	**312.5**	N/A	--	**363**	N/A	N/A	**0**
P6-C5	--	**347**	**337**	N/A	N/A	**312.5**	--	N/A	**91.5**	--	N/A	N/A	**0**
P7-C1	N/A	N/A	N/A	N/A	N/A	N/A	N/A	--	N/A	N/A	N/A	N/A	N/A
P8-C3	**112**	--	--	N/A	N/A	--	**91.5**	N/A	--	**368.5**	N/A	N/A	**0**
P8-C5	--	**426**	**363**	N/A	N/A	**363**	--	N/A	**368.5**	--	N/A	N/A	**0**
P8-C6	N/A	N/A	N/A	N/A	N/A	N/A	N/A	N/A	N/A	N/A	--	N/A	N/A
P9-C1	N/A	N/A	N/A	N/A	N/A	N/A	N/A	N/A	N/A	N/A	N/A	--	N/A
P10-C1	**0**	**0**	**0**	N/A	N/A	**0**	**0**	N/A	**0**	**0**	N/A	N/A	--

Gravimetric water content

	P1-C1	P1-C2	P1-C3	P2-C2	P5-C1	P6-C3	P6-C5	P7-C1	P8-C3	P8-C5	P8-C6	P9-C1	P10-C1
P1-C1	--	**3**	**26**	N/A	N/A	**0**	--	N/A	**114.5**	--	N/A	N/A	**0**
P1-C2	**3**	--	--	N/A	N/A	**0**	**414**	N/A	--	**507**	N/A	N/A	**0**
P1-C3	**26**	--	--	N/A	N/A	--	**336**	N/A	**281**	**403**	N/A	N/A	**0**
P2-C2	N/A	N/A	N/A	--	N/A	N/A	N/A	N/A	N/A	N/A	N/A	N/A	N/A
P5-C1	N/A	N/A	N/A	N/A	--	N/A	N/A	N/A	N/A	N/A	N/A	N/A	N/A
P6-C3	**0**	**0**	--	N/A	N/A	--	**437**	N/A	**389**	**529**	N/A	N/A	**0**
P6-C5	--	**414**	**336**	N/A	N/A	**437**	--	N/A	**295.5**	--	N/A	N/A	**0**
P7-C1	N/A	N/A	N/A	N/A	N/A	N/A	N/A	--	N/A	N/A	N/A	N/A	N/A
P8-C3	**114.5**	--	**281**	N/A	N/A	**389**	**295.5**	N/A	--	**347.5**	N/A	N/A	**0**
P8-C5	--	**507**	**403**	N/A	N/A	**529**	--	N/A	**347.5**	--	N/A	N/A	**0**
P8-C6	N/A	N/A	N/A	N/A	N/A	N/A	N/A	N/A	N/A	N/A	--	N/A	N/A
P9-C1	N/A	N/A	N/A	N/A	N/A	N/A	N/A	N/A	N/A	N/A	N/A	--	N/A
P10-C1	**0**	**0**	**0**	N/A	N/A	**0**	**0**	N/A	**0**	**0**	N/A	N/A	--

Table 15: Mann-Whitney *U* test comparison of median excess ice content and gravimetric water content in the top 1 m of ice bearing permafrost in four cores taken from University Valley. Only results indicative of a statistically significant (p-value = < 0.05) *W* statistic value are presented. A statistically significant result allows the rejection of the null hypothesis that the medians of variable x and variable y are equal. A N/A value appears where cores were less than 1 m in length.

Excess ice content													
	P1-C1	P1-C2	P1-C3	P2-C2	P5-C1	P6-C3	P6-C5	P7-C1	P8-C3	P8-C5	P8-C6	P9-C1	P10-C1
P1-C1	--	--	N/A	N/A	N/A	**437**	N/A	N/A	N/A	N/A	N/A	N/A	**153**
P1-C2	--	--	N/A	N/A	N/A	**500**	N/A	N/A	N/A	N/A	N/A	N/A	**191**
P1-C3	N/A	N/A	--	N/A	N/A	N/A	N/A	N/A	N/A	N/A	N/A	N/A	N/A
P2-C2	N/A	N/A	N/A	--	N/A	N/A	N/A	N/A	N/A	N/A	N/A	N/A	N/A
P5-C1	N/A	N/A	N/A	N/A	--	N/A	N/A	N/A	N/A	N/A	N/A	N/A	N/A
P6-C3	**437**	**500**	N/A	N/A	N/A	--	N/A	N/A	N/A	N/A	N/A	N/A	**331**
P6-C5	N/A	N/A	N/A	N/A	N/A	N/A	--	N/A	N/A	N/A	N/A	N/A	N/A
P7-C1	N/A	N/A	N/A	N/A	N/A	N/A	N/A	--	N/A	N/A	N/A	N/A	N/A
P8-C3	N/A	N/A	N/A	N/A	N/A	N/A	N/A	N/A	--	N/A	N/A	N/A	N/A
P8-C5	N/A	N/A	N/A	N/A	N/A	N/A	N/A	N/A	N/A	--	N/A	N/A	N/A
P8-C6	N/A	N/A	N/A	N/A	N/A	N/A	N/A	N/A	N/A	N/A	--	N/A	N/A
P9-C1	N/A	N/A	N/A	N/A	N/A	N/A	N/A	N/A	N/A	N/A	N/A	--	N/A
P10-C1	**153**	**191**	N/A	N/A	N/A	**331**	N/A	N/A	N/A	N/A	N/A	N/A	--
Gravimetric water content													
	P1-C1	P1-C2	P1-C3	P2-C2	P5-C1	P6-C3	P6-C5	P7-C1	P8-C3	P8-C5	P8-C6	P9-C1	P10-C1
P1-C1	--	**527**	N/A	N/A	N/A	**9**	N/A	N/A	N/A	N/A	N/A	N/A	**173.5**
P1-C2	**527**	--	N/A	N/A	N/A	**173.5**	N/A	N/A	N/A	N/A	N/A	N/A	**365**
P1-C3	N/A	N/A	--	N/A	N/A	N/A	N/A	N/A	N/A	N/A	N/A	N/A	N/A
P2-C2	N/A	N/A	N/A	--	N/A	N/A	N/A	N/A	N/A	N/A	N/A	N/A	N/A
P5-C1	N/A	N/A	N/A	N/A	--	N/A	N/A	N/A	N/A	N/A	N/A	N/A	N/A
P6-C3	**9**	**191**		N/A	N/A	--		N/A	N/A	N/A	N/A	N/A	**664**
P6-C5	N/A	N/A	N/A	N/A	N/A	N/A	--	N/A	N/A	N/A	N/A	N/A	N/A
P7-C1	N/A	N/A	N/A	N/A	N/A	N/A	N/A	--	N/A	N/A	N/A	N/A	N/A
P8-C3	N/A	N/A	N/A	N/A	N/A	N/A	N/A	N/A	--	N/A	N/A	N/A	N/A
P8-C5	N/A	N/A	N/A	N/A	N/A	N/A	N/A	N/A	N/A	--	N/A	N/A	N/A
P8-C6	N/A	N/A	N/A	N/A	N/A	N/A	N/A	N/A	N/A	N/A	--	N/A	N/A
P9-C1	N/A	N/A	N/A	N/A	N/A	N/A	N/A	N/A	N/A	N/A	N/A	--	N/A
P10-C1	**173.5**	**365**	N/A	N/A	N/A	**664**	N/A	N/A	N/A	N/A	N/A	N/A	--

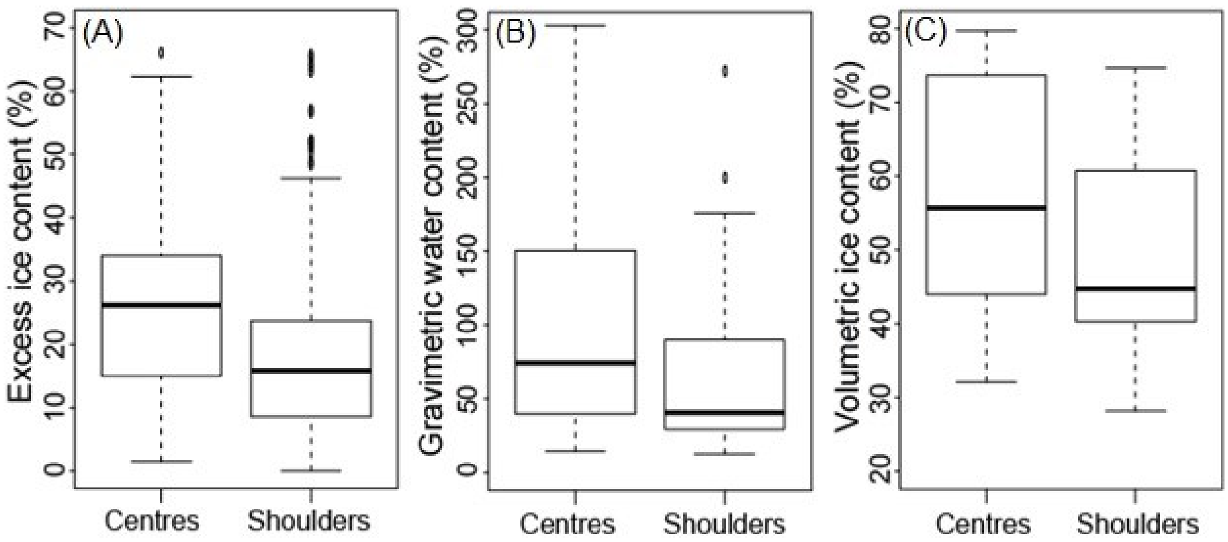

Figure 25: Boxplots illustrating the difference in median A) excess ice content (%), B) gravimetric water content (%) and C) volumetric ice content in the entire cores taken from the centres and shoulders of Polygons 1, 6 and 8.

4.2.11.2. Ground ice content variation in University Valley

The 15 cores obtained from University Valley allow the assessment of ice content at increasing distances from University Glacier. In upper University Valley, the centre of P8 showed a near-surface ice-rich layer at ca. 5 to 10 cm depth (excess ice and GWC reaching 50 and 100%, respectively); however, this ice-rich layer was not observed in the shoulders of the same polygons. Below 20 cm depth, excess ice and GWC in the centre and shoulders of the upper University Valley polygon predominantly increased with depth, reaching a plateau in ice content below ca. 70 cm. In central University Valley, a near-surface ice-rich layer was not observed in the centre of polygons (P1 and P6). However, as with the polygons in upper University Valley, the ground ice content in the centre and shoulders of the polygons mainly increased with depth (e.g. Tables 16 and 17) to reach a plateau below ca. 70 cm depth. The polygons in lower University Valley, which were sampled only on their shoulders as the ice table was too deep in their centres, had the highest ground ice contents. An ice-rich zone was apparent in the uppermost ca. 40 to 80 cm of the lower valley cores (excess ice and GWC reaching values > 85 and 725%, respectively) that was not observed in the polygons in upper and central University Valley. Below this ice-rich zone, ground ice content significantly decreased with depth (e.g. Tables 16 and 17) to reach values observed in the polygons from the upper and central portions of the valley (Figure 26).

Table 16: Results of the signal to noise variance ratio test between depth (cm) and excess ice content (%) for the 15 individual cores taken from University Valley. Statistically significant ratios are represented by bolded characters.

Core ID	Signal to noise ratio	Noise	Cross-correlation coefficent (multiple r)	p-value
P1-C1	**1.74**	**0.36**	0.64	**0.000**
P1-C2	**3.94**	**0.20**	-0.80	**0.000**
P1-C3	**2.41**	**0.29**	0.71	**0.000**
P2-C2	**1.14**	**0.47**	-0.53	**0.091**
P4-C1	0.59	0.63	0.37	0.413
P5-C1	**2.72**	**0.27**	0.73	**0.025**
P6-C3	**0.74**	**0.57**	0.43	**0.003**
P6-C5	**1.80**	**0.36**	0.64	**0.000**
P7-C1	**1.99**	**0.33**	0.67	**0.026**
P8-C3	**0.89**	**0.53**	0.47	**0.013**
P8-C5	**1.29**	**0.44**	0.56	**0.001**
P8-C6	0.40	0.71	0.29	0.264
P9-C1	**2.36**	**0.30**	-0.70	**0.035**
P9-C2	11.00	0.08	-0.92	0.083
P10-C1	**3.99**	**0.20**	-0.80	**0.000**

Table 17: Results of the signal to noise variance ratio test between depth (cm) and gravimetric water content (%) for the 15 individual cores taken from University Valley. Statistically significant ratios are represented by bolded characters.

Core ID	Signal to noise ratio	Noise	Cross-correlation coefficient (multiple r)	p-value
P1-C1	**2.16**	**0.32**	0.68	**0.000**
P1-C2	0.17	0.85	-0.15	0.332
P1-C3	**1.91**	**0.34**	0.66	**0.001**
P2-C2	1.00	0.50	0.50	0.117
P4-C1	2.21	0.31	0.69	0.087
P5-C1	**2.03**	**0.33**	0.67	**0.049**
P6-C3	**1.20**	**0.45**	0.55	**0.000**
P6-C5	**1.64**	**0.38**	0.62	**0.001**
P7-C1	0.88	0.53	0.47	0.146
P8-C3	**1.02**	**0.49**	0.51	**0.007**
P8-C5	**0.91**	**0.52**	0.48	**0.004**
P8-C6	**2.63**	**0.28**	0.72	**0.001**
P9-C1	**25.34**	**0.04**	-0.96	**0.000**
P9-C2	11.85	0.08	-0.92	0.078
P10-C1	**9.15**	**0.10**	-0.90	**0.000**

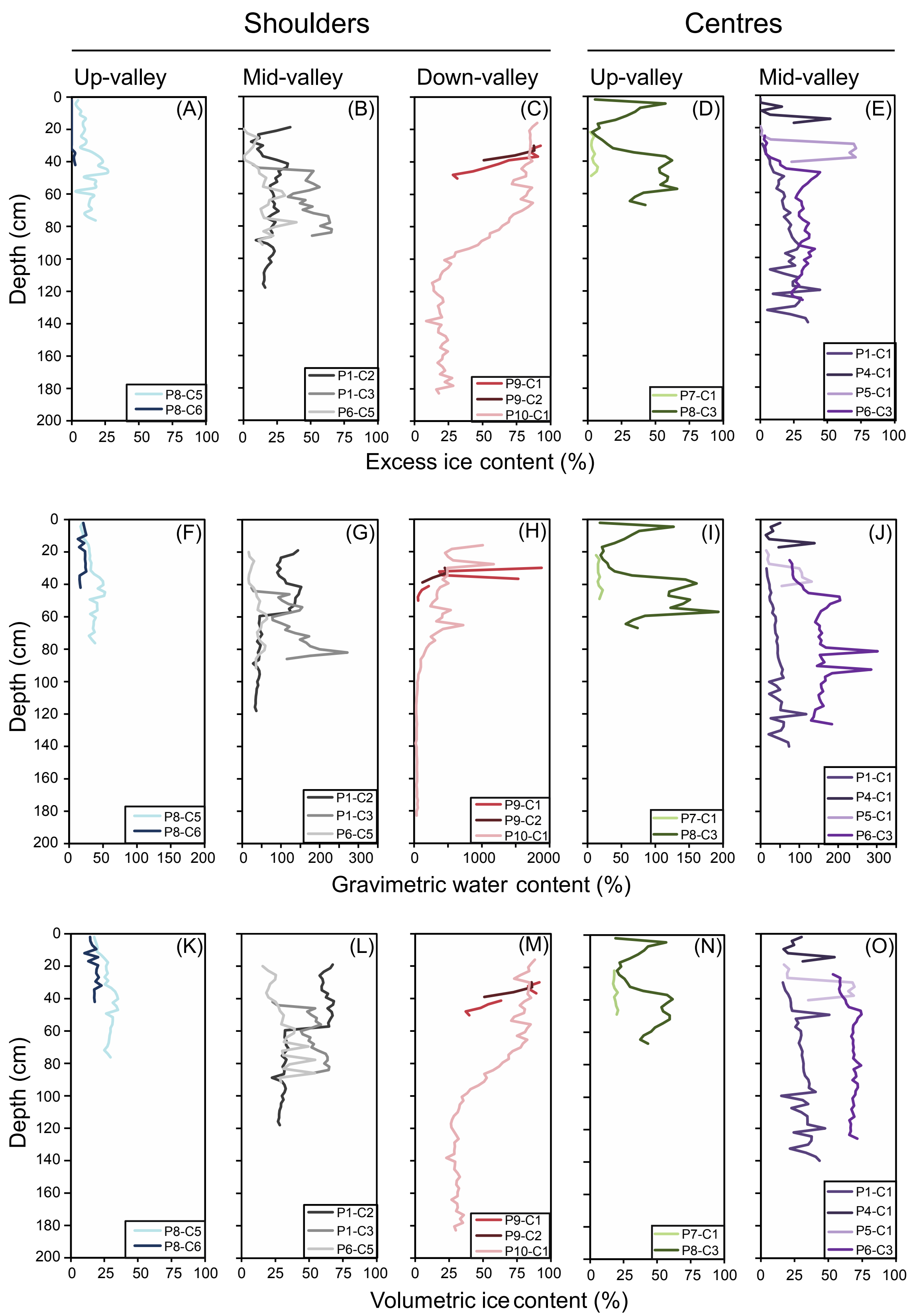

Figure 26: Distribution of excess ice content (%) (A, B, C, D, E), gravimetric water content (%) (F, G, H, I, J) and volumetric ice content (%) (K, L, M, N, O) in the shoulders (left) and centres (right) of up, mid and down-valley polygons in University Valley.

Figure 27 compares the median ice content for the top 20 cm of ice bearing permafrost in the centres and shoulders of the investigated polygons arranged at increasing distance from University Glacier. The median excess ice content and GWC in the top 20 cm of ice bearing permafrost in the centres of the seven polygons ranged from 3.4 to 37% and 16 and 104%, respectively. The median excess ice content and GWC in the top 20 cm of ice bearing permafrost in the shoulders of the eight polygons ranged from 0 to 85% and 22 to 495%, respectively. The median GWC, VIC and excess ice content in the shoulders of the polygons significantly increased down valley; but no significant trend was apparent in the centre cores along a down-valley transect (Table 18).

Figure 28 compares the median ice content in the entire cores taken from the centres and shoulders of the investigated polygons arranged in increasing distance from University Glacier. The median excess ice content and GWC in the centres of the eight polygons ranged from 3.4 to 35.1% and from 16.7 to 152.8%, respectively. However, linear regression analysis indicated that the visible decreasing trend in excess ice content and GWC (Figure 28) in the centres of the polygons with increasing distance from University Glacier was not statistically significant. Conversely, the median excess ice content and VIC in the shoulders of the polygons significantly increased down-valley (Table 19). For example, the median excess ice content in the polygons situated in lower University Valley was > 60%; whereas, the polygons located in the upper and central portions of the valley had < 40% excess ice.

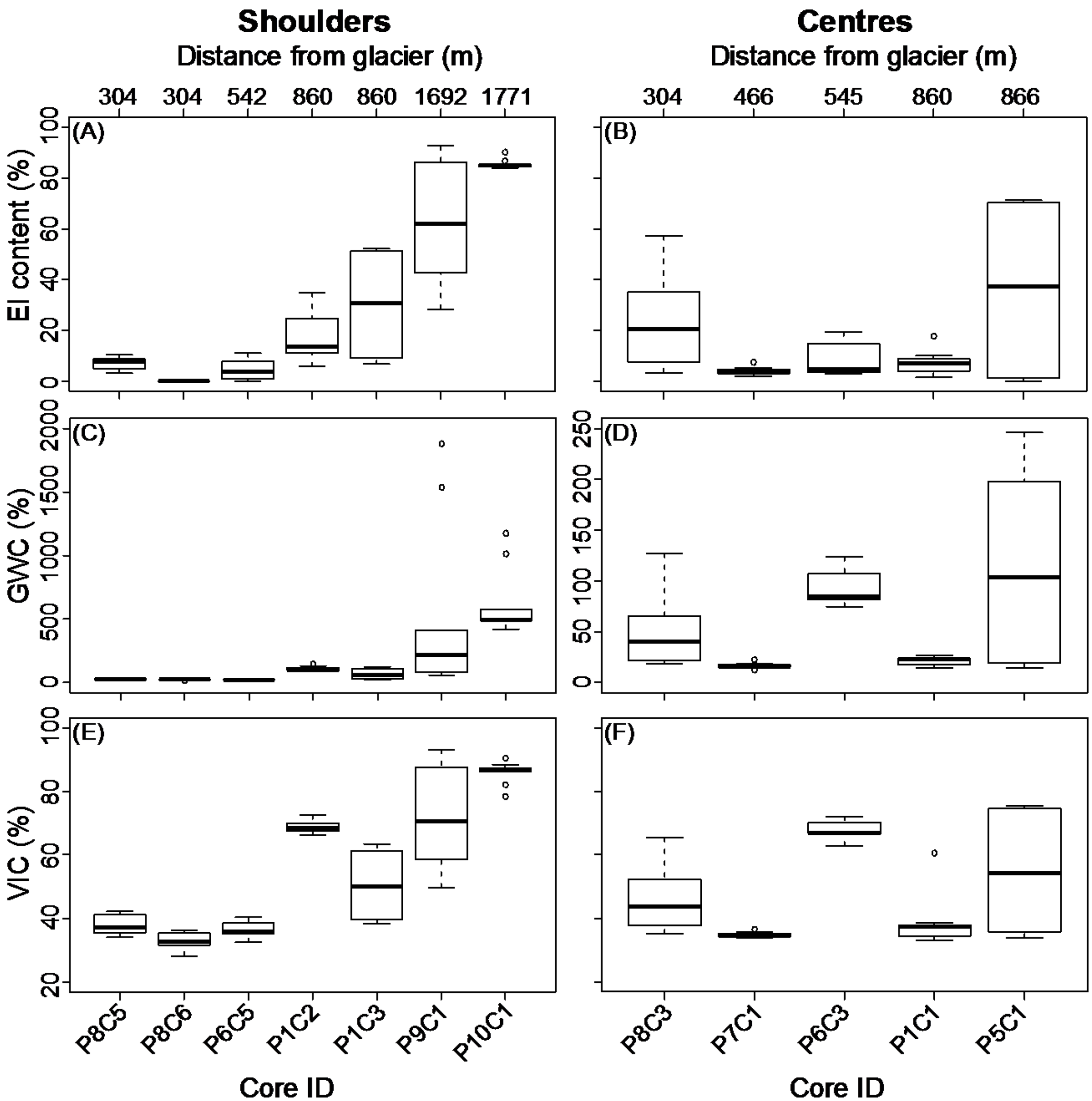

Figure 27: Boxplot illustrating the median excess ice content (EI, %) in the A) shoulders and B) centres of polygons in University Valley; boxplot illustrating median gravimetric water content (GWC, %) in the C) shoulders and D) centres of polygons in University Valley; boxplot illustrating the median volumetric ice content (VIC, %) in the E) shoulders and F) centres of polygons in University Valley in the top 20 cm of the permafrost cores arranged at increasing distance from University Glacier. Distances are measured from the “Glacier core” point indicated in Figure 7.

Table 18: Regression coefficients between the down-valley distance from University Glacier and median excess ice content (EI content), gravimetric water content (GWC) and volumetric ice content (VIC) in the top 20 cm of ice-bearing permafrost in the centres and shoulders of polygons in University Valley. Values significant at a 95 per cent level are bolded.

Shoulders				
	Slope	Intercept	r^2	*p*
EI content	17.8516	387.8144	0.9191	**0.0006**
GWC	3.0693	495.508	0.7688	**0.0095**
VIC	26.6247	-547.043	0.8453	**0.0034**
Centres				
	Slope	Intercept	r^2	*p*
EI content	5.327807	530.7498	0.0951	0.6135
GWC	2.1042	496.2804	0.1080	0.5898
VIC	1.3892	542.4315	0.0056	0.9051

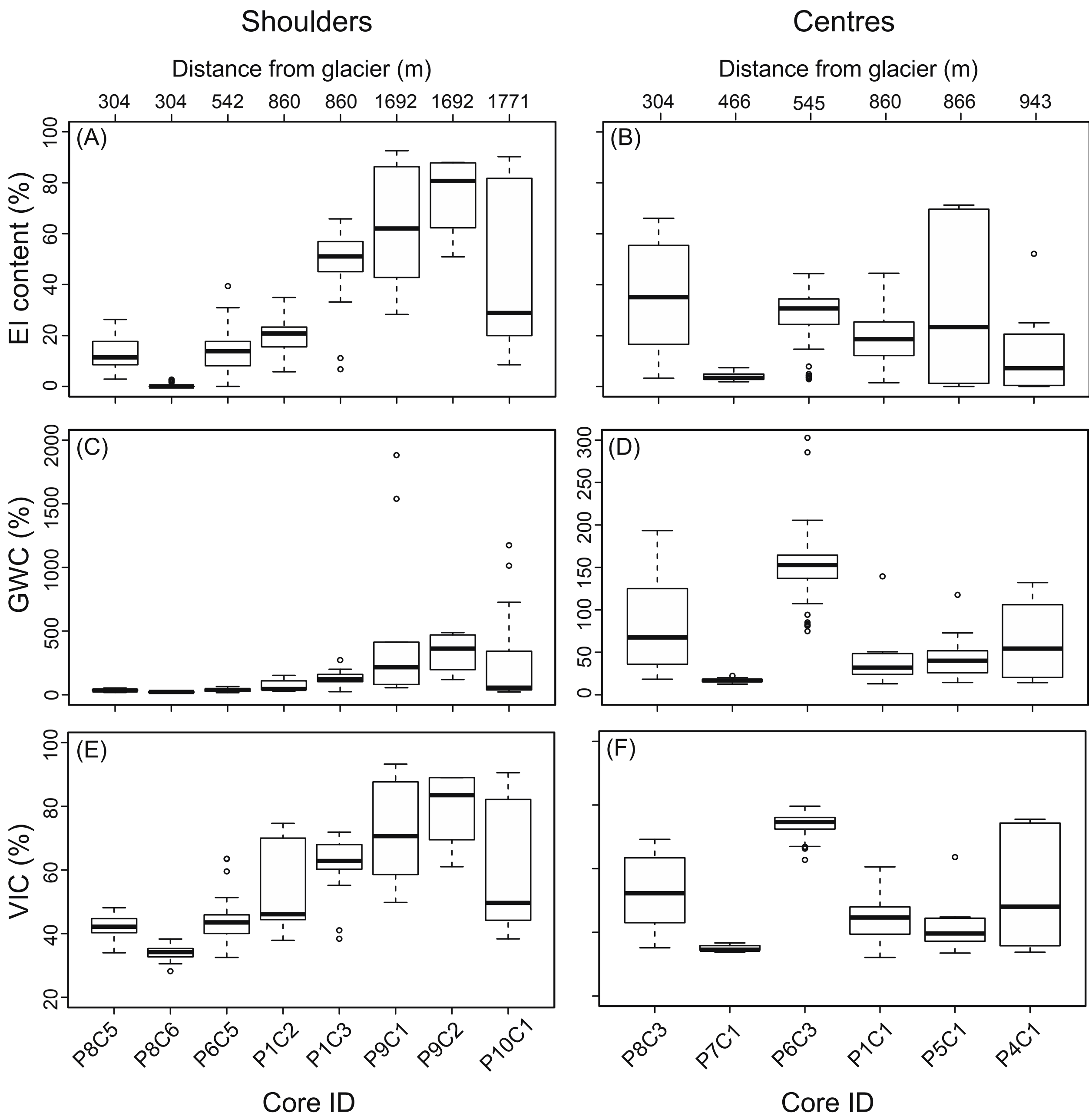

Figure 28: Boxplot illustrating the median excess ice content (EI, %) in the A) shoulders and B) centres of polygons in University Valley; boxplot illustrating median gravimetric water content (GWC, %) in the C) shoulders and D) centres of polygons in University Valley; boxplot illustrating median volumetric ice content (VIC, %) in the E) shoulders and F) centres of polygons in University Valley for the entire permafrost cores arranged at increasing distance from University Glacier. Distances are measured from the "Glacier core" point indicated in Figure 7.

Table 19: Regression coefficients between the down-valley distance from University Glacier and median excess ice content (EI content), gravimetric water content (GWC) and volumetric ice content (VIC) in the entire ice-bearing permafrost cores in the centres and shoulders of polygons in University Valley. Values significant at a 95 per cent level are bolded.

	Slope	Intercept	r^2	*p*
Shoulders				
EI content	0.0355	-1.6217	0.6071	**0.0227**
GWC	0.1305	-19.3631	0.4646	0.0626
VIC	0.0199	34.0804	0.5664	**0.0312**
Centres				
	Slope	Intercept	r^2	*p*
EI content	-0.0193	32.5533	0.1599	0.4321
GWC	-0.0530	95.7349	0.0812	0.5840
VIC	-0.0147	58.7443	0.0749	0.5999

4.3. Identification of cryostructures and derived volumetric ice content (CTVIC) through computed tomodensitometric scanning

4.3.1. Identification of cryostructures

Based on the stack of binary images of the CT-scans (e.g. Figure 29; Figure 30), structureless, suspended and crustal cryostructures were identified for six cores (P8-C3, P8-C6, P7-C1, P6-C5, P1-C1 and P2-C2) in University Valley. The cryostructures were predominantly composite in nature as different types were observed at the same depth. For example, a structureless cryostructure was often observed alongside suspended and crustal cryostructures. A structureless cryostructure was observed at all depths for the imaged core sections however, suspended and crustal cryostructures were not as frequently observed. Reticulate, layered and lenticular cryostructures were not observed in the cores. A full table of the depths at which each cryostructure was observed, as per Murton and French (1994), is provided in Appendix 6.

Structureless, crustal and suspended cryostructures were observed within the P8-C3 core section (44 cm segment; 2 to 47 cm depth) (Figure 31A). A crustal cryostructure was identified throughout the core except at 28 cm, 34 cm and 43 cm depths. Suspended cryostructures were more frequently observed in the uppermost section (up to 25 cm depth) of the core, with the exception of the 3 cm, 22 cm and 25 cm depths. Below 25 cm, a suspended cryostructure was observed less regularly, and only identified at 28 cm, 29 cm and 38 cm depths. An imaging error occurred between 6 cm and 7 cm depth which may have resulted in an error in the identification of observed cryostructures at these depths.

In contrast to the five other cores, suspended cryostructures were not observed in the P8-C6 core (38 cm segment; 2 to 40 cm depth) (Figure 31B). However, a structureless cryostructure was present throughout the core. Crustal cryostructures were identified in the uppermost 13 cm of the core except at 3 cm depth. The abundance of the crustal cryostructure decreased with depth and was only observed at 16 cm, 23 cm and 35 cm depth.

The P7-C1 core (21 cm segment; 22 to 43 cm depth) contained crustal, suspended and structureless cryostructures (Figure 31C). The structureless cryostructure present throughout the core. Compared to P6-C5, P2-C2 and P1-C1, the P7-C1 core had the least number of observed suspended cryostructures as only one was observed at 34 cm depth. Crustal cryostructures, however, were observed throughout the core except at 26 cm, 27 cm and 43 cm depths. The ice rim did not fully surround the pebble/aggregate at all the depths where a crustal cryostructure was observed.

The P6-C5 core (64 cm segment; 20 to 84 cm depth; e.g. Figure 30) contained suspended, structureless and crustal cryostructures (Figure 31D). Structureless cryostructures were present throughout the core. A crustal cryostructure was observed at most depths in the uppermost (21 to 28 cm and 31 to 44 cm depths) and lowermost (65 cm and 70 to 84 cm depths) parts of the core. The middle sections of the core showed crustal cryostructures at specific depths (47 to 50 cm and 52 cm depths). Suspended cryostructures were observed at all depths with the exception of 29 to 32 cm, where neither crustal nor suspended cryostructures were observed. The distribution of suspended cryostructures in P6-C5 became denser with depth. Furthermore, the observed thickness and frequency of ice within the cryostructures appeared greater in P6-C5 than in P1-C1 and P2-C2.

The P1-C1 core segment (62 cm segment; 30 to 92 cm depth) contained structureless, suspended and crustal cryostructures (Figure 31E). Structureless cryostructures were observed throughout the core segment. Suspended cryostructures were absent from the near surface (ca. 0 to 20 cm depth) but present at multiple depths in the middle section of the core (ca. 52 to 55 cm, 58 to 64 cm, 67 to 69 cm; 71 cm and 73 cm depths). Suspended cryostructures were observed throughout the lower section of the core (75 to 92 cm depth) with the thickness of the cryostructure generally increasing with depth. Crustal cryostructures were observed at two depths in the near surface (32 cm and 49 cm); however, the ice rim did not entirely surround the clast at 32 cm depth. Crustal cryostructures were present in the middle section of the core segment, although observed less frequently than the suspended cryostructure (ca. 53 cm, 54 cm, 57 cm, 70 cm and 71 cm depths), and absent from the end of the core segment (72 to 92 cm depth).

The P2-C2 core (28 cm segment; 20 to 48 cm depth) also contained crustal, suspended and structureless cyrostructures (Figure 31F). Structureless cryostructures were present throughout the core. A suspended cryostructure was only observed at 31 and 32 cm depth and both were thinner than those observed in the P1-C1 core. A crustal cryostructure was observed in the upper sections of the core (ca. 21 cm, 24 cm, 27 cm, 28 cm, 31 cm, 32 cm and 34 cm depths). Although neither a crustal nor a suspended cryostructure was observed between 15 and 23 cm depth, crustal cryostructures were observed in the lower sections of the core (44 to 46 cm depth). Many of the observed ice rims did not fully surround their pebbles/clasts.

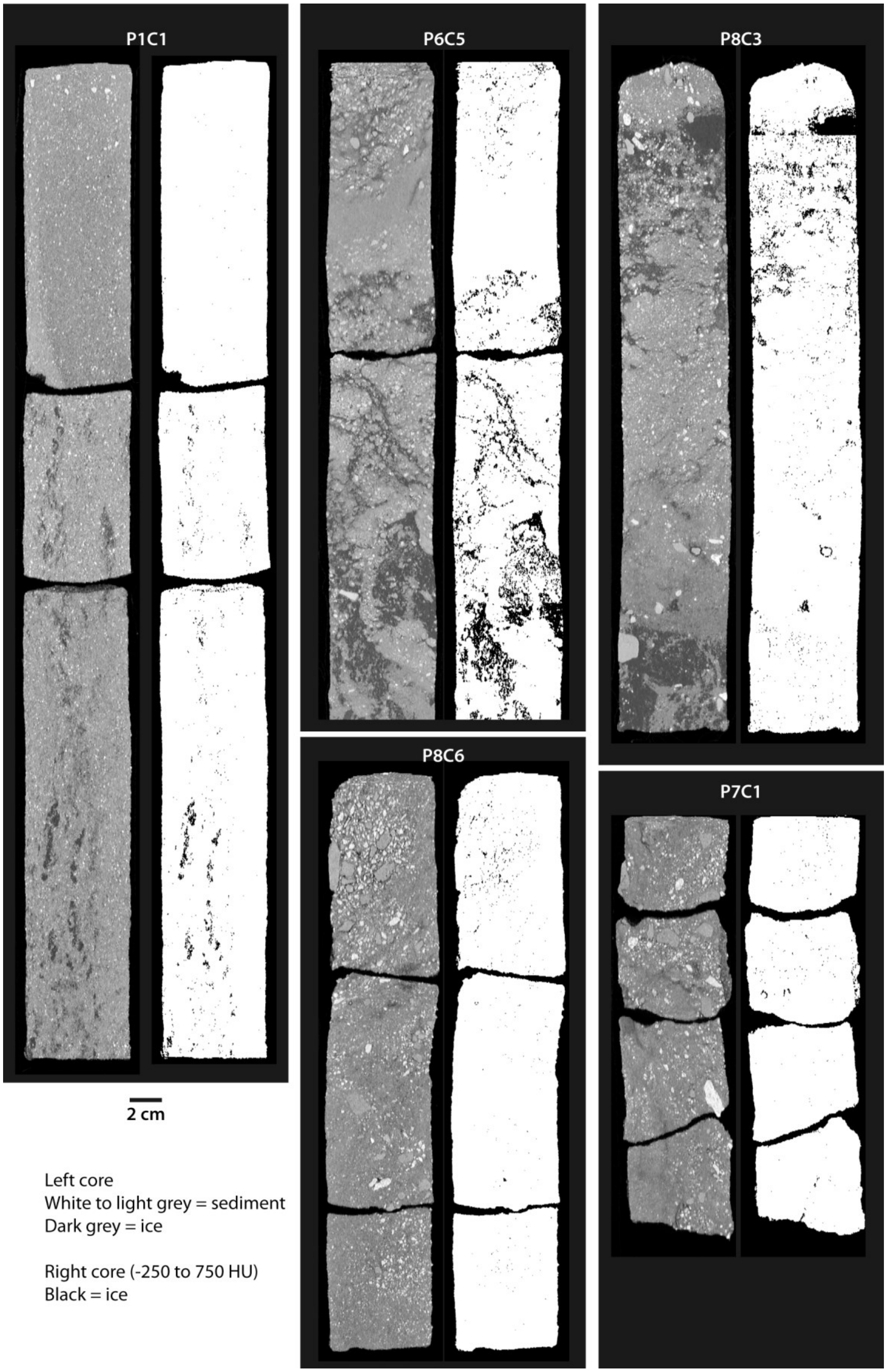

Figure 29: Montage of sample binary image slices for cores P1-C1, P6-C5, P8-C3, P8-C6 and P7-C1 illustrating crustal, suspended and structureless cryostructures.

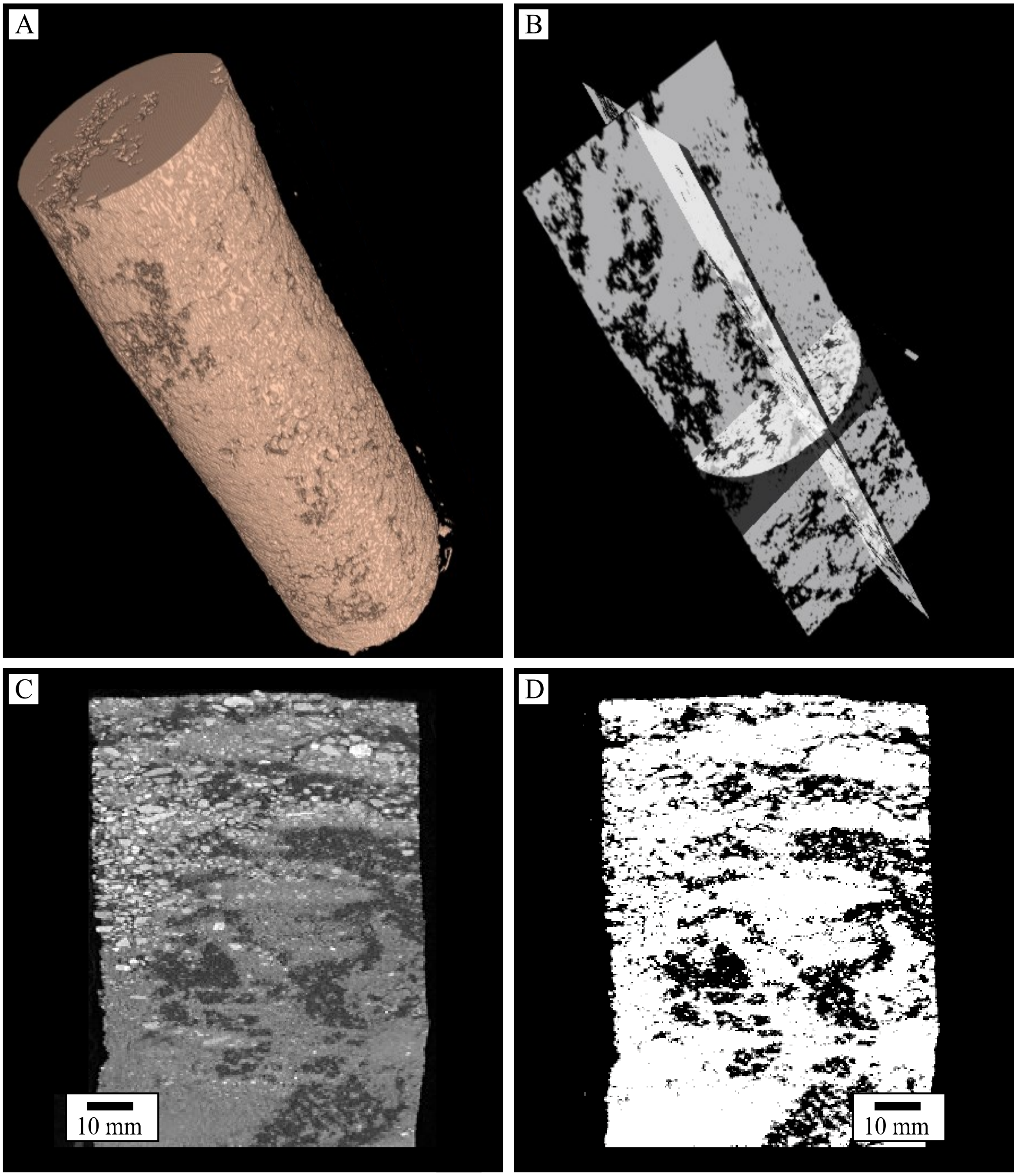

Figure 30: Montage of processed CT scan images of the 45 to 70 cm depth section of core P6-C5. A) 3D view projection of core section, B) Orthogonal reconstruction view of core section, C) contrast enhanced view of slice XZ322 on z axis, D) threshold for ice applied to slice XZ322 on z axis. The darker tones in each image are representative of ice in the core section.

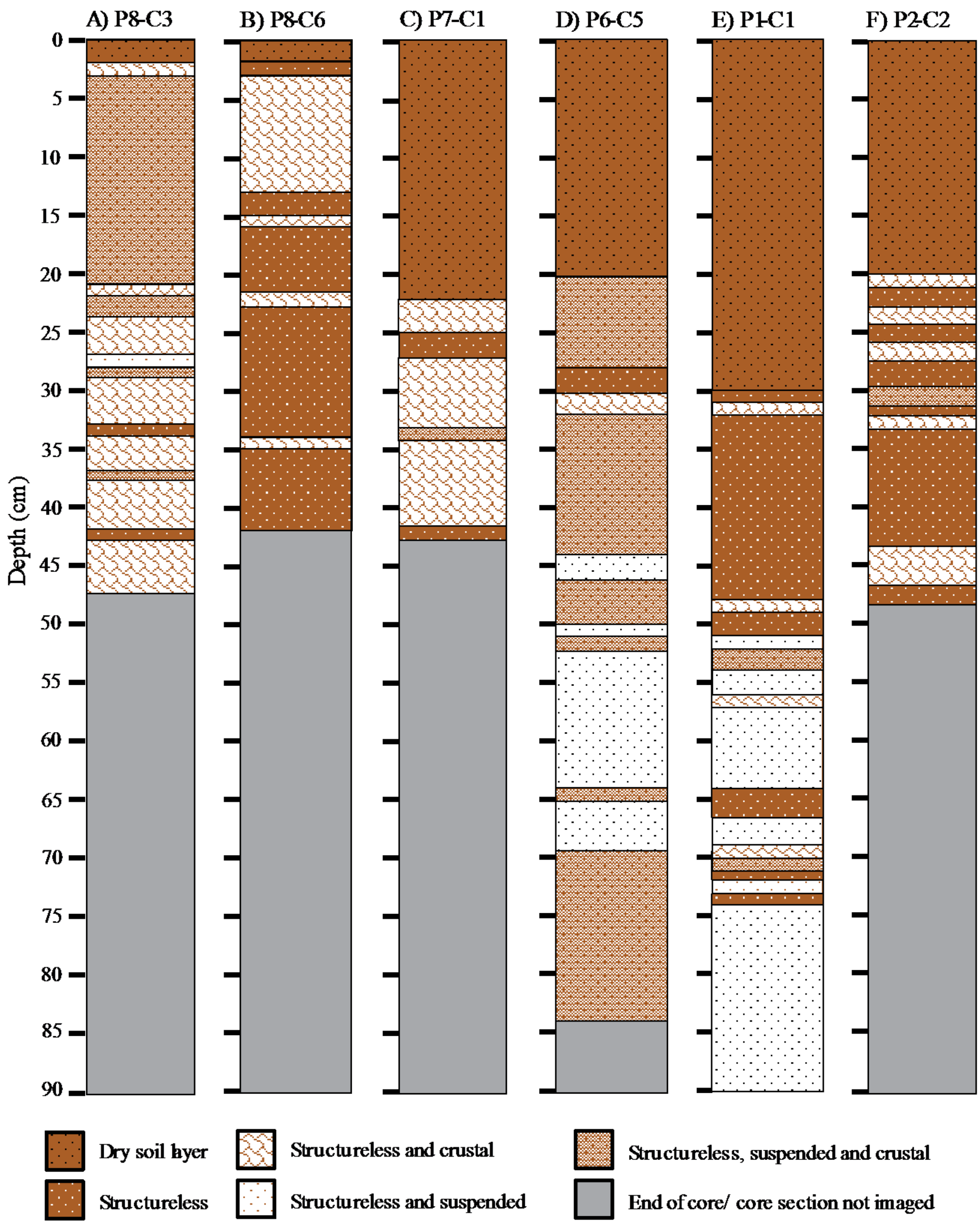

Figure 31: Schematic illustrating the depths at which cryostructures were observed within cores P8-C3, P8-C6, P7-C1, P6-C5, P1-C1 and P2-C2.

4.3.2. Derived volumetric ice contents (CTVIC) results from the binary CT-scan images

The volumetric ice content values derived from the stack of binary images for each CT scanned core (CTVIC) were plotted alongside the measured excess ice and volumetric ice contents for the associated core (Figure 32). Figure 32 illustrates that CTVIC largely underestimated the measured VIC values and more closely followed the distribution of excess ice with depth. CTVIC values were removed for depths associated with breaks in the core or where the core did not properly fit within the region of interest as they resulted in a large under or over-representation of pixels associated with ice. Core P8-C3 (Figure 32A) illustrates that the concentration pattern of CTVIC with depth for this core followed closely that of excess ice. CTVIC values and excess ice content for core P6-C5 (Figure 32D) also followed similar concentration patterns with depth; however, CTVIC values were slightly higher than those of excess ice throughout the majority of the core. In both the P8-C6 and P2-C2 cores (Figures 32B and 32F, respectively), CTVIC values were higher and illustrated more pronounced variations than excess ice where excess ice content values were 0%. However, the two variables showed similar distributions with depth as excess ice became present in the core. Cores P7-C1 and P1-C1 (Figures 32C and 32E, respectively) both illustrate similar concentration patterns between CTVIC and excess ice with depth, albeit CTVIC values both slightly over and underrepresent excess ice content at specific depths.

Figure 33 illustrates the relation between the CTVIC values averaged over the same depth interval as the measured volumetric ice and excess ice contents of the samples from the cores. The CTVIC and volumetric ice and excess ice content values can be fitted to linear regressions ($y = 0.4271x + 35.264$, $r^2 = 0.64$, $n = 92$; $y = 0.6777x + 2.6059$, $r^2 = 0.69$, $n = 92$, respectively).

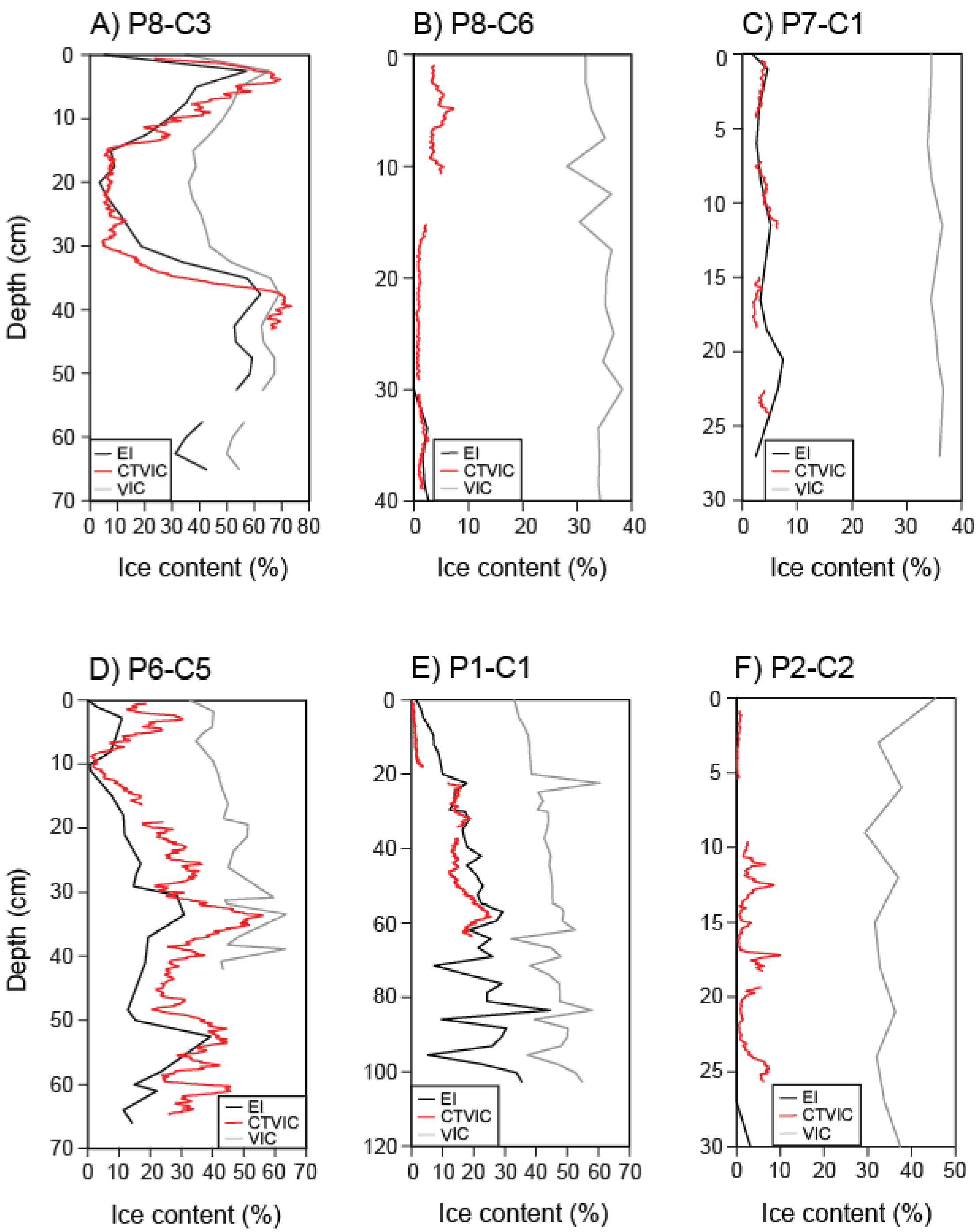

Figure 32: Measured excess ice content (EI; %), measured volumetric ice content (VIC; %) and volumetric ice contents derived from CT scan image analysis (CTVIC; %) for the A) P8-C3 (centre of P8), B) P8-C6 (left shoulder of P8), C) P7-C1 (centre of P7), D) P6-C5 (left shoulder of P6), E) P1-C1 (centre of P1) and F) P2-C2 (deflation surface of P2) cores in University Valley.

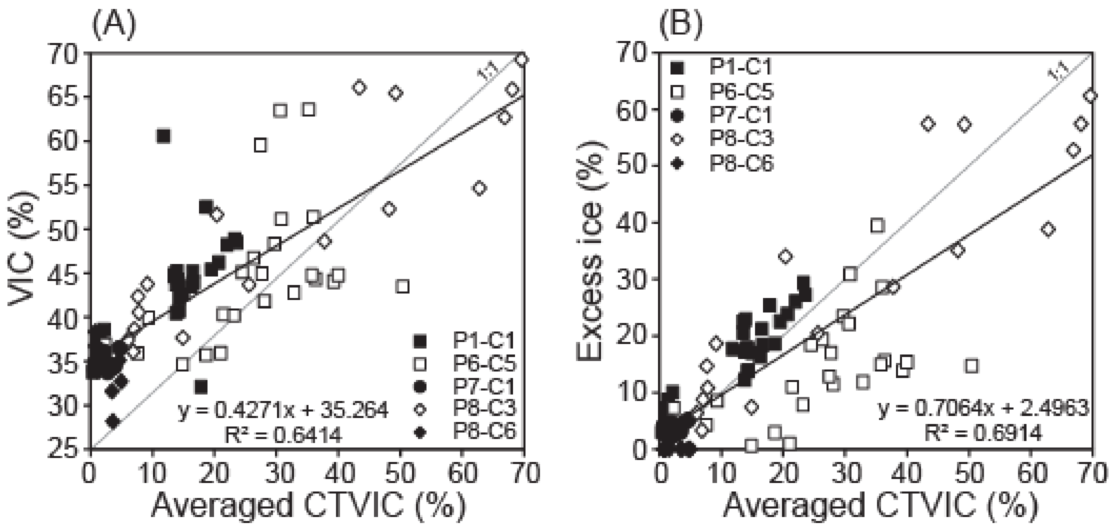

Figure 33: Graph illustrating the CTVIC (%) values averaged over the same depth interval as (A) the measured volumetric ice content (%) and (B) the measured excess ice content (%) for the polygon centre cores (P1-C1, P7-C1 and P8-C3) and shoulder cores (P6-C5, P8-C6).

5. Discussion

5.1. Digital processing and analyses of permafrost core CT-scans to derive ice content and cryostructures

5.1.1. Deriving ice contents from binary CT-scanned images

CT-scanned image analyses of ice-bearing permafrost have previously been used to extract and quantify VIC (CTVIC) in permafrost in palsas in northern Quebec and the Klondike region in the Yukon (e.g. Calmels and Allard, 2004; Calmels and Froese, 2009; Calmels *et al.*, 2010). In the six scanned cores from University Valley, the CTVIC and measured excess ice content showed a statistically significant positive linear relation ($r^2 = 0.69$; $p < 0.02$) (Figure 33). Conversely, CTVIC was much lower than the measured VIC (not shown). The detection of permafrost components (i.e. ground ice, sediments, gas inclusions) in CT-scanned images is limited to components that are greater than the pixel resolution of the image (0.4 mm) (e.g. Calmels and Allard, 2004). Since the average porosity of the medium sand in University Valley is ca. 0.42 ± 0.9 (Lacelle *et al.*, 2013), the pore space of the sediments is similar to the pixel resolution and the material found within the pore space cannot be spatially resolved by the CT-scanned image. As such, CTVIC in ice-bearing permafrost provides a valuable high-resolution approximation of the presence, distribution and abundance of excess ice in the mineral soils in University Valley, and other regions in the MDV (e.g. Figure 32).

5.1.2. Cryostructures in a cold and hyper-arid environment

Three types of cryostructures were observed in the ice-bearing permafrost in the six polygons in University Valley as per Murton and French (1994): structureless, suspended and crustal. The application of Murton and French's (1994) cryostructural classification scheme was appropriate in a hyper-arid environment. However, the differentiation between a structureless and suspended cryostructure was somewhat ambiguous at certain investigated depths. The difficulty of differentiating between the two cryostructures was a result of the presence of ice in the binary image larger than the surrounding pore ice (structureless cryostructure) without evidence of suspended aggregates (e.g. Figure 34). In these circumstances, the lack of suspended aggregates resulted in the classification of a structureless cryostructure. The inclusion of an additional cryostructure to address the distinction between the two sizes of pore ice may be of use in future cryostratigraphic analyses in the MDV. Kanevskiy *et al.* (2011; 2013; 2014) included the porphyritic (porous visible) cryostructure in their cryostratigraphic analyses in an Itkillik River exposure in northern Alaska and the Beaufort Sea Coast of Alaska. The *porphyritic* cryostructure is applied to random inclusions of visible ice that fill large pores, commonly observed in sandy soils, and sometimes accompanied by a structureless cryostructure. The CT scanned cores included multiple examples of cryostructures that could be defined as porphyritic (e.g. Figures 29, 30, 34). As such, porphyritic cryostructures should be considered in future studies in the MDV representing ice occupying larger pore spaces, visible to the naked eye and lacking observable suspended aggregates.

Previous Arctic studies by Murton and French (1994) and French and Shur (2010) have indicated that the crustal, structureless and suspended cryostructures form during the freezing of liquid water. For example, it has been suggested that structureless cryostructures form from the freezing of pore water in sands and gravels. The formation of suspended cryostructures remains elusive as the mechanism(s) by which soil aggregates are suspended during ice segregation or injection is(are) unclear. However, a suspended cryostructure can also be present in debris-rich basal glacier ice. The crustal cryostructure is a result of ice segregation around frost-susceptible clasts and is typically observed just below the permafrost table (French and Shur, 2010).

Polygon 8 is situated in the PCZ characterized by air and ground surface temperatures always below 0°C. Lapalme *et al.* (2015) found that the δD-$\delta^{18}O$ for P8-C3 was distributed along a regression slope resembling, but shifted lower than, the local meteoric line as a result of low D-excess. This distribution has previously been attributed to vapour deposition into the soil (Lacelle *et al.*, 2013; Fisher and Lacelle, 2014). Consequently, the structureless cryostructure in P8-C3 likely originated from water vapour diffusion and deposition in the pore spaces of the soil. Additionally, the continual diurnal and annual ground temperature cycles of the cryotic soils may result in fractures and cracks. These cracks could fill with ice formed from water vapour deposition, enriching the soil with ice contents above pore-filling capacity. The combination of vapour diffusion and deposition in the pore space and larger thermal cracks and fractures may therefore have caused the suspended and crustal cryostructures observed in the cores. The presence of liquid water is possible in both the transition zone and NCZ (Lacelle *et al.*, 2015); therefore cryostructures in these zones could form through the infiltration of liquid water, water vapour diffusion and deposition or a combination of both processes. Therefore, as the ground ice in cryostructures in University Valley can form either vapour diffusion or liquid water, care should be taken when inferring the process responsible for the formation of cryostructures in a cold and hyper-arid environment when drawing on studies based in most Arctic regions (e.g. Murton and French, 1994; French and Shur, 2010).

A crustal cryostructure, the least frequently observed in the Arctic (e.g. French and Shur, 2010), was the 2nd most commonly observed cryostructure in the CT scanned cores, being present in more than 50% of the investigated depths (131/256 investigated centimeters; Appendix 6). This suggests that at sites composed of coarser grained material, where water vapour diffusion and deposition can be responsible for the formation of ground ice, crustal cryostructures may be more commonly encountered. A study from the Beaufort Sea coast of Alaska (Kanevskiy *et al.*, 2013) observed crustal cryostructures to be commonly associated with structureless cryostructures in soil textures predominantly of gravelly sand. The presence of structureless cryostructures in conjunction with crustal cryostructures suggests a transition from the crustal cryostructure to a suspended cryostructure. This observation is similar to those made in University Valley as a structureless cryostructure was present at all depths where a crustal cryostructure was observed.

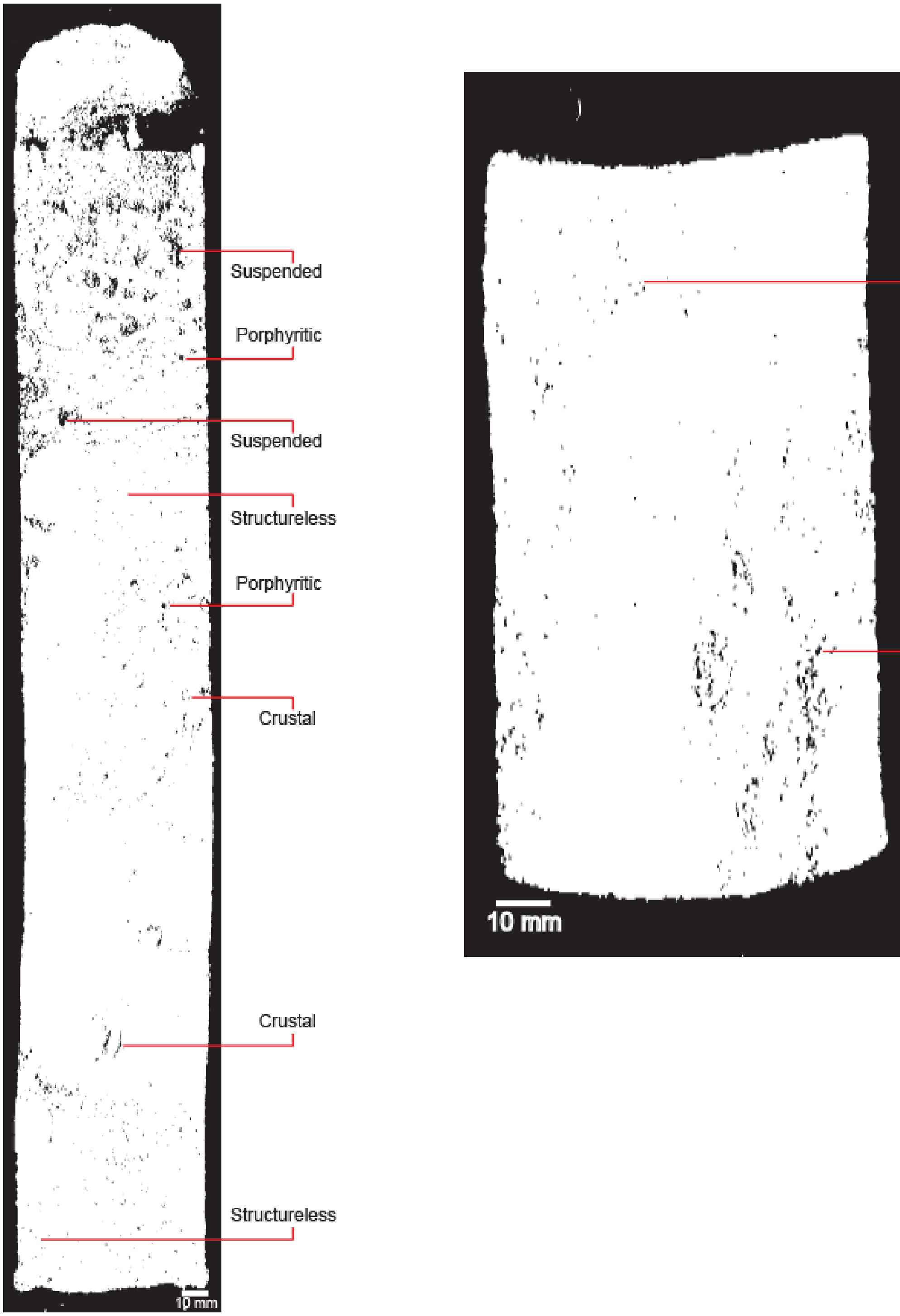

Figure 34: Left: Binary image slice (XZ232) of the full P8-C3 core showing composite cryostructures including porphyritic, crustal, suspended and structureless types. Right: Binary image slice (XZ257) of a section of the P1-C1 core (21-34 cm depth) illustrating composite porphyritic and structureless cryostructures.

5.2. Relation between gravimetric water content and soil texture

Regression analysis between GWC and fines, sand and gravel soil fractions yielded low r-squared values (0.026, 0.029 and 0.032, respectively), none of which were statistically significant (p-values = > 0.05; Figure 35). These results suggest that soil texture does not greatly influence the variability in GWC in University Valley. This conclusion contrasts with studies from western Arctic, Canada, where, for example, Kokelj and Burn (2005) documented an inverse association of sand content and the ice content of near-surface permafrost. O'Neil and Burn (2012) recorded a visible, albeit not statistically significant, relationship between soil texture and ice enrichment as excess ice content in near surface (50 cm) permafrost generally increased with increasing fine grain content.

In University Valley, a relation between GWC and excess ice content for the sandy soils was observed ($r^2 = 0.79$, p-value = < 0.05). However, further examination of the linear fit between the two variables suggested that the residuals were not normally distributed. As such, the significance of this relationship could not be tested despite the low p-value. Comparatively, Kokelj and Burn (2005) documented a statistically significant relation between excess ice content and GWC in silty loam sediments in northwestern Arctic Canada. Conversely, Morse *et al.* (2009) suggested that the GWC and excess ice are only strongly correlated in soils with organic matter content < 10%. Figure 36 compares the GWC and excess ice content from mineral soils in University Valley and the Kokelj and Burn (2005) study. The two datasets plot along different slopes and y-axis intercept values. The data points for University Valley reach a plateau near the maximum 100% excess ice threshold with increasing GWC; an observation that may account for the lower r^2 value for the University Valley data than for those from Arctic Canada. The different y-intercept values could suggest that the relation between excess ice content and GWC may be dependent on sediment type: medium sand for University Valley and silty loam for the Navy Road region in Arctic Canada.

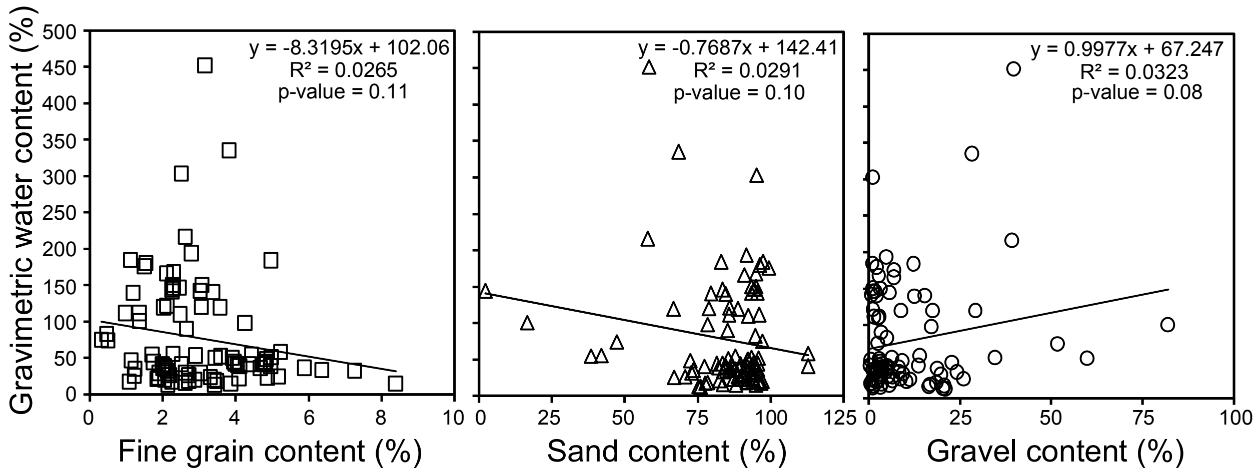

Figure 35: Comparison of gravimetric water content (%) with fine grain (left), sand (centre) and gravel (right) content (%) of permafrost samples taken from University Valley.

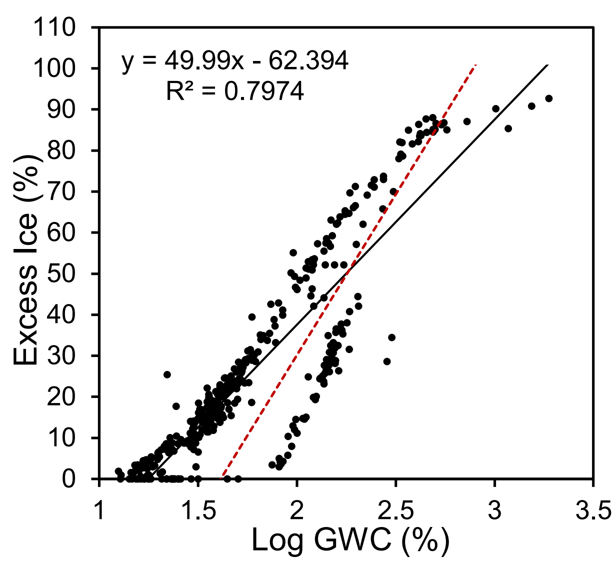

Figure 36: The logarithm of gravimetric water content compared to excess ice content for the predominantly sandy permafrost soil samples taken from University Valley. The dashed red line represents the slope of the regression analysis from Kokelj and Burn (2005) where the relation between log gravimetric water content and excess ice content was described by the equation y = 78.3x – 126.4.

5.3. Factors influencing ground ice variability in University Valley

Ground ice content diverged within an individual permafrost core, between the centre and shoulders of P1 (9 x 20 m), P6 (11 x 21 m) and P8 (13 x 8 m) and along University Valley. These results illustrate that ice content is variable throughout the valley, over a short horizontal distance, within and individual polygon and with depth. The GWC values of the cores taken from University Valley were generally greater than the few previously documented by Levy *et al.* (2008) for Upper Wright Valley situated in the IMZ and CTZ (2.4 – 4.7%, 8.9%, 10.4% and 13.2%). Further, the abundance of excess ice in the University Valley cores was greater than the map of permafrost distribution in the MDV suggests (Bockheim *et al*., 2007; Figure 3, p.11).

A near-surface ground ice map of VIC was created for the top 20 cm and 50 cm of ice-bearing permafrost in University Valley using the core results and the Kriging function in Spatial Analyst in ArcGIS10 (Figure 37). The map shows that the top 20 cm and 50 cm of ice-bearing permafrost in University Valley contain high amounts of ground ice (ca. 41% to 90%) and suggests increasing VIC with distance from University Glacier.

The difference in ground ice content between the University Valley cores could be attributed to the distinct ground surface temperature and RH conditions in the valley. The former is illustrated in Figure 7 (p.15), where two zones with differing ground surface temperatures are defined: i) the perennially cryotic zone and ii) the seasonally non-cryotic zone (Lacelle *et al.*, 2015). The latter is illustrated through the down-valley decrease in mean annual ground surface relative humidity (MAGSRH) in the centre of polygons in University Valley. MAGSRH decreases from $100\%_{ice}$ (expressed as saturated vapour pressure over ice) in the upper portion of the valley, where a thin perennial snow cover is present, to $87\%_{ice}$ in the central portion of the valley (Fisher *et al.*, in review). The high ground surface relative humidity (GSRH) values are notable as previous studies have used much lower RH values (measured above the ground surface) to model ice growth rates by vapour diffusion (e.g. Hindmarsh *et al.*, 1998, McKay *et al.*, 1998, Hagedorn *et al.*, 2007; Kowalewski *et al.*, 2011; Lui *et al.*, 2015).

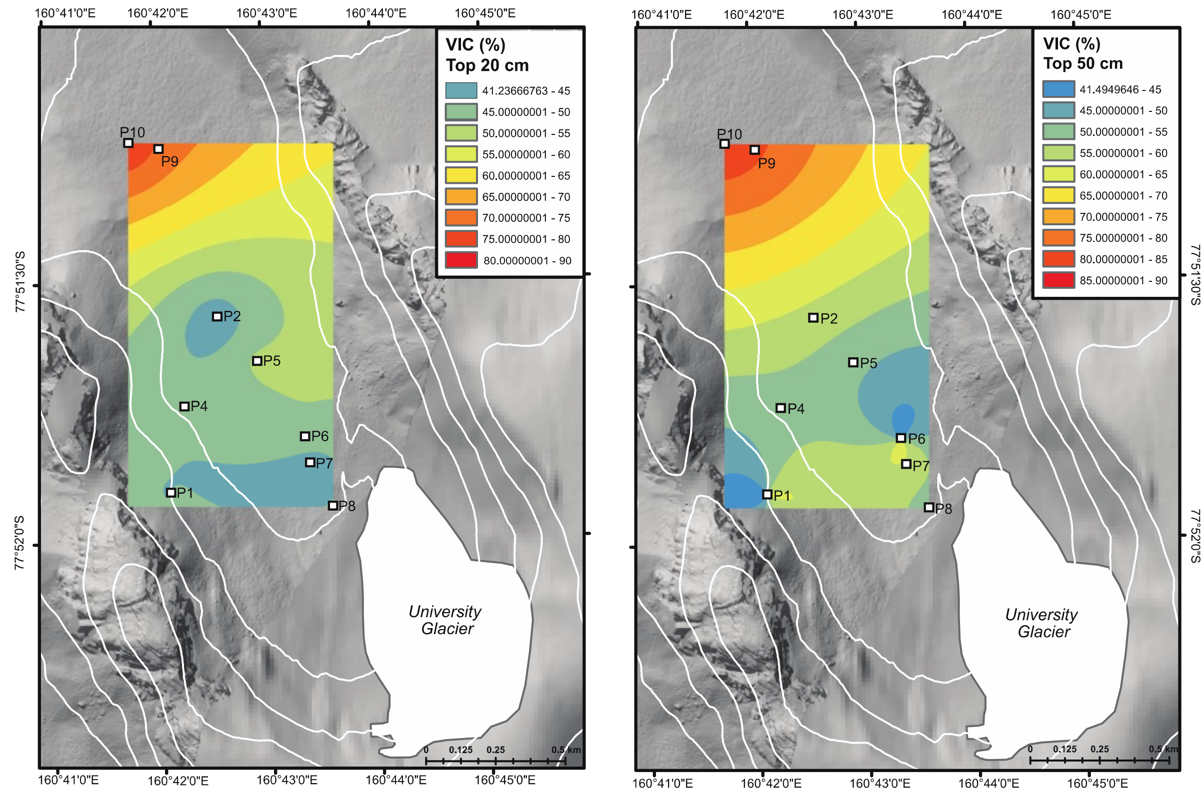

Figure 37: Volumetric ice content (%) in the top 20 cm (left) and 50 cm (right) of ice bearing permafrost in University Valley. The base map was generated using a LiDAR digital elevation model and a 15 m resolution ASTER digital elevation model (http://asterweb.jpl.nasa.gov/data.asp).

5.3.1. Ground ice variability in the seasonally non-cryotic zone (NCZ)

The lower portions of University Valley are mainly located in the NCZ while the areas in the south-east portion of the valley, in closer proximity to University Glacier, are generally located in the PCZ (Figure 7, p.15). Although snow overlies the ground surface near University Glacier, it only occupies the trough of polygons in middle and lower University Valley (e.g. Figure 11, p.36). Additionally, thaw degree hours increased from 0 in the PCZ to 400 near the mouth of the valley as a result of the increase in solar radiation received at the ground surface (Lacelle *et al.*, 2015; Figure 7, p.15). As a result, the snow present in the troughs of the polygons (e.g. Levy *et al.*, 2008; Bockheim *et al.*, 2009; Lacelle *et al.*, 2015; Figure 11, p.36) in the NCZ could partially melt on clear summer days when ground surface temperatures rise above 0°C. In this hypothesis, the shoulders and other areas surrounding the trough of the polygon would become saturated with snow melt water and increase the ice content in the underlying dry permafrost. For example, excavations of sand wedge polygons in Beacon Valley (a larger valley in the Quartermain Range located adjacent to University Valley; Figure 1, p.5) found segregated ice (primarily as ice veins but also including ice lenses) in the sand wedges of polygons. The origin of ice in the trough was suggested to result from snow melt that had accumulated in polygon wedges (Bockheim *et al.*, 2009). This interpretation is reasonable since Beacon Valley experiences ca. 30 days with mean soil surface temperatures > 0°C (TDD ca. 50; Figure 2, p.9) and is largely situated in the NCZ (Lacelle *et al*., 2015). Lacelle *et al.* (2015) also documented evidence of liquid water in University Valley in field photographs showing snowmelt water percolating into the underlying dry permafrost (Figure 38A) and frozen ponds (Figure 38B).

The significant increase in VIC, GWC and excess ice content measured in the top 20 cm of the permafrost cores taken from the shoulders of polygons, the significant increase in VIC and excess ice content measured in the full cores taken from the shoulders of the polygons and the increase in VIC observed down-valley in Figure 37 are likely associated with the change in ground surface temperature zone from the PCZ in upper University Valley to the NCZ down valley. The cores taken from the shoulders of polygons extracted the furthest down-valley (P1-C2, P1-C3, P9-C1, P9-C2 and P10-C1) are located in the NCZ, subjecting them to the possible presence of liquid water and resulting in faster growth and higher contents of ground ice. As the remaining core shoulders (P8-C6, P8-C5, P6-C5) are located in or near the PCZ, they are likely not exposed to snowmelt and subsequently require different processes and greater time periods to reach ice contents above pore filling capacity (e.g. Lacelle *et al.*, 2013).

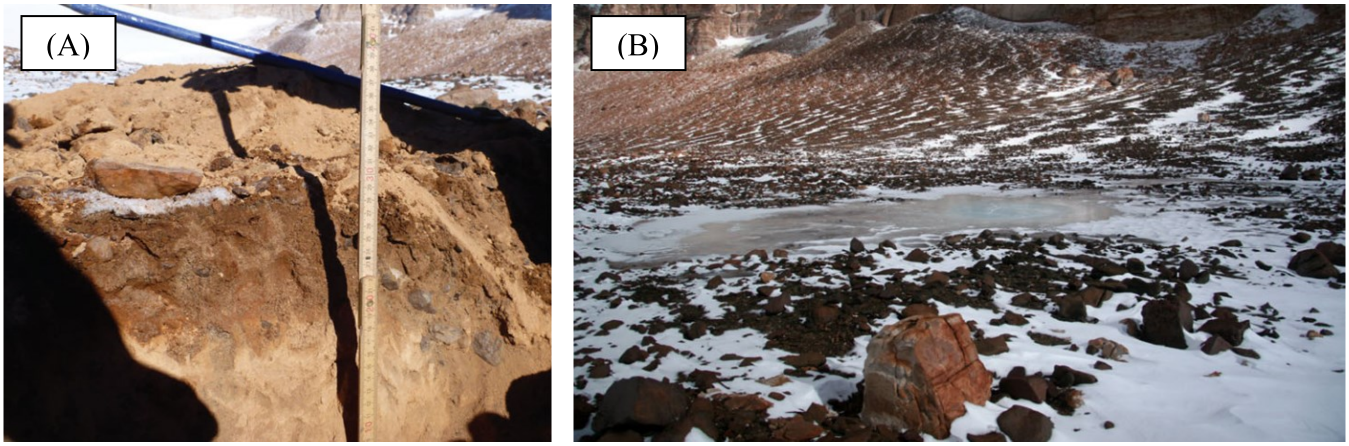

Figure 38: Field photographs of University Valley showing (A) snowmelt water percolating into the dry soil layer and (B) a frozen pond at least 30 cm deep and several metres wide. Source: Lacelle *et al.* (2015).

5.3.2. Ground ice variability in the perennially cryotic zone (PCZ)

Lacelle *et al.* (2013) and Fisher and Lacelle (2014) used the REGO model (a vapour-diffusion and advection model) to predict ice content variation in a 1 m soil column based on soil properties, ground surface temperature and humidity simulating conditions in the PCZ in University Valley. The results of a model run with MAGSRH > 90%$_{ice}$ showed a reasonable fit between the modeled and measured ground ice content distributions for two cores taken from the centres of polygons in the PCZ (Core 5 and Core 7; Figure 7, p.15). These results, coupled with isotopic analyses of Core 5, Core 7 and P8-C3 (Figure 7, p.15), suggested that the near-surface ground ice in these three cores was of water vapour diffusion and deposition origin (Lacelle *et al.*, 2013; Lapalme *et al.*, 2015). These interpretations, coupled with the results for the remaining cores studied in this thesis, may suggest an explanation for the lower ground ice contents measured in the cores taken from the shoulders of the up valley polygons. The lower ground ice content in the up valley polygons' shoulder cores (mainly situated in the PCZ) could be due to the vapour diffusion origin of ground ice in the PCZ compared to the potential for the ground ice in the down valley polygons' shoulder cores to be of liquid water origin.

An example of a ground ice profile from the REGO thermal contraction/expansion model, using input variables similar to those measured from the PCZ in University Valley, is shown in Figure 39 (Lacelle *et al.*, 2013). REGO produced a near surface ice rich layer in the upper most 5 – 10 cm of the ground ice depth profile when using a GSRH input fluctuating between 80 and 95% (similar to the GSRH fluctuations in upper University Valley; Fisher *et al.*, in review). In fact, two cores taken from the centres of polygons in upper University Valley (Core 5 (Lacelle *et al.*, 2013) and P8-C3) showed a near-surface ice-rich zone in their ground ice content depth profiles (Figure 39). As GSRH decreases down-valley, this could account for the lack of a near-surface ice rich zone in the other cores taken from the PCZ (Figure 26, p.69).

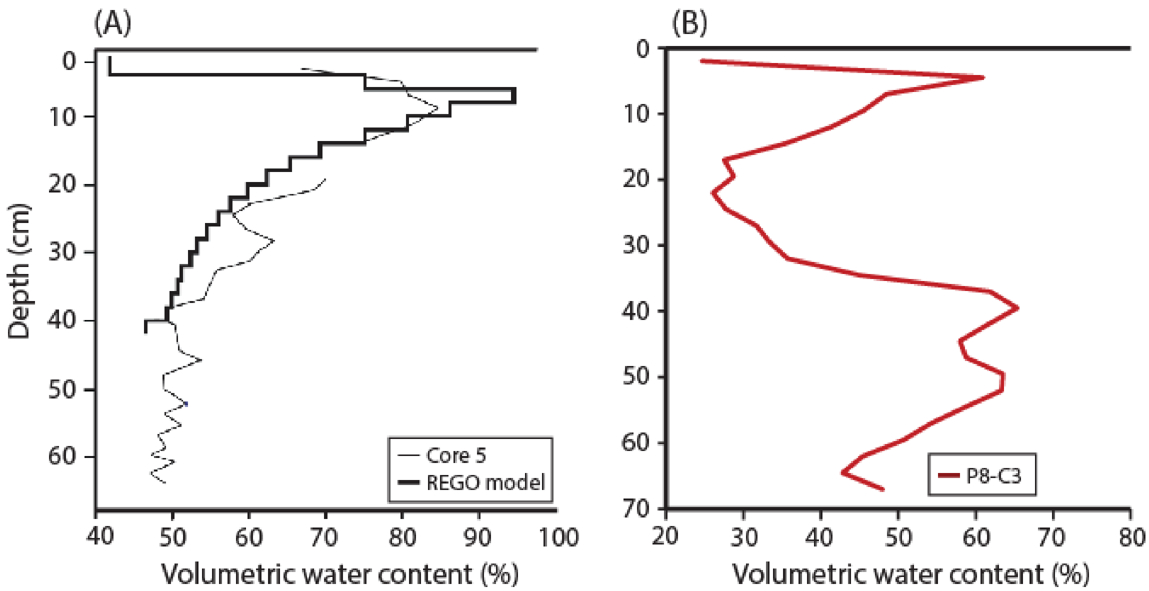

Figure 39: (A) Comparison of measured volumetric water content (%) in Core 5 (centre of polygon) taken from University Valley to the REGO model using variables and conditions similar to those from University Valley (source: Lacelle *et al.* (2013)). (B) Measured volumetric water content (%) in core P8-C3 (centre of polygon) in University Valley

Lacelle *et al.* (2013) estimated that it would require ca. 225 years to fill the pore space of a dry soil column with ice of water vapour diffusion origin under the annual range of climate conditions in University Valley. However, excess ice was present in all of the investigated cores taken from the PCZ in this thesis. The ice enrichment process in University Valley has been suggested to result from thermal waves travelling downward through the dry permafrost and causing the thermal contraction and subsequent expansion of the ice-bearing permafrost below. The resulting cracks would increase the pore-filling capacity of the ice-bearing soil allowing the growth of excess ice through vapour migration, albeit, at a slower rate of accumulation (Lacelle *et al.*, 2013). Evidence of cracking in the McMurdo Dry Valleys has been documented by Lacelle *et al.* (2011), Fisher and Lacelle (2014) and through the analysis of the CT scanned images (Figure 40).

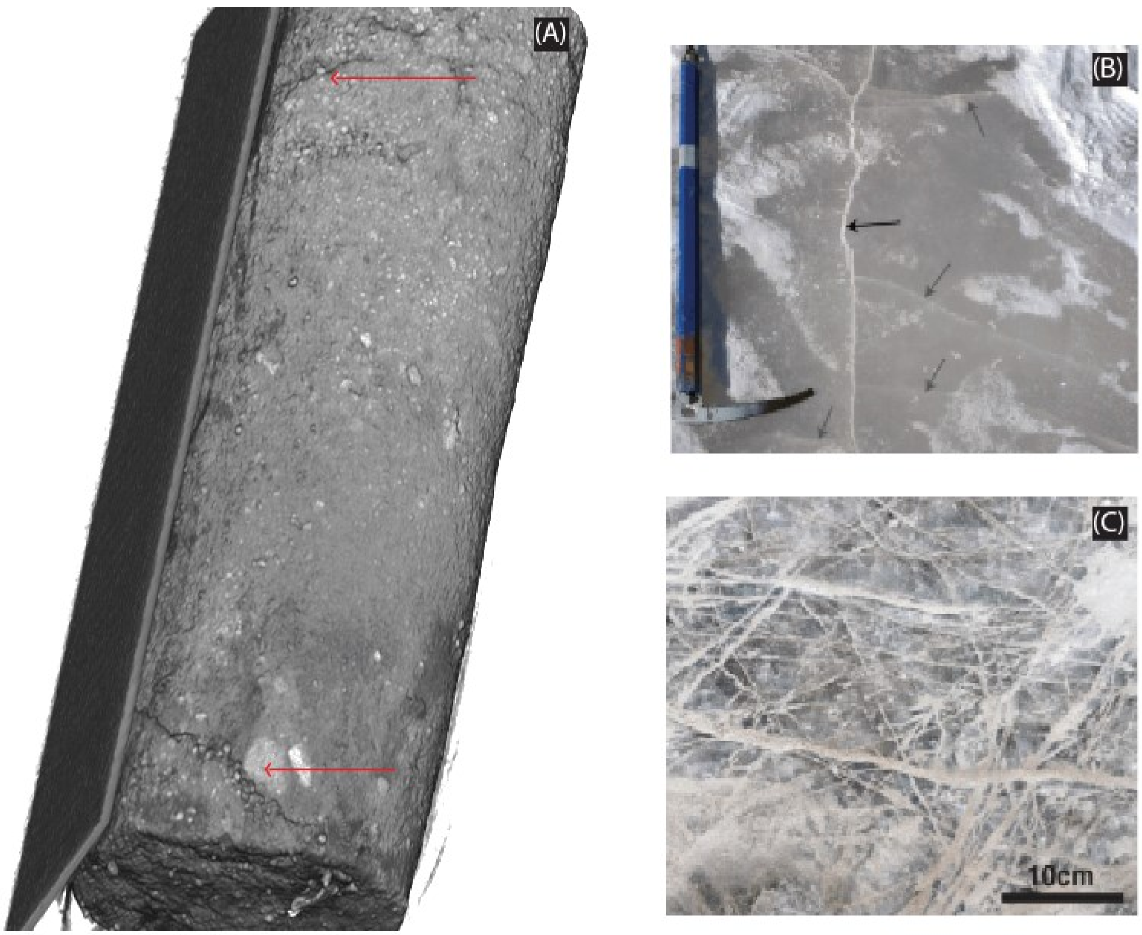

Figure 40: Evidence of cracking in the McMurdo Dry Valleys. (A) Processed CT scanned image illustrating cracks present in part of the P8-C3 University Valley core (0-46 cm core section); (B) cracks in the ice of a frozen pond in the Dry Valleys (source: Fisher and Lacelle (2014)); (C) cracks in massive ice in University Valley exposed under 30 cm of dry soil (source: Lacelle *et al.* (2011)).

5.3.3. Intra-polygon ground ice variability

The observed variations in ground ice content between the centres and shoulders of P1, P6 and P8 may be attributed to their respective ground surface temperature zone and the processes responsible for polygonal development. Levy *et al.* (2008) previously suggested that the water found to be preferentially stored in the interior of wet-top polygons in upper Wright Valley in the MDV was a result of the higher fine grained fraction in the centre of the polygon. However, this is likely not applicable for P1, P6 and P8 as the fine grain content in their respective cores was always < 8% and no relationship was found between GWC and soil texture properties (Figure 35, p.88).

The higher ground ice content in the cores taken from the centres of P6 and P8, located predominantly in the PCZ, may be linked to the processes responsible for the development of the sand-wedge polygons. The cooling of the ground surface and subsurface results in tensile stresses that can cause cracks and fractures in ice-bearing permafrost if the stresses exceed the tensile strength of the frozen soil (Lachenbruch, 1962; e.g. Figure 40). The resulting cracks that open at the surface of the ground are less than a millimeter in width and fine-grained sediments or sand from the adjacent dry soil layer can fall into the opening (Mellon *et al.*, 2014). The continued cycle of polygon development could cause an unstable surface near the shoulder of the polygon, whereas the centre of the polygon would experience less ground disturbance as tensile stresses are largely relieved near the cracks (e.g. Lachenbruch, 1962). As a result, the sediments near the shoulder of the polygon shoulder should experience more disturbance than the centre allowing the centres of the polygons to undergo a continual process of water vapour diffusion and deposition without ground disturbance. Cosmogenic isotope results (Be-10) from polygons in the nearby Table Mountains support this concept with much younger Be-10 ages given to the shoulders of polygons (Dickinson, unpublished data).

Polygon 1, however, contained higher ground ice contents in the cores taken from the shoulders of the polygon. The contrast between the distribution of ground ice in P1 and the two polygons located in the PCZ could be that P1 is located in the NCZ where the presence of liquid water is plausible. The shoulders of the polygons are located adjacent to the commonly snow-covered troughs (Levy *et al*., 2008; Bockheim *et al*., 2009; Lacelle *et al*., 2015; Figure 11, p.36) allowing snowmelt water to infiltrate the soils and freeze. Additionally, fractures and cracks in the ice-bearing permafrost, resulting from the continued diurnal and annual ground temperature cycles of the cryotic soils, could fill with the snowmelt water from the overlying dry permafrost. The centres of polygons located further down-valley are largely snow-free and therefore would not be subject to the same snowmelt water processes that could increase ground ice content.

6. Conclusion

This thesis provided the first comprehensive study of ground ice content in the McMurdo Dry Valleys of Antarctica. The following conclusions were reached based on the results from the 15 permafrost cores taken from University Valley:

1. Ground is present throughout University Valley and its conditions are not homogenous: variable ground ice contents were measured within individual polygons, at increasing distance from University Glacier and with depth. Additionally, the high excess ice contents (ranging between 0 to 93%) measured in the permafrost cores suggested much higher ground ice contents in University Valley than the permafrost classification map for the McMurdo Dry Valleys (Bockheim *et al.*, 2007; Figure 3, p.11) suggests.

2. The median GWC, VIC and excess ice content in the top 20 cm of the permafrost cores taken from the shoulders of the polygons significantly increased from upper to lower University Valley. The median GWC and VIC in the shoulders of the polygons for the entire permafrost cores also significantly increased with distance from University Glacier. The median ice content was higher in the centre than in the shoulders for both P6 and P8 that are predominantly located in the PCZ. The median ice content was higher in the shoulders of P1 (located in the NCZ) than in the centre.

3. The mechanisms responsible for the measured variability in ground ice content in University Valley are likely related to the polygons' respective ground surface temperature zone and differences in GSRH.

4. Based on the stack of binary images of the CT-scans, structureless, suspended, crustal and porphyrtic cryostructures were identified in six cores (P8-C3, P8-C6, P7-C1, P6-C5, P1-C1 and P2-C2) taken from University Valley, all of which were composite in nature. Structureless cryostructures were observed at all investigated depths of the six imaged core sections. The reticulate, layered and lenticular cryostructures were not observed in the cores.

5. The application of Murton and French's (1994) cryostructural classification scheme was appropriate in a hyper-arid environment as it allowed for the classification of the suspended,

crustal and structureless cryostructures observed in the binary images. However, the porphyritic cryostrucure (e.g. Kanevskiy *et al.*, 2011; 2013; 2014) should be included in future cryostratigraphic analyses in the MDV to address the distinction between the two observed sizes of pore ice in the processed CT scanned images. In addition, as ground ice in University Valley can be from either liquid water or vapour diffusion origin (e.g. Lacelle *et al.*, 2013), care should be taken when inferring the process(es) responsible for the formation of crysotructures in cold and hyper-arid environments, particularly when drawing on studies from most Arctic regions.

6. CTVIC was useful in assessing the distribution of excess ice in permafrost cores; CTVIC underestimated the measured VIC in the permafrost cores. CT scan image analysis allowed for the identification of cryostructures at a sub-mm scale, resulting in a more detailed description than would be possible when undergoing field-based cryostructural classification.

7. The mineral soils in University Valley were predominantly classified as medium sand. In each polygon, little changes in grain size distribution were observed with depth. However, the gravel-size sediment content significantly increased down-valley for the shoulders of the polygons only.

Future work concentrating on factors influencing ground ice distribution in the McMurdo Dry Valleys should be undertaken. The ground surface temperature zone map (Lacelle *et al.*, 2015) should be utilized when planning future ground ice quantification work in the MDV that may further contribute to results and hypotheses put forth in this thesis. Valleys that include both the PCZ and NCZ should be investigated (e.g. Turnabout Valley) to determine if similar intra-polygonal and ground surface temperature zone ground ice trends are present. The new findings, in addition to the results from this thesis and Bockheim *et al.* (2007) (Figure 3, p.11), could help contribute to a full and updated ground ice map for the MDV. The ground ice map for University Valley created in this thesis (Figure 37, p.90) does not account for differences in GSRH, ground surface temperature zone and the core location in a polygon. Future mapping should include the aforementioned variables in order to create a more detailed and accurate ground ice content picture.

Salt aggregations within soils may lead to greater water contents than the surrounding soils subsequently influencing geochemical and thermal states (Campbell and Claridge, 2006). McKay (2009) also suggested that films of liquid water could transport water through the active layer of permafrost and possibly through the dry permafrost as a result of the presence of salt. Further, Dickinson and Rosen (2003) suggested that ground ice could form from the downward migration and freezing of briny films. Therefore, the salinity of the soil samples from this study and future studies should be analyzed to determine if a relation between ice content and soil salinity exists.

Isotopic analysis should be run on the remaining supernatant water from the University Valley cores in order to determine the mechanism responsible for the emplacement of ground ice in the cores (i.e. vapour diffusion or liquid water). This information could help determine the origin of the ground ice in the cryostructures observed in all three ground surface zones (PCZ, NCZ and transition zone). Further, RH measurements should be measured or modeled for multiple locations in polygons (trough, shoulder and centre), along a down valley transect and in all three ground temperature zones in order to establish possible micro-variability.

Lastly, cryostructures in cores taken from the shoulders and centres of polygons located in the PCZ, NCZ and transition zone in the MDV should be classified to investigate the effects of liquid water on cryostructural distribution in a cold and dry environment.

References

Acevedo, M. F. 2013. *Data analysis and statistics for geography, environmental science and engineering*. CRS Press Taylor & Francis Group. Boca Raton, FL.

Adlam, L. S., Balks, M. R., Seybold, C. A. and Campbell, D. I. 2010. Temporal and spatial variation in active layer depth in the McMurdo Sound Region, Antarctica. *Antarctic Science, 22*(1), 45-53.

Barrett, P. J. 1981. History of the Ross Sea region during the deposition of the Beacon Supergroup 400–180 million years ago. *Journal of the Royal Society of New Zealand, 11*, 447–458.

Bockheim, J. G. 1982. Properties of a chronosequence of ultraxerous soils in the Trans-Antarctic Mountains. *Geoderma, 28,* 142-152.

Bockheim, J. G. 1990. Soil development rates in the Transantarctic Mountains. *Geoderma, 47,* 59-77.

Bockheim, J. G. 1995. Permafrost distribution in the southern circumpolar region and its relation to the environment: A review and recommendations for further research. *Permafrost and Periglacial Processes, 6*, 27-45.

Bockheim, J. G. 1997. Properties and classification of cold desert soils from Antarctica. *Soil Science Society of America Journal, 61,* 224-231.

Bockheim, J. G. 2002. Landform and soil development in the McMurdo Dry Valleys, Antarctica: A regional synthesis. *Arctic, Antarctic, and Alpine Research, 34(*3), 308-317.

Bockheim, J. G. and Hall, K. J. 2002. Permafrost, active-layer dynamics and periglacial environments of continental Antarctica. *South African Journal of Science, 98,* 82-90.

Bockheim, J. G. and McLeod, M. 2006. Soil formation in Wright Valley, Antarctica since the late Neogene. *Geoderma, 137*, 109-116.

Bockheim, J. G., Campbell, I. B. and McLeod, M. 2007. Permafrost distribution and active-layer depths in the McMurdo Dry Valleys, Antarctica. *Permafrost and Periglacial Processes, 18*, 217-227.

Bockheim, J.G., Campbell, I.B., Guglielmin, M. and Lopez-Martinez, J. 2008. *Distribution of permafrost types and buried ice in ice-free areas of Antarctica.* Paper presented at the 9th International Conference on Permafrost, Fairbanks, Alaska, 125–130.

Bockheim, J. G., Kurz, M. D., Soule, S. A. and Burke, A. 2009. Genesis of active sand-filled polygons in lower and central Beacon Valley, Antarctica. *Permafrost and Periglacial Processes, 20*, 295 – 308.

Bockheim J. G. and McLeod, M. 2015. Soils of central Victoria Land, the McMurdo Dry Valleys. In J. G. Bockheim (Ed.), *The soils of Antarctica* (pp. 117-149). Springer International Publishing.

Bockheim, J. G. (Ed.). 2015. *The soils of Antarctica.* Springer International Publishing, New York.

Burt, T. P. and Williams, P. J. 1976. Hydraulic conductivity in frozen soils. *Earth Surface Processes, 1*, 349-360.

Calmels, F. and Allard, M. 2004. Ice segregation and gas distribution in permafrost using tomodensitometric analysis. *Permafrost and Periglacial Processes, 15,* 367-378.

Calmels, F. and Allard, M. 2008. Segregated ice structures in various heaved permafrost landforms through CT Scan. *Earth Surface Processes and Landforms, 33,* 209-225.

Calmels, F., Delisle, G. and Allard, M. 2008. Internal structure and the thermal and hydrological regime of a typical lithalsa: significance of permafrost growth and decay. *Canadian Journal of Earth Sciences, 45,* 31-43.

Calmels, F. and Froese, D. G. 2009. Cryostratigraphic record of permafrost degradation and recovery following historic surface disturbances, Klondike area, Yukon. In: *Yukon Exploration and Geology 2008*, L.H. Weston, L.R. Blackburn and L.L. Lewis (eds.), Yukon Geological Survey, 85-97.

Calmels, F., Clavano, W. R. and Froese, D. G. 2010. *Progress on X-ray computed tomography (CT) scanning in permafrost studies.* Paper presented at the 6th Canadian Conference on Permafrost and of the 63rd Canadian Geotechical Conference: Calgary 2010, Calgary, Canada, 1353-1358.

Campbell, I. B. and Claridge, G. G. C. 1969. A classification of frigic soils – the zonal soils of the Antarctic continent. *Soil Science, 107*(2), 75-85.

Campbell, I. B. and Claridge, G. G. C. 1975. Morphology and age relationships in Antarctic soils. In: R. P. Suggate and M. M. Cresswell (Eds.). *Quaternary Studies. Royal Society of New Zealand Bulletin, 13*, 83-88.

Campbell, I. B. and Claridge, G. G. C. 1978. Soils and Late Cenozoic history of the Upper Wright Valley area, Antarctica. *New Zealand Journal of Geology and Geophysics, 21*, 635-643.

Campbell, I. B. and Claridge, G. G. C. 1981. Soil research in the Ross Sea region of Antarctica. *Journal of the Royal Society of New Zealand, 11*, 401-410.

Campbell, I. B. and Claridge, G. G. C. 2006. Permafrost properties, patterns and processes in the Transantarctic Mountains region. *Permafrost and Periglacial Processes, 17,* 215-232.

Cheng, G. 1983. The mechanism of repeated segregation for the formation of thick-layered ground ice. *Cold Regions Science and Technology, 8*, 57-66.

Clow, G. D., McKay, C. P., Simmons Jr., G. M. and Wharton Jr., R. A. 1988. Climatological observations and predicted sublimation rates at Lake Hoare, Antarctica. *Journal of Climate, 1*(7), 715-728.

Cold Regions Research and Engineering Laboratory. 2012. Permafrost: Cryostructures. Retrieved from http://permafrosttunnel.crrel.usace.army.mil/permafrost/cryostructures.html.

Cox, S. C., Turnbull, I. M., Isaac, M. J., Townsend, D. B., Smith, B. L. (compilers). 2012. Geology of southern Victoria Land Antarctica. Institute of Geological and Nuclear Sciences, 1:250 000 geological map 22. Lower Hutt, New Zealand, GNS Science. 135 pp.

Dana, G. L., Wharton Jr., R. A. and Dubayah, R. 1998. Solar radiation in the McMurdo Dry Valleys, Antarctica. In J. C. Priscu (Ed.) *Ecosystem Dynamics in a Polar Desert: The McMurdo Dry Valleys, Antarctica, Research Series, 72,* (39-64). Washington, D. C.: AGU.

Denton, G. H., Prentice, M. L., Kellogg, D. E. and Kellogg, T. B. 1984. Late Tertiary history of the Antarctic ice sheet: Evidence from the Dry Valleys. *Geology, 12*(5), 263-265.

Denton, G. H., Sugden, D. E., Marchant, D. R., Hall, B. L. and Wilch, T. I. 1993. East Antarctic ice sheet sensitivity to Pliocene climatic change from a dry valleys perspective. *Geografiska Annaler*, *75A*(4), 155-204.

Dickinson, W. W. and Rosen, M. R. 2003. Antarctic permafrost: An analogue for water and diagenetic minerals on Mars. *Geological Society of America, 31*(3), 199-202.

Dickinson, W. W. *Unpublished data*.

Doran, P. T., McKay, C. P., Clow, G. D., Dana, G. L., Fountain, A. G., Nylen, T. and Lyons W. B. 2002. Valley floor climate observations from the McMurdo dry valleys, Antarctica, 1986-2000. *Journal of Geophysical Research, 107*(D24), ACL 13-1- ACL 13-12.

Fisher, D. A., Reeh, N., Clausen, H. B. 1985. Stratigraphic noise in time series derived from ice cores. *Annals of Glaciology, 7*, 76-83.

Fisher, D. A. and Lacelle, D. 2014. A model for co-isotopic signatures of evolving ground ice in the cold dry environment of Earth and Mars. *Icarus, 243*, 454-470.

Fisher, D. A., Lacelle, D., Pollard, W., Davila, A. and McKay, C. P. Ground surface temperature and humidity, soil airflow and the geothermal gradient determine the ice table depth in University Valley, McMurdo Dry Valleys of Antarctica. *Journal of Geophysical Research. In review.*

Fountain, A. G., Lyons, W. B., Burkins, M. B., Dana, G. L., Doran, P. T., Lewis, K. J., McKnight, D. M., Moorhead, D. L., Parsons, A. N., Priscu, J. C., Wall, D. H., Wharton, R. A. and Virginia, R. A. 1999. Physical controls on the Taylor Valley ecosystem, Antarctica. *Bioscience, 49*, 961–971.

Fountain, A. G., Nylen, T. H., Monaghan, A., Basagic, H. J. and Bromwich, D. 2009. Snow in the McMurdo Dry Valleys, Antarctica. *International Journal of Climatology, 30*(5), 633-642.

Fountain, A. G., Levy, J. S., Gooseff, M. N. and Van Horn, D. 2014. The McMurdo Dry Valleys: A landscape on the threshold of change. *Geomorphology, 225,* 25-35.

French, H. M. 1998. An appraisal of cryostratigraphy in North-West Arctic Canada. *Permafrost and Periglacial Processes, 9,* 297-312.

French, H. and Shur, Y. 2010. The principles of cryostratigraphy. *Earth-Science Reviews*, *101*, 190-206.

Hagedorn, B., Sletten, R. S. and Hallet, B. 2007. Sublimation and ice condensation in hyperarid soils: Modeling results using field data from Victoria Valley, Antarctica. *Journal of Geophysical Research, 112*(F3), F03017.

Hagedorn, B., Sletton, R. S., Hallet, B., McTigue, D. F. and Steig, E. J. 2010. Ground ice recharge via brine transport in frozen soils of Victoria Valley, Antarctica: Insights from modelling $\delta^{18}O$ and δD profiles. *Geochimica and Cosmochimica Acta, 74*, 435-448.

Hindmarsh, R. C. A., van der Wateren, F.M., Verbers, A. 1998. Sublimation of ice through sediment in Beacon Valley, Antarctica. *Geografiska Annaler Series a-Physical Geography 80A*(3–4), 209–219.

Iwahana, G., Takano, S., Petrov, R. E. , Tei, S., Shingubara, R., Maximov, T. C., Federov, A. N., Desyatkin, A. R., Nikolaev, A. N., Desyatkin, R. V. and Sugimoto, A. 2014. Geocryological characteristics of the upper permafrost in a tundra-forest transition of the Indigirka River Valley, Russia. *Polar Science, 8*(2), 96-113.

Jouzel, J., Masson-Delmotte, V., Cattani, O., Dreyfus, G., Falourd, S., Hoffman, G., Minster, B., Nouet, J., Barnola, J. M., Chappellaz, J., Fischer, H., Gallet, J. C., Johnsen, S., Leuenberger, M., Loulergue, L., Leuthi, D., Oerter, H., Parrenin, F., Raisbeck, G., Raynaud, D., Shilt, A., Schwander, J., Selmo, E., Souchez, R., Spahni, R., Stauffer, B., Steffensen, J. P., Stenni, B., Stocker T. F., Tilson, J. L., Werner, M. and Wolff, E. W. 2007. Orbital and millennial Antarctic climate variability over the past 800,000 years. *Science, 317,* 793-796.

Kanevskiy, M., Shur, Y., Fortier, D., Jorgenson, M. T., Stephani, E. 2011. Cryostratigraphy of late Pleistocene syngenetic permafrost (yedoma) in northern Alaska, Itkillik River exposure. *Quaternary Research, 75*, 584-596.

Kanevskiy, M., Shur, Y., Jorgenson, M. T., Ping, C-L., Michaelson, G. J., Fortier, D., Stephani, E., Dillon, M. and Tumskoy, V. 2013. Ground ice in the upper permafrost of the Beaufort Sea coast of Alaska. *Cold Regions Science and Technology, 85*, 56-70.

Kanevskiy, M., Jorgenson, T., Shur, Y., O'Donnell, J. A., Harden, J. W., Zhuang, Q. and Fortier, D. 2014. Cryostratigraphy and permafrost evolution in the lacustrine lowlands of West-Central Alaska. *Permafrost and Periglacial Processes, 25*, 14-34.

Katasonov, E. M. 1969. Composition and cryogenic structure of permafrost. In *Permafrost invesigations in the field.* National Research Council of Canada, Ottawa, Technical Translation 1358, 25-36.

Kawamura, K. Parrenin, F., Lisiecki, L., Uemura, R., Vimeux F., Severinghaus, J. P., Hutterli, M. A., Nakazawa, T., Aoki, S., Jouzel, J., Raymo, M. E., Matsumoto, K., Nakata, H., Motoyama, H., Fujita, S. Goto-Azuma, K., Fujii, Y. and Watanabe, O. 2007. Northern Hemisphere forcing of climatic cycles in Antarctica over the past 360 000 years. *Nature, 448*, 912-916.

Kokelj, S. V. and Burn, C. R. 2003. Ground ice and soluble cations in near-surface permafrost, Inuvik, Northwest Territories, Canada. *Permafrost and Periglacial Processes, 14,* 275-289.

Kokelj, S. V. and Burn, C. R. 2005. Geochemistry of the active layer and near-surface permafrost, Mackenzie delta region, Northwest Territories, Canada. *Canadian Journal of Earth Sciences, 42*(1), 37-48.

Kokelj, S. V., Lacelle, D., Lantz, T. C., Tunnicliffe, J., Malone, L., Clark, I. D. and Chin, K.S. 2013. Thawing of massive ground ice in mega slumps drives increases in stream sediment and solute flux across a range of watershed scales. *Journal of Geophysical Research: Earth Surface, 118*, 681-692.

Kowalewski, D. E., Marchant, D. R., Levy, J. S. and Head, J. W. 2006. Quantifying low rates of summertime sublimation for buried glacier ice in Beacon Valley, Antarctica. *Antarctic Science, 18*(3), 421-428.

Kowalewski, D. E., Marchant, D. R., Head III, J. W. and Jackson, D. W. 2012. A 2D model for characterising first-order variability in sublimation of buried glacier ice, Antarctica: Assessing the influence of polygon troughs, desert pavements and shallow subsurface salts. *Permafrost and Periglacial Processes, 23*, 1-14.

Kudriavstev, V. A. (Ed.). 1978. *General Permafrost Science* (2^{nd} ed). Moscow University Editions, Moscow (In Russian).

Lacelle, D., Bjornson, J., Lauriol, B., Clark, I. D. and Troutet, Y. 2004. Segregated-intrusive ice of subglacial meltwater origin in retrogressive thaw flow headwalls, Richardson Mountains, NWT, Canada. *Quaternary Science Review, 23*, 681–696.

Lacelle, D., Davila, A. F., Pollard, W. H., Andersen, D., Heldmann, J., Marinova, M. and McKay, C. P. 2011. Stability of massive ground ice bodies in University Valley, McMurdo Dry Valleys of Antarctica: Using stable O-H isotope as tracers of sublimation in hyper-arid regions. *Earth and Planetary Science Letters, 301,* 403-411.

Lacelle, D., Davila, A. F., Fisher, D., Pollard, W. H., DeWitt, R., Heldmann, J., Marinova, M. M. and McKay, C. P. 2013. Excess ground ice of condensation-diffusion origin in University Valley, McMurdo Dry Valleys of Antarctica: Evidence from isotope geochemistry and numerical modeling. *Geochimica et Cosmochimica Acta, 120,* 280-297.

Lacelle, D., Fontaine, M., Forest, A. P. and Kokelj, S. 2014. High-resolution stable water isotopes as tracers of thaw unconformities in permafrost: A case study from western Arctic Canada. *Chemical Geology, 368,* 85-96.

Lacelle, D., Lapalme, C., Davila, A. F., Pollard, W., Marinova, M., Heldmann, J. and McKay, C. P. 2015. Solar radiation and air and ground temperature relations in the cold and hyper-arid Quartermain Mountains, McMurdo Dry Valleys of Antarctica, *Permafrost and Periglacial Processes,* doi: 10.1002/ppp.1859.

Lachenbruch, A.H. 1962. Mechanics of thermal contraction cracks and ice-wedge polygons in permafrost, *Geologic Society of America Special Papers, 70,* 1-66.

Lapalme, C. M., Lacelle, D., Davila, A. F., Pollard, W., Fortier, D. and McKay, C. P. 2015. *Cryostratigraphy of near-surface permafrost in University Valley, McMurdo Dry Valleys of Antarctica.* Paper presented at GeoQuebec 2015, Quebec, Canada.

Levy, J. S., Head, J. W. and Marchant, D. R. 2008. The role of thermal contraction crack polygons in cold-desert fluvial systems. *Antarctic Science, 20*, 565-579.

Levy, J. S., Fountain, A. G., Gooseff, M. N., Welch, K. A. and Lyons, W. B. 2011. Water tracks and permafrost in Taylor Valley, Antarctica: Extensive and shallow groundwater connectivity in a cold desert ecosystem. *Geological Society of America Bulletin*, *123*(11/12), 2295-2311.

Linell, K. A. and Kaplar, C. W. 1966. Description and classification of frozen soils. Paper presented at the 1st International Permafrost Conference, National Academy of Science - National Research Council of Canada Publication 1287, 481-487.

Levy, J. 2013. Short note: How big are the McMurdo Dry Valleys? Estimating ice-free area using Landsat image data. *Antarctic Science 25*(1), 119-120.

Liu, L., Sletten, R. S., Hagedorn, B., Hallet, B., McKay, C. P. and Stone, J. O. 2015. An enhanced model of the contemporary and long-term (200 ka) sublimation of the massive subsurface ice in Beacon Valley, Antarctica. *Journal of Geophysical Research: Earth Surface*, *120*(8), 1596-1610.

Mackay, J. R. 1972. The world of underground ice. *ANNALS of the association of American geographers, 62(*1), 1-22.

Mackay, J. R. 1974. Reticulate ice veins in permafrost, Northern Canada. *Canadian Geotechnical Journal, 11*, 230-237.

Mackay, J. R. 1984. The frost heave of stones in the active layer above permafrost with downward and upward freezing. *Arctic and Alpine Research, 16*, 439-446.

Mackay, J. R. 1985. Permafrost growth in recently drained lakes, western Arctic coast. In *Current research, part B*. Geological Survey of Canada, 85-1B, 177-189.

Mackay, J. R. and Dallimore, S. R. 1992. Massive ice of the Tuktoyaktuk area, western Arctic coast, Canada. *Canadian Journal of Earth Sciences, 29*, 1235-1249.

Marchant, D. R., Denton, G. H. and Swisher III, C. C. 1993. Miocene-Pliocene-Pleistocene glacial history of Arena Valley, Quartermain Mountains, Antarctica. *Geografiska Annaler, 75A*(4), 269-302.

Marchant, D. R. and Denton, G. H. 1996. Miocene and Pliocene paleoclimate of the Dry Valleys region, southern Victoria Land: A geomorphological approach. *Marine Micropaleontology, 27*, 253-271.

Marchant, D. R., Phillips, W. M., Moore, E. J., Souchez, R. A., Denton, G. H., Sugden, D. E., Potter Jr., N. and Landis, G. P. 2002. Formation of patterned ground and sublimation till over Miocene glacier ice in Beacon Valley, southern Victoria Land, Antarctica. *Geological Society of America, 144*(6), 718-730.

Marchant, D. R. and Head III, J. W. 2007. Antarctic dry valleys: Microclimate zonation, variable geomorphic processes, and implications for assessing climate change on Mars. *Icarus, 192,* 187-222.

Marinova, M. M., Mckay, C. P., Pollard, W. H., Heldmann, J. L., Davila, A. F., Anderson, D. T., Jackson, W. A., Lacelle, D., Paulsen, G. and Zacny, K. 2013. Distribution of depth to ice-cemented soils in the high elevation Quartermain Mountains, McMurdo Dry Valleys, Antarctica. *Antarctic Science, 25*(4), 575-582.

McKay, C. P., Mellon, M. T. and Friedmann, E. I. 1998. Soil temperature and stability of ice cemented ground in the McMurdo Dry Valleys, Antarctica. *Antarctic Science, 10*(1), 31-38.

McKay, C. P. 2009. Snow recurrence sets the depth of dry permafrost at high elevations in the McMurdo Dry Valleys of Antarctica. *Antarctic Science, 10*, 31-38.

McKay, C. P. 2015. Testing the Doran summer climate rules in Upper Wright Valley, Antarctica. *Antarctic Science*, doi.10.1017/S095410201500005X.

Mellon, M. T., McKay, C. P. and Heldmann, J. L. 2014. Polygonal ground in the McMurdo Dry Valleys of Antarctica and its relationship to ice-table depth and the recent Antarctic climate history. *Antarctic Science, 26*(4), 413-426.

Morse, P. D., Burn, C. R. and Kokelj, S. V. 2009. Near-surface ground-ice distribution, Kendall Island Bird Sanctuary, western Arctic coast, Canada. *Permafrost and Periglacial Processes, 20*, 155-171.

Murton, J. B. and French, H. M. 1994. Cryostructures in permafrost, Tuktoyaktuk coastlands, western arctic Canada. *Canadian Journal of Earth Sciences, 31,* 737-747.

Ng, F., Hallet, B., Sletten, R. S. and Stone, J. O. 2005. Fast-growing till over ancient ice in Beacon Valley, Antarctica. *Geology, 33,* 121-124.

Nylen, T. H., Fountain, A. G., and Doran, P. T. 2004. Climatology of katabatic winds in the McMurdo dry valleys, southern Victoria Land, Antarctica. *Journal of Geophysical Research, 109,* D03114.

O'Neill, H. B. and Burn, C.R. 2012. Physical and temporal factors controlling the development of near-surface ground ice at Illisarvik, western Arctic coast, Canada. *Canadian Journal of Earth Sciences*, *49***,** 1096-1110.

O'Sullivan, D. and Unwin, D. J. 2003. *Geographic information analysis.* John Wiley & Sons, Inc. Hoboken, NJ.

Pollard, W.H. and French, H.M. 1980. A first approximation of the volume of ground ice, Richards Island, Pleistocene Mackenzie Delta, Northwest Territories, Canada. *Canadian Geotechnical Journal, 17*, 509-516.

Pollard, W., Doran, P. and Wharton, R. 2002. The nature and significance of massive ground ice in Ross Sea Drift, Garwood Valley, McMurdo Sound. *Royal Society of New Zealand Bulletin, 35,* 397-404.

Pollard, W. H., Lacelle, D., Davila, A. F., Andersen, D., McKay, C. P., Marinova, M. and Heldmann, J. 2012. Ground ice conditions in University Valley, McMurdo Dry Valleys, Antarctica. Paper presented at *the Tenth International Conference on Permafrost (TICOP), Salekhard, Russia, 1*, 305-310.

Popov, A. I. Cryolithogenesis, the composition and structure of frozen rocks, and ground ice (the current state of the problem). *Biuletyn Peryglacjalny, 27*, 155-169.

Popov, A. I., Rozenbaum, G. E., Renfrew, I. A. and Anderson, P. S. 2002. The surface climatology of an ordinary katabatic wind regime in Coats Land, Antarctica. *Tellus A, 54*(5), 463-484.

Reeh, N. and Fisher, D. A. 1983. *Noise in accumulation rate and δ(^{18}O) time series as determined from comparison of adjacent Greenland and Devon Island ice cap cores.* Ottawa, Polar Continental Shelf Project (Internal Report).

Renfrew, I. A. and Anderson, P. S. 2002. The surface climatology of an ordinary katabatic wind regime in Coats Land, Antarctica, *Tellus A, 54*(5), 463-484.

Sheskin, D. J. 2011. *Handbook of parametric and nonparametric statistical procedures. Fifth edition.* CRC Press Taylor & Francis Group. Boca Raton, FL.

Shur, Y., French, H. M., Bray, M. T. and Anderson, D. A. 2004. Syngenetic permafrost growth: cryostratigraphic observations from the CRREL tunnel near Fairbanks, Alaska. *Permafrost and Periglacial Processes, 15*, 339-347.

Smith, S. L. and Williams, P. J. 1990. Ice lens orientation around a chilled buried pipe. Proceedings, *5th Canadian Permafrost Conference*, *Collection Nordicana.* Centre d'études Nordiques, Université Lavel, 54, 83-87.

Stuiver, M., Yang I. C., Denton, G. H., Kellogg, T. B. 1981. Oxygen isotope ratios of Antarctic permafrost and glacier ice. *Dry Valley Drilling Project, Antarctic Research Series, 33,* 131-139.

Sugden, D.E., Denton, G. H., Souchez, R. A., Marchant, D. R., Potter, N., Swisher III, C. C. and Tison, J-L. 1995. Preservation of Miocene glacier ice in East Antarctica. *Nature, 376*, 412-414.

Trinh-Le., C. *Unpublished data.*

van Everdingen, R. (Ed.). 1998, revised May 2005. *Multi-language glossary of permafrost and related ground-ice terms*. Boulder, CO: National Snow and Ice Data Center.

Appendix 1: Step by step image analysis in Fiji

1. **Install Fiji (http://fiji.sc/Fiji)**
2. **Open image**

i) Under the *File* menu, scroll to *Import* and then point to *Image Sequence.*

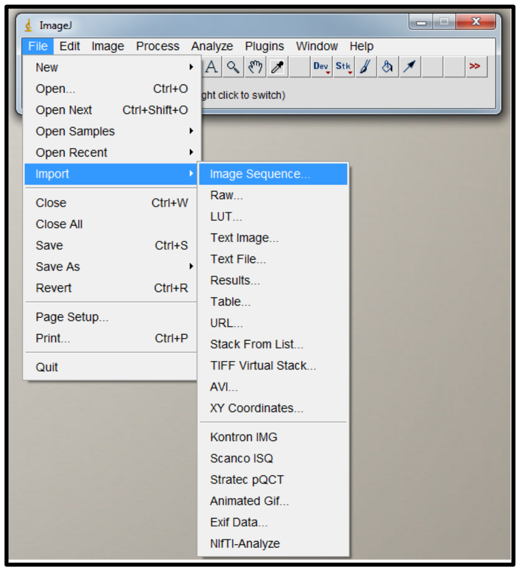

ii) In the *Open Image Sequence* dialogue box, navigate to the folder that contains the images of the core and click *Open.*

iii) Select the first image file within the folder and then click *Open.*

iv) In the *Sequence Options* dialogue box, ensure *Starting image* is set to *1* and the box to the left of the *Sort names numerically* option is checked.

v) Press *OK.*

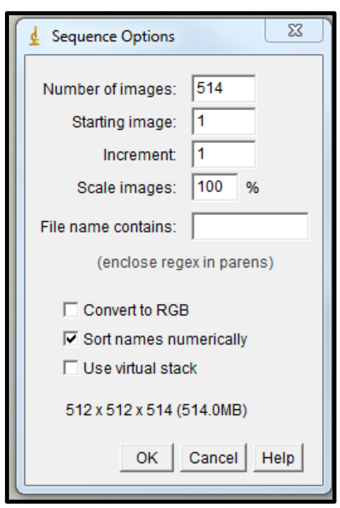

vi) A window will open with the title of the folder that contains the images. To scroll through images use the left and right cursors.

3. Determine the density class for ice

i. Cores must be analyzed one at a time.

ii. To adjust the contrast, navigate to the *Image* menu, scroll the cursor down to *Adjust* and click *Brightness/Contrast*. Alternatively, type Ctrl+Shift+C on the keyboard.

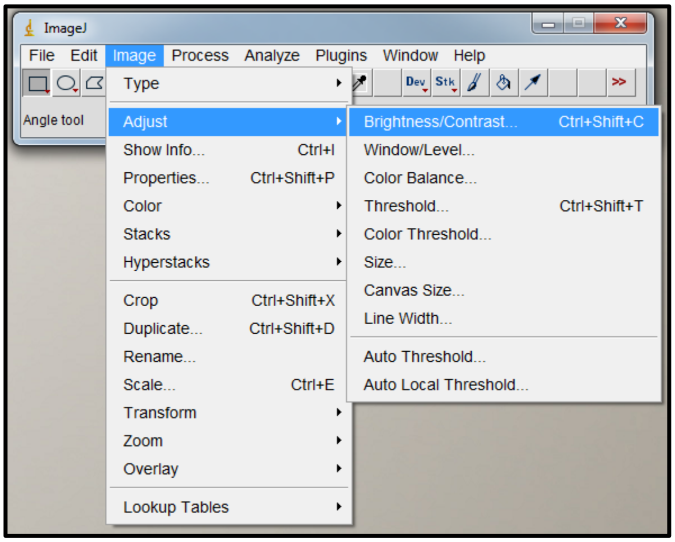

a. Scroll to an image where the core is visible in the image viewer window.

b. In the *B&C* dialogue box, click the *Auto* tab and then close the *B&C* dialogue box.

iii. Classifying the pixels

a. Navigate to the *Image* dropdown menu, and scroll down to *Adjust* and then point to *Threshold.* Alternatively, press "Ctrl+Shift+T" on the keyboard.

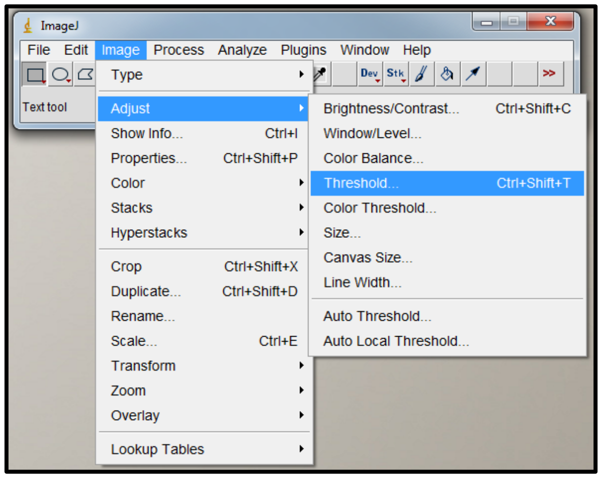

i. Once the *Threshold* dialogue box appears, click the *Set* button.

ii. In the *Set Threshold Levels* dialogue box, set the threshold to that of ice

1. E.g:
    a. Lower Threshold level = -200
    b. Upper Threshold Level = 700

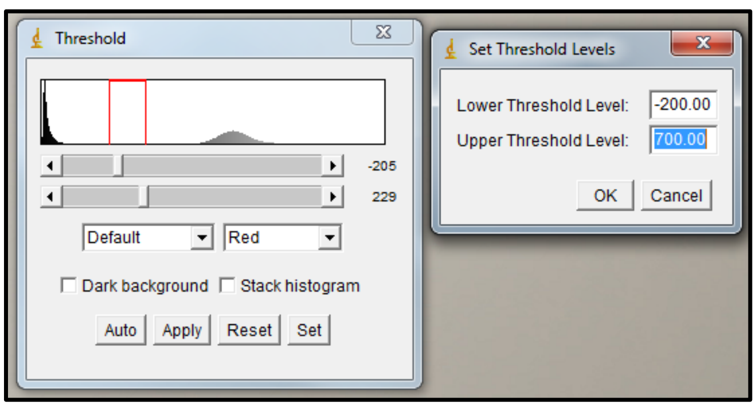

2. Click *OK.*

iii. The red colour in the image viewer window for the core corresponds to the threshold selection.

iv. A binary image must be created before calculations can be performed. In order to do this, click *Apply* in the *Threshold* dialogue box.

  1. When the *Convert Stack to Binary* dialogue box appears, click *OK*.

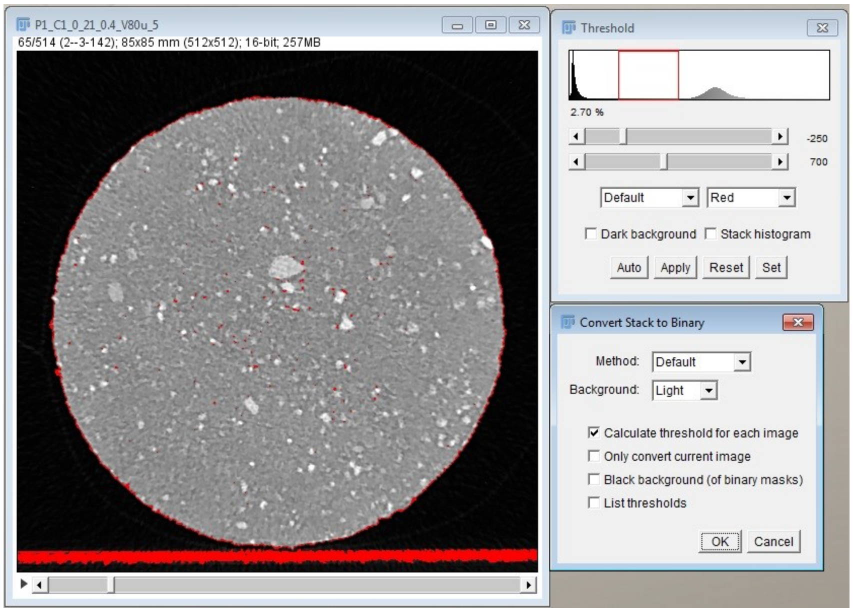

  2. In the resulting set of images, the black corresponds to your threshold selection (in this example, the black corresponds to ice), while the white represents everything else. It is important to note that this method allows the representation of only two density classes; as a result, only one element (i.e. ice) can be visualized at a time.

b. Analyze the data using the histogram

i. Click the *Oval* tool and draw a circle around the arbitrary region of interest (ROI) for the core.

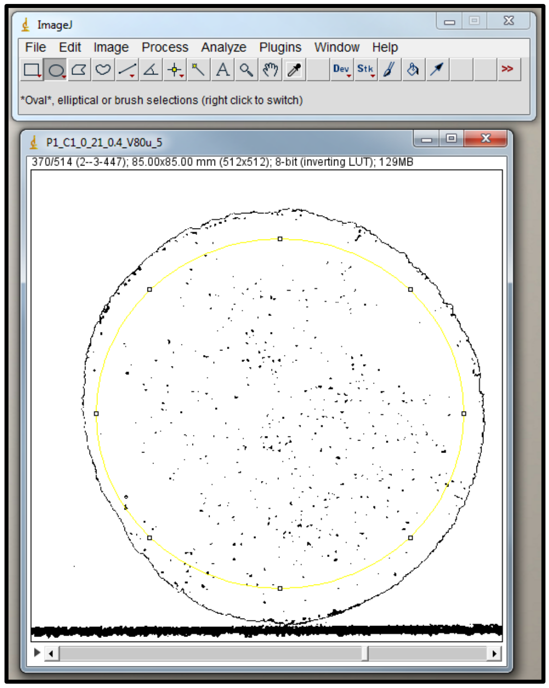

ii. Click the *Stk* (stack) tool on the toolbar and point to *Plot Z-axis Profile*. The resulting plot represents the ROI selection mean gray value on the y axis, and the slice number on the x axis (http://rsbweb.nih.gov/ij/docs/guide/146.html).

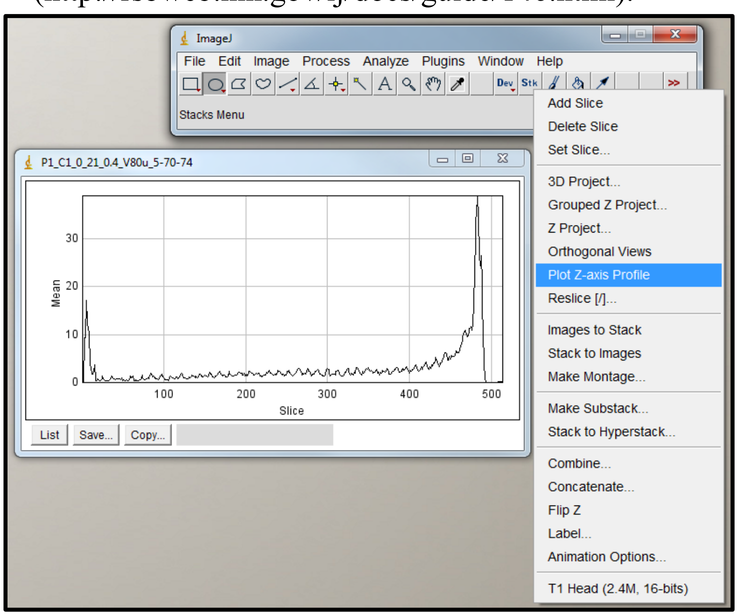

iii. From the *File* menu, click *Save as* in the *Results* dialogue box in order to export the data from the plot into an excel format.

iv. Scroll through your stack of images to identify those which would have been too small to fit inside the ROI and note the slice number(s).

v. In the excel document saved from the *Results* dialogue box, multiply the column "Mean" by the value in the "Max" column (255). Multiply the result by 100. The result is the percentage of VIC/excess ice in the core.

vi. Remove the slice numbers previously noted that did not fit inside the ROI as these values will over/underpresent the ice content.

iv. Changing the views of the image stack for cryostructural classification

a. Download the *Radial Reslice* plugin (http://rsb.info.nih.gov/ij/plugins/radial-reslice/index.html).

1) Once the file is downloaded drag and drop the file into the grey area in Image J under the tool bar.

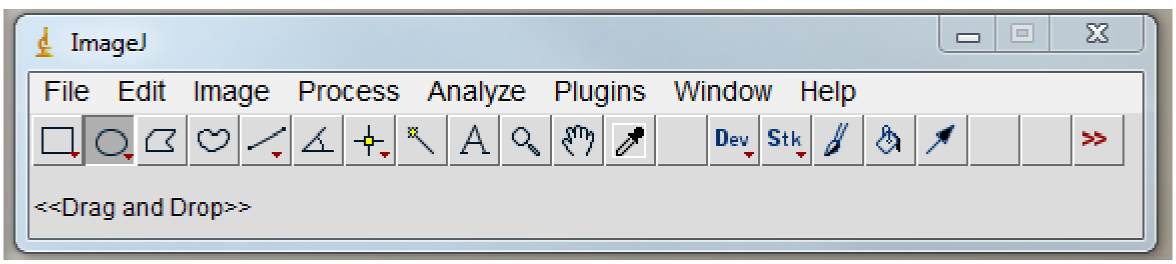

2) From the Toolbar click the line tool and draw a line down the middle of the core image.

3) From the Plugins dropdown menu choose *Radial Reslice.*

4) In the *Radial Reslice* dialogue box check the *Rotate around center* option and click *OK*.

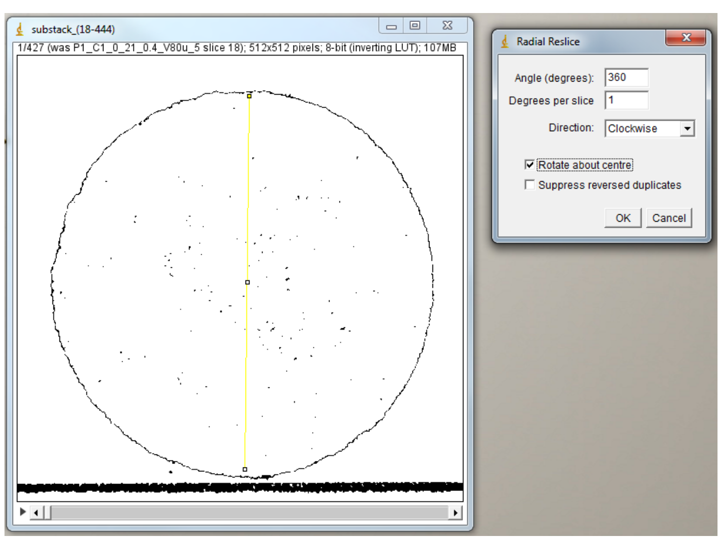

5) The output created is an orthogonal reconstruction of the image stack. It is created through the rotation of the specified line of ROI around the center of the image (http://rsb.info.nih.gov/ij/plugins/radial-reslice/index.html).
6) Investigating cryostructures
   a. Under the *Image* tab, choose *Stacks,* and point to *Orthogonal Views.*
   b. The resulting windows allow the investigation of cryostructures at different depths, from three different views.

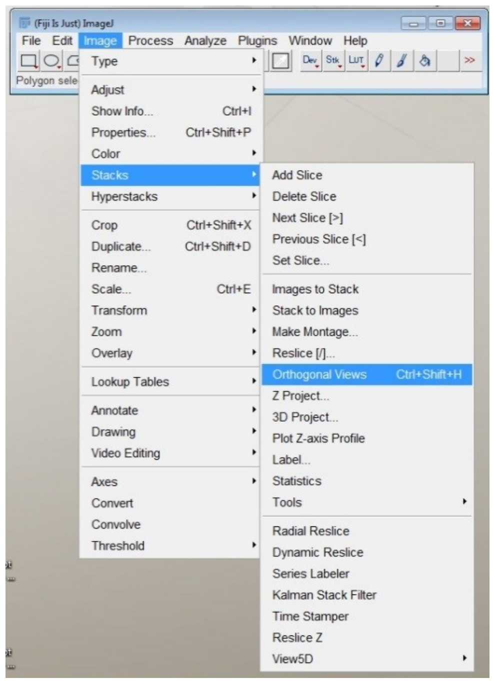

Appendix 2: Summary of the Spatial Autocorrelation Tool (Global Moran's I statistic)

Appendix 2: Summary of the Spatial Autocorrelation Tool (Global Moran's I statistic) results for the mean VIC (%), GWC (%) and excess ice content (%) in the entire core for the fifteen cores sampled in University Valley. The null hypothesis for the test is that the feature values are randomly distributed across University Valley.

Statistic	VIC	GWC	Excess ice content
Moran's index	0.082	0.358	0.085
Expected index	-0.071	-0.071	-0.071
Variance	0.109	0.078	0.104
z-score	0.467	1.533	0.484
p-value	0.640	0.125	0.628

Appendix 3: Results of the Shaprio-Wilk test

Appendix 3A: Results of the Shapiro-Wilk test on mean excess ice contents in the top 20 cm, 50 cm and 1 m of 15 cores taken from University Valley. N/A values represent cores that do not reach the designated length. A high p-value (> 0.05) indicates that there is no evidence to reject the null hypothesis that the sample is normally distributed (e.g. Acevedo, 2013).

H0 = sample is normally distributed
H1 = sample is not normally distributed

	Top 20 cm				Top 50 cm				Top 1 m			
Core ID	W statistic	P-value	Reject null hypothesis?	Sample is normally distributed?	W statistic	P-value	Reject null hypothesis?	Sample is normally distributed?	W statistic	P-value	Reject null hypothesis?	Sample is normally distributed?
P1-C1	0.906	0.286	no	yes	0.940	0.222	no	yes	0.9671	0.2766	no	yes
P1-C2	0.879	0.126	no	yes	0.964	0.549	no	yes	0.9811	0.6639	no	yes
P1-C3	0.792	0.089	no	yes	0.847	0.006	yes	no	N/A	N/A	N/A	N/A
P2-C2	Error: all values are identical				N/A	N/A	N/A	N/A	N/A	N/A	N/A	N/A
P4-C1	N/A	N/A	N/A	N/A	N/A	N/A	N/A	N/A	N/A	N/A	N/A	N/A
P5-C1	0.717	0.003	yes	no	N/A	N/A	N/A	N/A	N/A	N/A	N/A	N/A
P6-C3	0.792	0.012	yes	no	0.895	0.020	yes	no	0.863	0.000	yes	no
P6-C5	0.917	0.403	no	yes	0.944	0.305	no	yes	N/A	N/A	N/A	N/A
P7-C1	0.931	0.488	no	yes	N/A	N/A	N/A	N/A	N/A	N/A	N/A	N/A
P8-C3	0.908	0.301	no	yes	0.869	0.009	yes	no	N/A	N/A	N/A	N/A
P8-C5	0.940	0.557	no	yes	0.884	0.012	yes	no	N/A	N/A	N/A	N/A
P8-C6	Error: all values are identical				N/A	N/A	N/A	N/A	N/A	N/A	N/A	N/A
P9-C1	0.905	0.246	no	yes	N/A	N/A	N/A	N/A	N/A	N/A	N/A	N/A
P9-C2	N/A	N/A	N/A	N/A	N/A	N/A	N/A	N/A	N/A	N/A	N/A	N/A
P10-C1	0.704	0.001	yes	no	0.871	0.008	yes	no	0.814	0.000	yes	no

Appendix 3B: Results of the Shapiro-Wilk test on mean gravimetric water contents in the top 20 cm, 50 cm and 1 m in 15 cores taken from University Valley. N/A values represent cores that do not reach the designated length. A high p-value (> 0.05) indicates that there is no evidence to reject the null hypothesis that the sample is normally distributed (e.g. Acevedo, 2013)

H0 = sample is normally distributed
H1 = samples is not normally distributed

	Top 20 cm				Top 50 cm				Top 1 m			
Core ID	W statistic	P-value	Reject null hypothesis?	Sample is normally distributed?	W statistic	P-value	Reject null hypothesis?	Sample is normally distributed?	W statistic	P-value	Reject null hypothesis?	Sample is normally distributed?
P1-C1	0.945	0.631	no	yes	0.934	0.162	no	yes	0.852	0.000	yes	no
P1-C2	0.855	0.066	no	yes	0.885	0.013	yes	no	0.800	0.000	yes	no
P1-C3	0.868	0.288	no	yes	0.941	0.278	no	yes	N/A	N/A	N/A	N/A
P2-C2	0.784	0.019	yes	no	N/A	N/A	N/A	N/A	N/A	N/A	N/A	N/A
P4-C1	N/A	N/A	N/A	N/A	N/A	N/A	N/A	N/A	N/A	N/A	N/A	N/A
P5-C1	0.792	0.024	yes	no	N/A	N/A	N/A	N/A	N/A	N/A	N/A	N/A
P6-C3	0.859	0.074	no	yes	0.920	0.066	no	yes	0.857	0.000	yes	no
P6-C5	0.836	0.068	no	yes	0.928	0.159	no	yes	N/A	N/A	N/A	N/A
P7-C1	0.905	0.283	no	yes	N/A	N/A	N/A	N/A	N/A	N/A	N/A	N/A
P8-C3	0.848	0.071	no	yes	0.857	0.006	yes	no	N/A	N/A	N/A	N/A
P8-C5	0.880	0.131	no	yes	0.930	0.109	no	yes	N/A	N/A	N/A	N/A
P8-C6	0.811	0.027	yes	no	N/A	N/A	N/A	N/A	N/A	N/A	N/A	N/A
P9-C1	0.711	0.002	yes	no	N/A	N/A	N/A	N/A	N/A	N/A	N/A	N/A
P9-C2	N/A	N/A	N/A	N/A	N/A	N/A	N/A	N/A	N/A	N/A	N/A	N/A
P10-C1	0.688	0.001	yes	no	0.799	0.000	yes	no	0.880	0.000	yes	no

Appendix 4: Complete results of the Mann-Whitney *U* test comparison

Appendix 4A: The complete Mann-Whitney *U* test comparison of the median excess ice content and gravimetric water content in the top 20 cm of ice bearing permafrost in 13 cores taken from University Valley. Results indicative of a statistically significant (p-value = < 0.05) W statistic are bolded. A statistically significant result allows the rejection of the null hypothesis that the medians of variable x and variable y are equal. Cores P4-C1 and P9-C2 were not included as they measured less than 20 cm in length.

Excess ice content

	P1-C1	P1-C2	P1-C3	P2-C2	P5-C1	P6-C3	P6-C5	P7-C1	P8-C3	P8-C5	P8-C6	P9-C1	P10-C1
P1-C1	N/A	**11**	6	**72**	30	45	49	58	**18**	41	**81**	**0**	**0**
P1-C2	**11**	N/A	16	**80**	39	**78**	**76**	**89**	42	**92**	**90**	**2**	**0**
P1-C3	6	16	N/A	**32**	15	33	**29**	**35**	22	34	**36**	6	**0**
P2-C2	**72**	**80**	**32**	N/A	**4**	**0**	**4**	**0**	**0**	**0**	36	**0**	**0**
P5-C1	30	39	15	**4**	N/A	47	44	45	39	45	**68**	23	**0**
P6-C3	45	**78**	33	**0**	47	N/A	55	65	**20**	42	**90**	**90**	**0**
P6-C5	49	**76**	**29**	**4**	44	55	N/A	33	**10**	22	**68**	**0**	**0**
P7-C1	58	**89**	**35**	**0**	45	65	33	N/A	**7**	**14**	**81**	**0**	**0**
P8-C3	**18**	42	22	**0**	39	**20**	**10**	**7**	N/A	67	**81**	**9**	**0**
P8-C5	41	**92**	34	**0**	45	42	22	**14**	67	N/A	**90**	**0**	**0**
P8-C6	81	**90**	**36**	36	**68**	**90**	**68**	**81**	**81**	**90**	N/A	**0**	**0**
P9-C1	**0**	**2**	6	**0**	23	**90**	**0**	**0**	**9**	**0**	**0**	N/A	32
P10-C1	**0**	**0**	**0**	**0**	**0**	**0**	**0**	**0**	**0**	**0**	**0**	32	N/A

Gravimetric water content

	P1-C1	P1-C2	P1-C3	P2-C2	P5-C1	P6-C3	P6-C5	P7-C1	P8-C3	P8-C5	P8-C6	P9-C1	P10-C1
P1-C1	N/A	**0**	**2**	36	25	**0**	38	**65.5**	19.5	30.5	40	**0**	**0**
P1-C2	**0**	N/A	30	**80**	**54**	**77**	**80**	**90**	**82**	**100**	**90**	32	**0**
P1-C3	**2**	30	N/A	26	19	15	**29**	**36**	24	32	**35**	7	**0**
P2-C2	36	**80**	26	N/A	18	**0**	28	52	**13**	29	37	0	**0**
P5-C1	25	**54**	19	18	N/A	32	44	**60**	37	50	44	**13**	**0**
P6-C3	**0**	**77**	15	**0**	32	N/A	**80**	**90**	**79**	**100**	**90**	30	**0**
P6-C5	38	**80**	**29**	28	44	**80**	N/A	**13**	**11.5**	25	30	**0**	**0**
P7-C1	**65.5**	**90**	**36**	52	**60**	**90**	**13**	N/A	**3.5**	**8.5**	19	**0**	**0**
P8-C3	19.5	**82**	24	**13**	37	**79**	**11.5**	**3.5**	N/A	64	58	**8**	**0**
P8-C5	30.5	**100**	32	29	50	**100**	25	**8.5**	64	N/A	54	**0**	**0**
P8-C6	40	**90**	**35**	37	44	**90**	30	19	58	54	N/A	**0**	**0**
P9-C1	**0**	32	7	0	**13**	30	**0**	**0**	**8**	**0**	**0**	N/A	**20**
P10-C1	**0**	**0**	**0**	**0**	**0**	**0**	**0**	**0**	**0**	**0**	**0**	**20**	N/A

Appendix 4B: The complete Mann-Whitney *U* test comparison of the median excess ice content and gravimetric water content in the top 50 cm of ice bearing permafrost in eight cores taken from University Valley. Results indicative of a statistically significant (p-value = < 0.05) W statistic are bolded. A statistically significant result allows the rejection of the null hypothesis that the medians of variable x and variable y are equal. Cores P2-C2, P4-C1, P5-C1, P7-C1, P8-C6, P9-C1 and P9-C2 were not included as they measured less than 50 cm in length.

Excess ice content								
	P1-C1	P1-C2	P1-C3	P6-C3	P6-C5	P8-C3	P8-C5	P10-C1
P1-C1	N/A	**100**	**30**	**150**	232.5	**112**	259	**0**
P1-C2	**100**	N/A	**43**	236	**347**	183	**426**	**0**
P1-C3	**30**	**43**	N/A	**394**	**337**	252	**411**	**0**
P6-C3	**150**	236	**394**	N/A	**312.5**	169	**363**	**0**
P6-C5	232.5	**347**	**337**	**312.5**	N/A	**91.5**	211	**0**
P8-C3	**112**	183	252	169	**91.5**	N/A	**368.5**	**0**
P8-C5	259	**426**	**411**	**363**	211	**368.5**	N/A	**0**
P10-C1	**0**	**0**	**0**	**0**	**0**	**0**	**0**	N/A
Gravimetric water content								
	P1-C1	P1-C2	P1-C3	P6-C3	P6-C5	P8-C3	P8-C5	P10-C1
P1-C1	N/A	**3**	**26**	**0**	175	**114.5**	214.5	**0**
P1-C2	**3**	N/A	180	**0**	**414**	319	**507**	**0**
P1-C3	**26**	180	N/A	174	**336**	**281**	**403**	**0**
P6-C3	**0**	**0**	174	N/A	**437**	**389**	**529**	**0**
P6-C5	175	**414**	**336**	**437**	N/A	**295.5**	217.5	**0**
P8-C3	**114.5**	319	**281**	**389**	**295.5**	N/A	**347.5**	**0**
P8-C5	214.5	**507**	**403**	**529**	217.5	**347.5**	N/A	**0**
P10-C1	**0**	**0**	**0**	**0**	**0**	**0**	**0**	N/A

Appendix 4C: The complete Mann-Whitney *U* test comparison of the median excess ice content and gravimetric water content in the top 50 cm of ice bearing permafrost in four cores taken from University Valley. Results indicative of a statistically significant (p-value = < 0.05) W statistic are bolded. A statistically significant result allows the rejection of the null hypothesis that the medians of variable x and variable y re equal. Cores P1-C3, P2-C2, P4-C1, P5-C1, P6-C5, P7-C1, P8-C3, P8-C5, P8-C6 and P9-C2 were not included as they measured less than 1 m in length.

Excess ice content				
	P1-C1	P1-C2	P6-C3	P10-C1
P1-C1	N/A	841	**437**	**153**
P1-C2	841	N/A	**500**	**191**
P6-C3	**437**	**500**	N/A	**331**
P10-C1	**153**	**191**	**331**	N/A
Gravimetric water content				
	P1-C1	P1-C2	P6-C3	P10-C1
P1-C1	N/A	**527**	**9**	**173.5**
P1-C2	**527**	N/A	**191**	**365**
P6-C3	**9**	**191**	N/A	**664**
P10-C1	**173.5**	**365**	**664**	N/A

Appendix 4D: Complete results of the Mann-Whitney U test comparison of the differences in the medians of excess ice content, gravimetric water content and volumetric ice content in the centres and shoulders of Polygons 1, 6 and 8. Results indicative of a statistically significant (p-value = < 0.05) W statistic are bolded. A statistically significant result allows the rejection of the null hypothesis that the medians of variable x and variable y are equal.

H0 : x= y; H1: x does not = y
Are medians equal?
Low p = reject null hypothesis = different

X variable	Y variable	W	P-value	Reject null hypothesis?	Equal?
Excess ice content					
Shoulders	Centres	11290.5	0.00	yes	no
GWC					
Shoulders	Centres	11603	0.00	yes	no
VIC					
Shoulders	Centres	11832	0.00	yes	no

Appendix 5: Complete results of the K-S test comparison

Appendix 5A: The complete Kolomogrov-Smirnov (K-S) test results between two cores for excess ice and gravimetric water content in the top 20 cm of ice bearing permafrost in 13 cores taken from University Valley. Results indicative of a statistically significant (p-value = < 0.05) D statistic are bolded. A statistically significant result allows the rejection of the null hypothesis that variable x and variable y are of equal distributions. Cores P4-C1 and P9-C2 were not included as they measured less than 20 cm in length.

Excess ice content

	P1-C1	P1-C2	P1-C3	P2-C2	P5-C1	P6-C3	P6-C5	P7-C1	P8-C3	P8-C5	P8-C6	P9-C1	P10-C1
P1-C1	N/A	**0.79**	0.64	**1**	0.5	0.27	0.39	0.56	0.56	0.23	**1**	**1**	**1**
P1-C2	**0.79**	N/A	0.5	**1**	0.5	**0.6**	**0.8**	**0.9**	0.34	**0.8**	**1**	**0.9**	**1**
P1-C3	0.64	0.5	N/A	**1**	0.5	0.6	**0.75**	**0.89**	0.39	0.75	**1**	0.7	**1**
P2-C2	**1**	**1**	**1**	N/A	**0.88**	**1**	**0.88**	**1**	**1**	**1**	0	**1**	**1**
P5-C1	0.5	0.5	0.5	**0.88**	N/A	0.5	0.5	0.64	0.5	0.5	**0.88**	0.5	**1**
P6-C3	0.27	**0.6**	0.6	**1.0**	0.5	N/A	0.4	0.4	**0.56**	0.4	**1**	**1**	**1**
P6-C5	0.39	**0.8**	**0.75**	**0.88**	0.5	0.4	N/A	0.38	**0.56**	0.53	**0.88**	**1**	**1**
P7-C1	0.56	**0.9**	**0.89**	**1**	0.64	0.4	0.38	N/A	**0.78**	**0.59**	**1**	**1**	**1**
P8-C3	0.56	0.34	0.39	**1**	0.5	**0.56**	**0.56**	**0.78**	N/A	0.56	**1**	**0.69**	**1**
P8-C5	0.23	**0.8**	0.75	**1**	0.5	0.4	0.53	**0.59**	0.56	N/A	**1**	**1**	**1**
P8-C6	**1**	**1**	**1.0**	0.00	**0.88**	**1**	**0.88**	**1**	**1**	**1**	N/A	**1**	**1**
P9-C1	**1**	**0.9**	0.7	**1**	0.5	**1**	**1**	**1**	**0.69**	**1**	**1**	N/A	0.6
P10-C1	**1**	**1**	**1.0**	**1**	**1**	**1**	**1**	**1**	**1**	**1**	**1**	0.6	N/A

Gravimetric water content

	P1-C1	P1-C2	P1-C3	P2-C2	P5-C1	P6-C3	P6-C5	P7-C1	P8-C3	P8-C5	P8-C6	P9-C1	P10-C1
P1-C1	N/A	**1**	**0.78**	0.38	0.5	**1**	0.31	**0.56**	0.56	0.4	0.22	**1**	**1**
P1-C2	**1**	N/A	0.55	**1**	0.5	**0.6**	**1**	**1**	**0.89**	**1**	**1**	0.56	**1**
P1-C3	**0.78**	0.55	N/A	0.63	0.5	0.5	**0.75**	**1**	0.44	0.5	**0.89**	0.56	**1**
P2-C2	0.38	**1**	0.63	N/A	0.5	**1**	0.38	0.43	**0.63**	0.53	0.40	**1**	**1**
P5-C1	0.5	0.5	0.5	0.5	N/A	0.5	0.5	**0.65**	0.39	0.5	0.5	**0.56**	**1**
P6-C3	**1**	**0.6**	0.5	**1**	0.5	N/A	**1**	**1**	**0.79**	**1**	**1**	0.57	**1**
P6-C5	0.31	**1**	**0.75**	0.38	0.5	**1**	N/A	**0.56**	**0.56**	0.4	0.42	**1**	**1**
P7-C1	**0.56**	**1**	**1**	0.43	**0.65**	**1**	**0.56**	N/A	**0.78**	**0.7**	0.67	**1**	**1**
P8-C3	0.56	**0.89**	0.44	**0.63**	0.39	**0.79**	**0.56**	**0.78**	N/A	0.6	0.56	**0.67**	**1**
P8-C5	0.4	**1**	0.5	0.53	0.5	**1**	0.43	**0.69**	0.56	N/A	0.4	**1**	**1**
P8-C6	0.222	**1**	**0.89**	0.40	0.5	**1**	0.42	0.67	0.56	0.4	N/A	**1**	**1**
P9-C1	**1**	0.56	0.56	**1**	**0.56**	0.57	**1**	**1**	**0.67**	**1**	**1**	N/A	**0.78**
P10-C1	**1**	**1**	**1**	**1**	**1**	**1**	**1**	**1**	**1**	**1**	**1**	**0.78**	N/A

Appendix 5B: The complete Kolomogrov-Smirnov (K-S) test results between two cores for excess ice and gravimetric water content in the top 50 cm of ice bearing permafrost in eight cores taken from University Valley. Results indicative of a statistically significant (p-value = < 0.05) D statistic are bolded. A statistically significant result allows the rejection of the null hypothesis that variable x and variable y are of equal distributions. Cores P2-C2, P4-C1, P5-C1, P7-C1, P8-C6, P9-C1 and P9-C2 were not included as they measured less than 50 cm in length.

Excess ice content								
	P1-C1	P1-C2	P1-C3	P6-C3	P6-C5	P8-C3	P8-C5	P10-C1
P1-C1	N/A	**0.5528**	**0.8947**	**0.5652**	0.213	**0.5714**	0.2717	**1**
P1-C2	**0.5528**	N/A	**0.8513**	0.3913	**0.5904**	**0.4803**	**0.5652**	**1**
P1-C3	**0.8947**	**0.8513**	N/A	**0.7208**	**0.8947**	0.4135	**0.8947**	**1**
P6-C3	**0.5652**	0.3913	**0.7208**	N/A	**0.46**	0.381	**0.5652**	**1**
P6-C5	0.213	**0.5904**	**0.8947**	**0.46**	N/A	**0.5238**	0.2311	**1**
P8-C3	**0.5714**	**0.4803**	0.4135	0.381	**0.5238**	N/A	**0.5714**	**1**
P8-C5	0.2717	**0.5652**	**0.8947**	**0.5652**	0.2311	**0.5714**	N/A	**1**
P10-C1	**1**	**1**	**1**	**1**	**1**	**1**	**1**	N/A
Gravimetric water content								
	P1-C1	P1-C2	P1-C3	P6-C3	P6-C5	P8-C3	P8-C5	P10-C1
P1-C1	**0.957**	**0.895**	**1**	0.263	**0.571**	0.217	**1**	**1**
P1-C2	N/A	0.228	**0.435**	**0.783**	**0.429**	**0.783**	**1**	**1**
P1-C3	0.228	N/A	0.268	**0.895**	**0.514**	**0.895**	**1**	**1**
P6-C3	**0.435**	0.268	N/A	**1**	**0.576**	**1**	**1**	**1**
P6-C5	**0.783**	**0.895**	**1**	N/A	**0.524**	0.179	**1**	**1**
P8-C3	**0.429**	**0.514**	**0.576**	**0.524**	N/A	**0.571**	**1**	**1**
P8-C5	**0.783**	**0.895**	**1**	0.179	**0.571**	N/A	**1**	**1**
P10-C1	**1**	**1**	**1**	**1**	**1**	**1**	N/A	N/A

Appendix 5C: The complete Kolomogrov-Smirnov (K-S) test results between two cores for excess ice and gravimetric water content in the top 1 m of ice bearing permafrost in four cores taken from University Valley. Results indicative of a statistically significant (p-value = < 0.05) D statistic are bolded. A statistically significant result allows the rejection of the null hypothesis that variable x and variable y are of equal distributions. Cores P1-C3, P2-C2, P4-C1, P5-C1, P6-C5, P7-C1, P8-C3, P8-C5, P8-C6 and P9-C2 were not included as they measured less than 1 m in length.

Excess ice content				
	P1-C1	P1-C2	P6-C3	P10-C1
P1-C1	N/A	0.1995	**0.5648**	**0.75**
P1-C2	0.1995	N/A	**0.6222**	**0.7727**
P6-C3	**0.5648**	**0.6222**	N/A	**0.75**
P10-C1	**0.75**	**0.7727**	**0.75**	N/A
Gravimetric water content				
	P1-C1	P1-C2	P6-C3	P10-C1
P1-C1	N/A	**0.3756**	**0.9756**	**0.771**
P1-C2	**0.3756**	N/A	**0.6444**	**0.6591**
P6-C3	**0.9756**	**0.6444**	N/A	**0.5692**
P10-C1	**0.771**	**0.6591**	**0.5692**	N/A

Appendix 6: Presence of cryostructures in the six CT-scanned permafrost cores with depth

Appendix 6: Presence of cryostructures with depth in the six CT-scanned cores with depth. The number "1" is used to represent the presence of the cryostructure and not the frequency at which the cryostructure was observed at the specified depth. "N/A" represents an imaging error within the core.

	P1C1			P2-C2			P6-C5			P7-C1			P8C3			P8C6		
	Cryostructure			Cryostructure			Cryostructure			Cryostructure			Cryostructure			Cryostructure		
Depth (cm)	Struct.	Susp.	Crust.	Struct.	Susp.	Crust.	Struct.	Susp.	Crust.	Struct.	Susp.	Crust.	Struct.	Susp.	Crust.	Struct.	Susp.	Crust.
1																		
2																		
3													1		1	1		
4													1	1	1	1		1
5													1	1	1	1		1
6													1	1	1	1		1
7													1	1	1	1		1
8													1	1	1	1		1
9													1	1	1	1		1
10													1	1	1	1		1
11													1	1	1	1		1
12													1	1	1	1		1
13													1	1	1	N/A	N/A	N/A
14													1	1	1	N/A	N/A	N/A
15													1	1	1	1		
16													1	1	1	1		1
17													1	1	1	1		
18													1	1	1	1		
19													1	1	1	1		
20													1	1	1	1		
21				1		1	1	1	1				1	1	1	1		
22				1			1	1	1				1		1	1		
23				1			1	1	1	1		1	1	1	1	1		1
24				1		1	1	1	1	1		1	1	1	1	1		
25				1			1	1	1	1		1	1		1	1		
26				1			1	1	1	1			1		1	1		
27				1		1	1	1	1	1			1		1	1		
28				1		1	1	1	1	1		1	1	1		1		
29				1			1			1		1	1	1	1	1		
30				1			1			1		1	1		1	1		
31	1			1	1	1	1		1	1		1	1		1	1		
32	1		1	1	1	1	1		1	1		1	1		1	1		

33	1			1			1	1	1	1		1	1		1	1		
34	1			1		1	1	1	1	1	1	1	1			1		
35	1			1			1	1	1	1		1	1		1	1		1
36	1			1			1	1	1	1		1	1		1	1		
37	1			1			1	1	1	1		1	1		1	1		
38	1			1			1	1	1	1		1	1	1	1	1		
39	1			1			1	1	1	1		1	1		1	1		
40	1			1			1	1	1	1		1	1		1	1		
41	1			1			1	1	1	1		1	1		1			
42	1			1			1	1	1	1		1	1		1			
43	1			1			1	1	1	1			1					
44	1			1		1	1	1	1				1		1			
45	1			1		1	1	1					1		1			
46	1			1		1	1	1					1		1			
47	1			1			1	1	1				1		1			
48	1			1			1	1	1									
49	1						1	1	1									
50	1						1	1	1									
51	1						1	1										
52	1	1					1	1	1									
53	1	1	1				1	1										
54	1	1	1				1	1										
55	1	1					1	1										
56	1	1					1	1										
57	1		1				1	1										
58	1	1					1	1										
59	1	1					1	1										
60	1	1					1	1										
61	1	1					1	1										
62	1	1					1	1										
63	1	1					1	1										
64	1	1					1	1										
65	1						1	1	1									
66	1						1	1										
67	1	1					1	1										
68	1	1					1	1										
69	1	1					1	1										
70	1		1				1	1	1									
71	1	1	1				1	1	1									
72	1						1	1	1									
73	1	1					1	1	1									
74	1						1	1	1									
75	1	1					1	1	1									
76	1	1					1	1	1									
77	1	1					1	1	1									
78	1	1					1	1	1									
79	1	1					1	1	1									
80	1	1					1	1	1									
81	1	1					1	1	1									
82	1	1					1	1	1									

83	1	1					1	1	1
84	1	1					1	1	1
85	1	1							
86	1	1							
87	1	1							
88	1	1							
89	1	1							
90	1	1							
91	1	1							
92	1	1							